NASA/TM-2010-216182

Ares I-X Flight Test Vehicle Modal Test

Ralph D. Buehrle, Justin D. Templeton, Mercedes C. Reaves, Lucas G. Horta, and James L. Gaspar
Langley Research Center, Hampton, Virginia

Paul A. Bartolotta
Glenn Research Center, Cleveland, Ohio

Russel A. Parks and Daniel R. Lazor
Marshall Space Flight Center, Huntsville, Alabama

January 2010

NASA STI Program . . . in Profile

Since its founding, NASA has been dedicated to the advancement of aeronautics and space science. The NASA scientific and technical information (STI) program plays a key part in helping NASA maintain this important role.

The NASA STI program operates under the auspices of the Agency Chief Information Officer. It collects, organizes, provides for archiving, and disseminates NASA's STI. The NASA STI program provides access to the NASA Aeronautics and Space Database and its public interface, the NASA Technical Report Server, thus providing one of the largest collections of aeronautical and space science STI in the world. Results are published in both non-NASA channels and by NASA in the NASA STI Report Series, which includes the following report types:

- TECHNICAL PUBLICATION. Reports of completed research or a major significant phase of research that present the results of NASA programs and include extensive data or theoretical analysis. Includes compilations of significant scientific and technical data and information deemed to be of continuing reference value. NASA counterpart of peer-reviewed formal professional papers, but having less stringent limitations on manuscript length and extent of graphic presentations.

- TECHNICAL MEMORANDUM. Scientific and technical findings that are preliminary or of specialized interest, e.g., quick release reports, working papers, and bibliographies that contain minimal annotation. Does not contain extensive analysis.

- CONTRACTOR REPORT. Scientific and technical findings by NASA-sponsored contractors and grantees.

- CONFERENCE PUBLICATION. Collected papers from scientific and technical conferences, symposia, seminars, or other meetings sponsored or co-sponsored by NASA.

- SPECIAL PUBLICATION. Scientific, technical, or historical information from NASA programs, projects, and missions, often concerned with subjects having substantial public interest.

- TECHNICAL TRANSLATION. English-language translations of foreign scientific and technical material pertinent to NASA's mission.

Specialized services also include creating custom thesauri, building customized databases, and organizing and publishing research results.

For more information about the NASA STI program, see the following:

- Access the NASA STI program home page at *http://www.sti.nasa.gov*

- E-mail your question via the Internet to help@sti.nasa.gov

- Fax your question to the NASA STI Help Desk at 443-757-5803

- Phone the NASA STI Help Desk at 443-757-5802

- Write to:
  NASA STI Help Desk
  NASA Center for AeroSpace Information
  7115 Standard Drive
  Hanover, MD 21076-1320

NASA/TM-2010-216182

Ares I-X Flight Test Vehicle Modal Test

Ralph D. Buehrle, Justin D. Templeton, Mercedes C. Reaves, Lucas G. Horta, and James L. Gaspar
Langley Research Center, Hampton, Virginia

Paul A. Bartolotta
Glenn Research Center, Cleveland, Ohio

Russel A. Parks and Daniel R. Lazor
Marshall Space Flight Center, Huntsville, Alabama

National Aeronautics and
Space Administration

Langley Research Center
Hampton, Virginia 23681-2199

January 2010

Acknowledgments

Thanks go to Winifred Feldhaus of NASA Langley Research Center for her assistance with finite element model development. The test execution phase at Kennedy Space Center (KSC) could not have been done without the support of many individuals. Special thanks go to the KSC instrumentation team led by Frank Walker, which routed approximately 28000 feet of cable for the Flight Test Vehicle alone. Logistics and test hardware integration went smoothly due to the dedicated KSC crew that included Russ Brucker, Trip Healey, Stephanie Heffernan, Teresa Kinney, Todd Reeves, Kara Schmitt, Mark Tillett, and Jim Wiltse. Lastly, thanks to our independent verification team of Jeff Lollock, Ryan Tuttle, and Joshua Hwung from Aerospace Corporation.

Available from:

NASA Center for AeroSpace Information
7115 Standard Drive
Hanover, MD 21076-1320
443-757-5802

Table of Contents

Abstract

The first test flight of NASA's Ares I crew launch vehicle, called Ares I-X, was launched on October 28, 2009. Ares I-X used a 4-segment reusable solid rocket booster from the Space Shuttle heritage with mass simulators for the 5th segment, upper stage, crew module and launch abort system. Flight test data will provide important information on ascent loads, vehicle control, separation, and first stage reentry dynamics. As part of hardware verification, a series of modal tests were designed to verify the dynamic finite element model (FEM) used in loads assessments and flight control evaluations. Based on flight control system studies, the critical modes were the first three free-free bending mode pairs. Since a test of the free-free vehicle was not practical within project constraints, modal tests for several configurations during vehicle stacking were defined to calibrate the FEM. Test configurations included two partial stacks and the full Ares I-X flight test vehicle on the Mobile Launcher Platform. This report describes the test requirements, constraints, pre-test analysis, test execution and results for the Ares I-X flight test vehicle modal test on the Mobile Launcher Platform. Initial comparisons between pre-test predictions and test data are also presented.

1.0 Introduction

The 327 foot 1.8 million-pound Ares I-X flight test vehicle [1] is shown in Figure 1. Ares I-X consists of a 4-segment reusable solid rocket motor from the Space Shuttle heritage with mass simulators for the 5th segment, upper stage, crew module (CM) and launch abort system (LAS). NASA Langley Research Center (LaRC) built the CM/LAS simulator. NASA Glenn Research Center (GRC) built the upper stage simulator and ATK built the first stage. Integration of the vehicle was performed in the Vehicle Assembly Building (VAB) at NASA's Kennedy Space Center (KSC). Ares I-X was successfully launched on October 28, 2009. This was the first flight test for NASA's Ares I crew launch vehicle. Flight test data will provide important information on ascent loads, vehicle control, separation, and first stage reentry dynamics.

As part of hardware verification for Ares I-X, a series of modal tests were designed to verify the dynamic finite element model (FEM) used in loads assessments and flight control evaluations. The first three free-free bending mode pairs were defined as the target modes for the modal test based on the flight control requirements. Since a test of the free-free vehicle configuration was not practical within the projects constraints, calibration of the FEM was done using modal test data for three configurations in the nominal KSC integration flow. The first of these modal tests was performed in May 2009 on the Stack 5 subassembly, which included the topmost hardware from the Spacecraft Adapter Simulator to the Launch Abort System Simulator. The second test was performed in July 2009 on the Stack 1 hardware, which included the center section from the 5th Segment Simulator through the Interstage. Finally, the fully integrated Ares I-X flight test vehicle (FTV) mounted to the Mobile Launcher Platform (MLP) was tested in August 2009.

This report focuses on the modal test of the full Ares I-X FTV on the MLP that was conducted from August 27-30, 2009. Separate reports are under development for the partial stack tests. The requirements are derived from the free-free bending target modes. Based on these requirements, FEM pre-test analysis is used to define the response transducer and shaker locations. Project constraints on instrumentation numbers and vehicle accessibility are also discussed as part of the transducer/shaker placement studies. Schedule constraints required that the team conduct the tests and verify the sufficiency of the data in a short four-day test period. Details of the modal test planning, setup, operation, and results are described. Comparisons between pre-test predictions and test data are also presented.

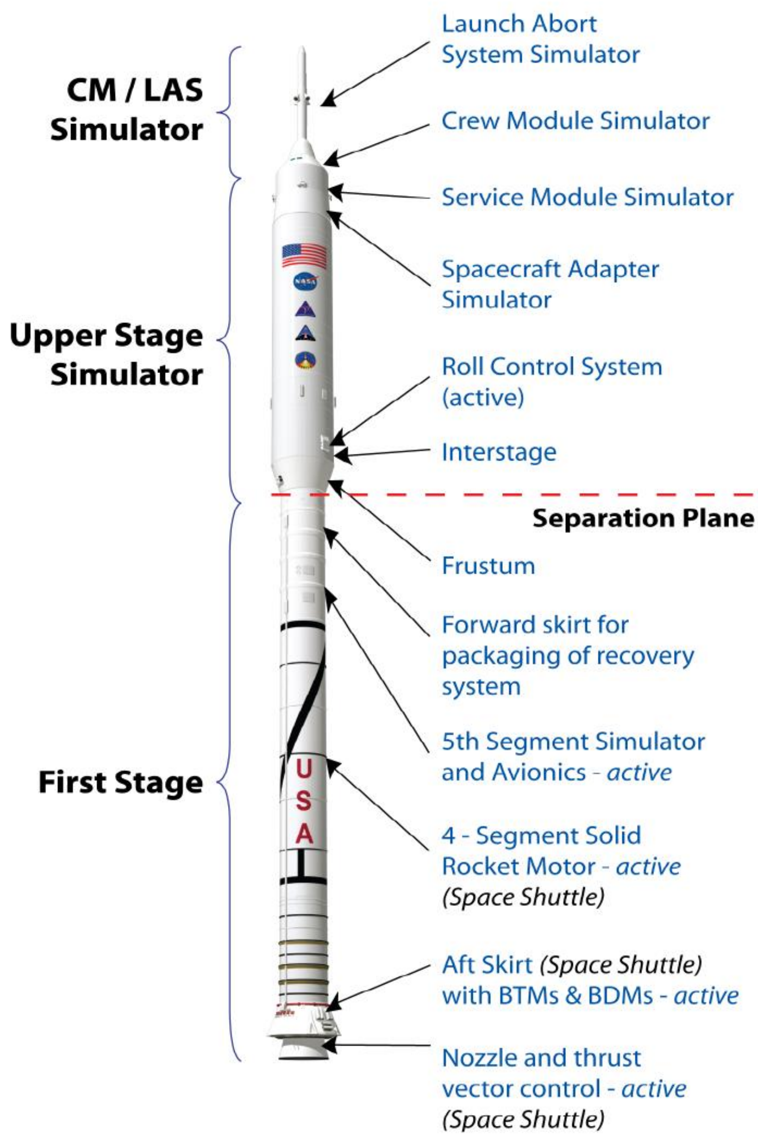

Figure 1. Ares I-X Flight Test Vehicle [1].

2.0 Test Planning

2.1 Test Configurations

The modal verification for Ares I-X focused on new hardware components. Shuttle heritage hardware like the first stage (see Figure 1) had FEMs that had been test verified. However, the 5^{th} segment simulator, upper stage, and CM/LAS were all new hardware that needed to be test verified.

For flight control, the target free-free bending modes shown in Figure 2 are critical. Due to vehicle symmetry, a companion set of modes also occur in the orthogonal bending plane (not shown). These orthogonal "mode pairs" appear at nearly the same frequency. Based on visual inspection of the first three free-free bending mode shapes shown in Figure 2, the center section of the vehicle displays significant deformations for the 1^{st} and 2^{nd} bending modes but the CM/LAS deformations dominate the 3^{rd} bending mode. These areas of the vehicle are also new hardware without previous test verification. Consequently, the Stack 1 and Stack 5 subassemblies shown in Figure 3 were selected for modal tests. These tests were meant to provide an early assessment of FEM adequacy for the subassemblies. To minimize impact to the program schedule and cost, test durations and configurations were restricted to what was available during the normal vehicle integration flow. Because no special provisions were made for testing, subassemblies were tested with unknown boundary conditions and without mass loading of the unsupported edges. Early in the planning stage the test team recognized the risk associated with unknown boundaries and proceeded with an effort to correct for boundary interface compliance [2], and planned for additional measurements across the boundaries.

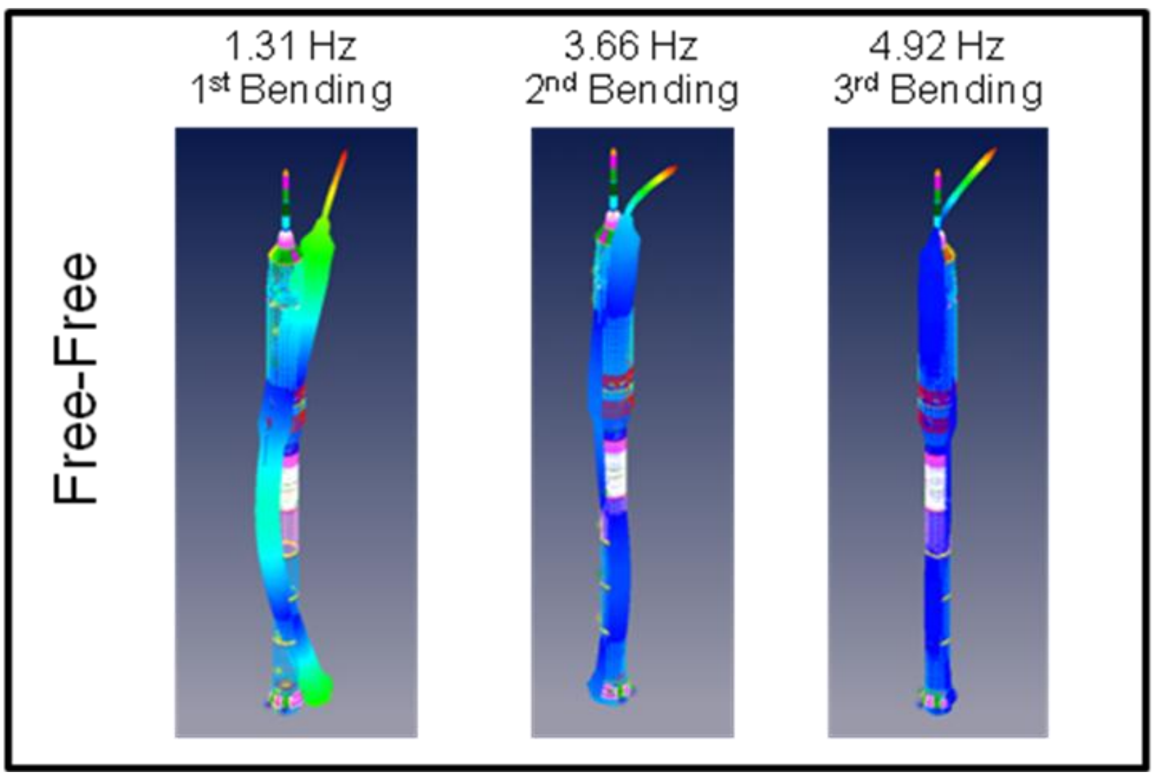

Figure 2. Free-free bending target modes.

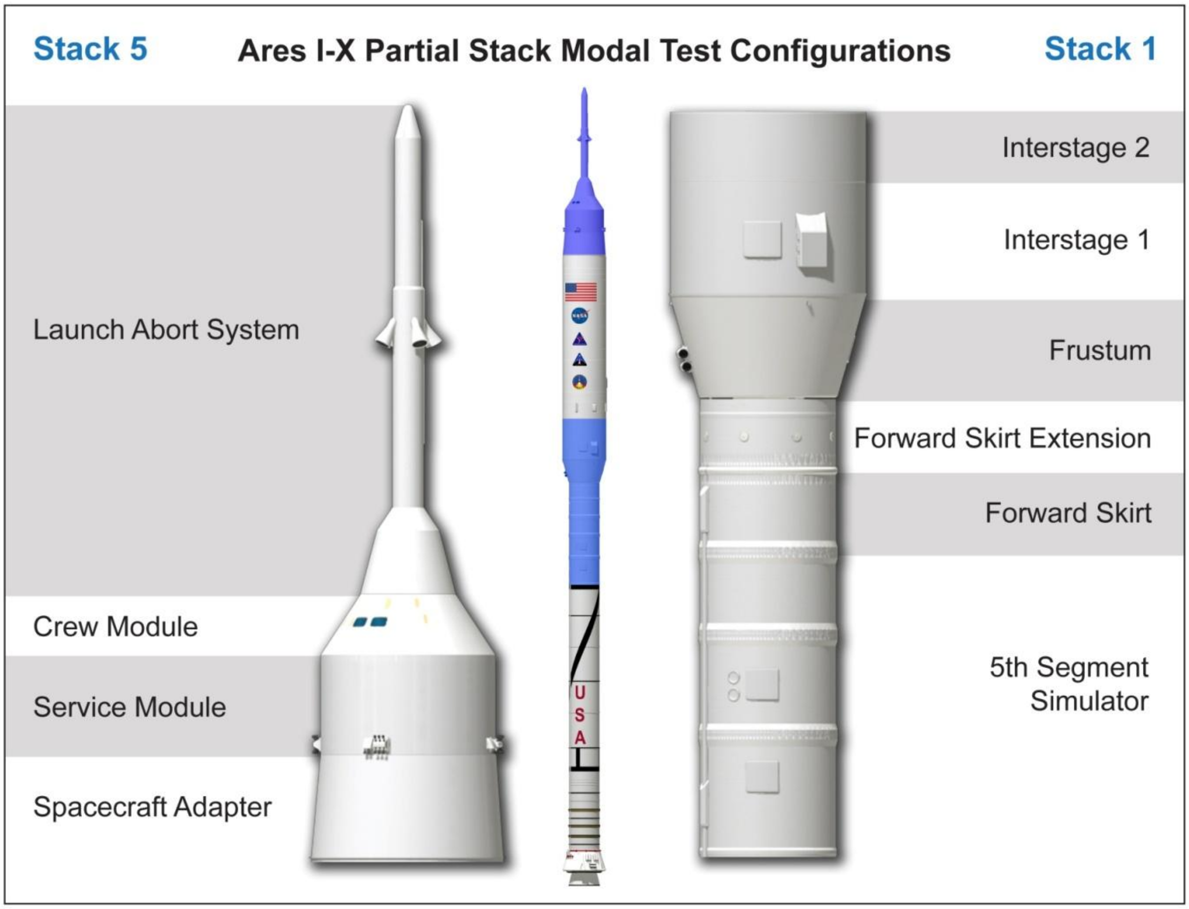

Figure 3. Ares I-X Subassembly Modal Test Configurations

Before flight, the final check in the verification process called for testing of the full Ares I-X FTV on the MLP, as shown in Figure 4. Because the hardware components were fabricated at various sites, hardware suppliers also provided the FEM for their components. This included a CM/LAS model from NASA LaRC, an upper stage model from NASA GRC, a first stage model from ATK, and an MLP model from NASA KSC. After integration of the models at LaRC, initial model checkouts were performed and then the model was used for coupled loads analysis and control system evaluations. The modal test results provided a needed check on the fidelity of the integrated model. The remainder of the report will focus on the modal test of the FTV on MLP configuration. Separate reports are in development for the partial stack modal tests.

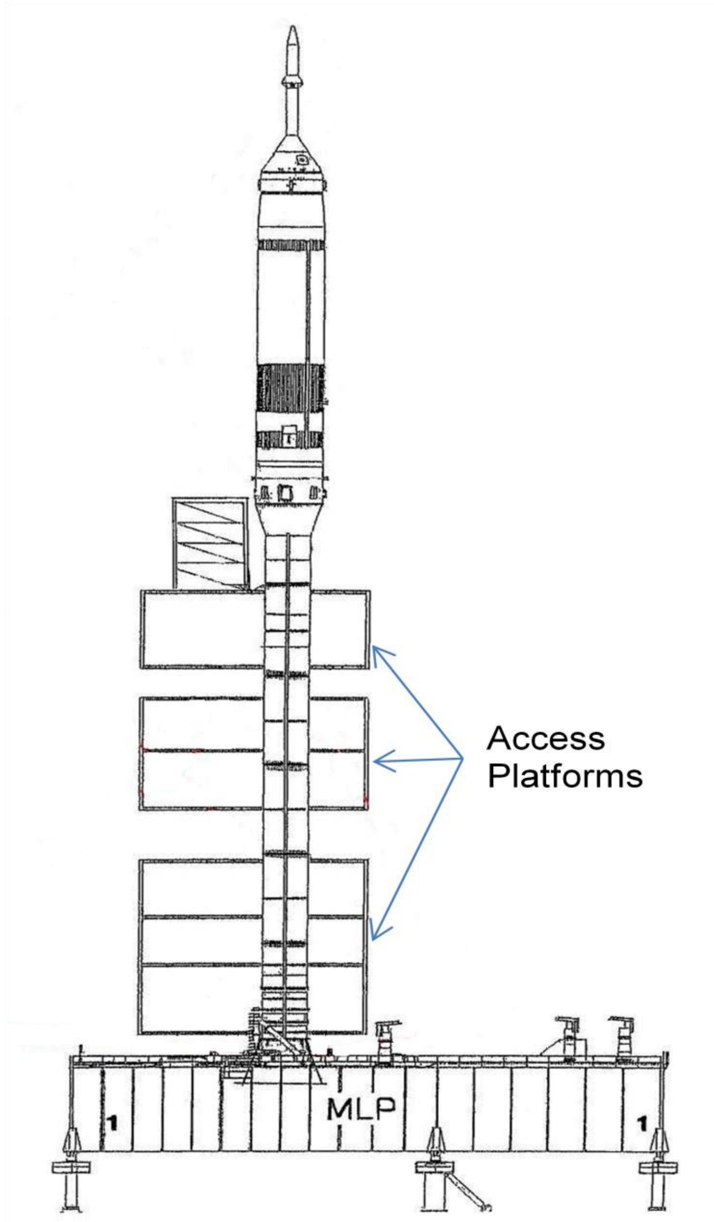

Figure 4. Schematic of Ares I-X FTV on the MLP with VAB access platforms.

2.2 Test Requirements

The modal tests were designed to minimize impact to the project integration flow and schedule. As such, the project emphasized minimal instrumentation to characterize the bending modes and did not provide hard limits on test/analysis orthogonality metrics. Metrics for the tests, derived from Monte Carlo simulations of the flight control system, were provided to the test group in terms of variances. For instance, allowable variances were set to: 10% for 1st bending mode frequency and 20% for higher modes; node locations within +/- 100 inches; and modal deformations within 20% of nominal for the 1st bending mode pair and 50% for higher modes.

While these requirements could not be verified on the free-free configuration, calibration of the model for comparable modes for the FTV on the MLP was deemed sufficient to verify the FEM. Hence, predictions of the free-free modes were assumed to have similar test/analysis variances as comparable modes for the FTV on MLP.

Figure 5 shows the flow down from the free-free target modes to the comparable modes for the FTV on the MLP. There is a strong similarity between the first three free-free bending modes and the 2nd through 4th bending modes on the MLP. Therefore, the target modes selected for the FTV on the MLP are the first four bending mode pairs. Although the 1st bending mode pair on the MLP was not important for controls, it was critical for transportation to the launch pad.

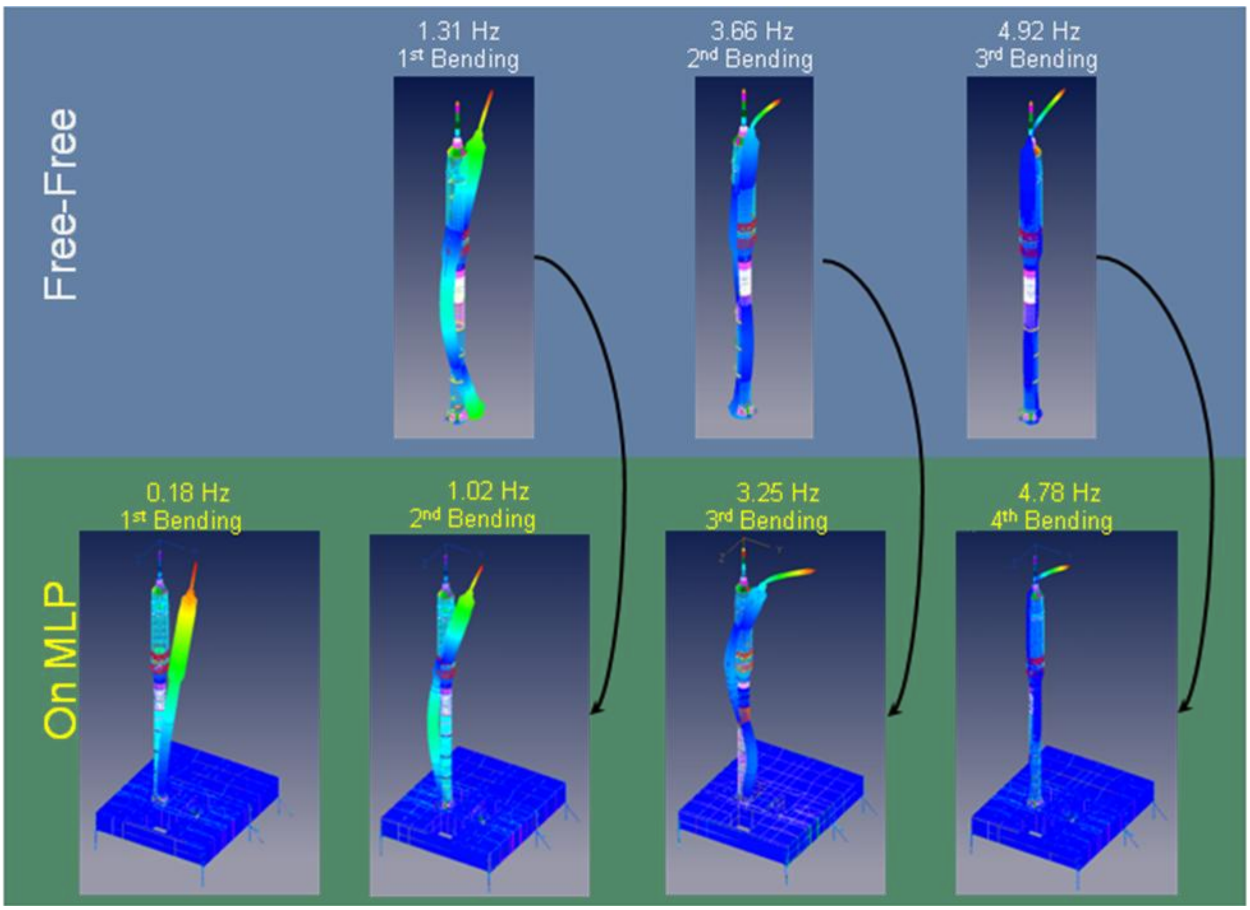

Figure 5. Mode shapes for Ares I-X free-free and on MLP.

2.3 Pre-Test Analysis

To control cost, the project emphasized minimal instrumentation to characterize the bending modes and did not provide targets on test/analysis orthogonality metrics. Initially, the goal prior to conducting the pre-test analysis was for approximately 20 sensor locations with biaxial accelerometers for capturing the bending modes. As will be shown, the sensor count was expanded to approximately 40 locations in an effort to improve the orthogonality results. Sensor and shaker placement was performed using the pre-test FEM. For component tests, the effective independence [3] technique along with engineering judgment was used for sensor placement. In contrast, for the FTV physical access constraints dominated the instrumentation placement process. Shaker and accelerometer placement on the exterior of the first stage focused on areas accessible from existing facility platforms. Because no external access for shaker or accelerometer mounting was available above the first stage, as shown in Figure 4, all instrumentation was mounted internally for the upper stage and CM/LAS.

Table 1 lists the FEM predictions of the first 14 modes with the target modes highlighted. The corresponding target mode shapes for the X-Y plane are those shown in Figure 5. Based on the target bending modes, a line of sensors reachable from existing facility platforms and internal ladders was selected. Orthogonality was then used to evaluate the sensor set and to make adjustments. In addition, triaxial accelerometers (numbers 24-26) were located at the three control sensor locations. Except for locations 24-26, all vehicle sensors were mounted to the vehicle outer shell. The resulting measurement locations shown on Figure 6 include a combination of radial, biaxial and triaxial accelerometers at 34 locations on the vehicle and MLP, as defined in Table 2. Also listed in Table 2 are the four shaker locations that were determined to be optimal with platform access for mounting. A cross reference between the instrumentation locations and the finite element model (version IVM_13b) node numbers is provided in Table 2.

Cross-orthogonality between the reduced model (corresponding to the test instrumentation set) and the full model was used to assess the adequacy of the test instrumentation set. Figure 7 shows a plot of the orthogonality results with numerical values provided in Table 3. It is important to note that the 346,860 degree of freedom (DOF) FEM was reduced to an 82 DOF test model. As a result, system modes at 4.66 Hz and 4.92 Hz were not predicted in the reduced order model, which produced a frequency offset in the diagonal of the orthogonality plot. Also note that the diagonal terms for the target modes are >0.85 and the off-diagonal terms were generally less than 0.1. However, the torsion mode at 3.58 Hz and the system mode (significant MLP motion) at 4.66 Hz have high off-diagonal terms. Nonetheless, this was acceptable within the project constraints on instrumentation. To alleviate the problem with torsion and system modes, the measured data can be sieved to eliminate these modes and to focus the correlation effort on the bending modes of interest. The MLP and 1st stage (including aft skirt) are considered validated models based on Shuttle test heritage and were therefore not a focus of this test.

Pre-test analysis also included simulations of the test to evaluate the required force and expected acceleration amplitudes. This was used in the selection of the shakers, accelerometers, and for test planning.

Table 1 FTV on MLP Predicted Modes

Mode No.	Frequency (Hz)	Mode Description
1	0.176	1st Bending Mode of Ares I-X (X-Y Plane)
2	0.216	1st Bending Mode of Ares I-X (X-Z Plane)
3	1.02	2nd Bending Mode of Ares I-X (X-Y Plane)
4	1.17	2nd Bending Mode of Ares I-X (X-Z Plane)
5	1.87	Ares I-X / MLP System lateral mode
6	2.66	Ares1-X / MLP System lateral mode
7	3.25	3rd Bending Mode of Ares1-X (X-Y Plane)
8	3.49	Ares1-X / MLP System mode
9	3.50	3rd Bending Mode of Ares1-X (X-Z Plane)
10	3.58	Ares1-X Torsion
11	4.22	Ares1-X / MLP System mode
12	4.66	Ares1-X / MLP System mode
13	4.78	4th Bending Mode of Ares1-X (X-Y Plane)
14	4.84	4th Bending Mode of Ares1-X (X-Z Plane)

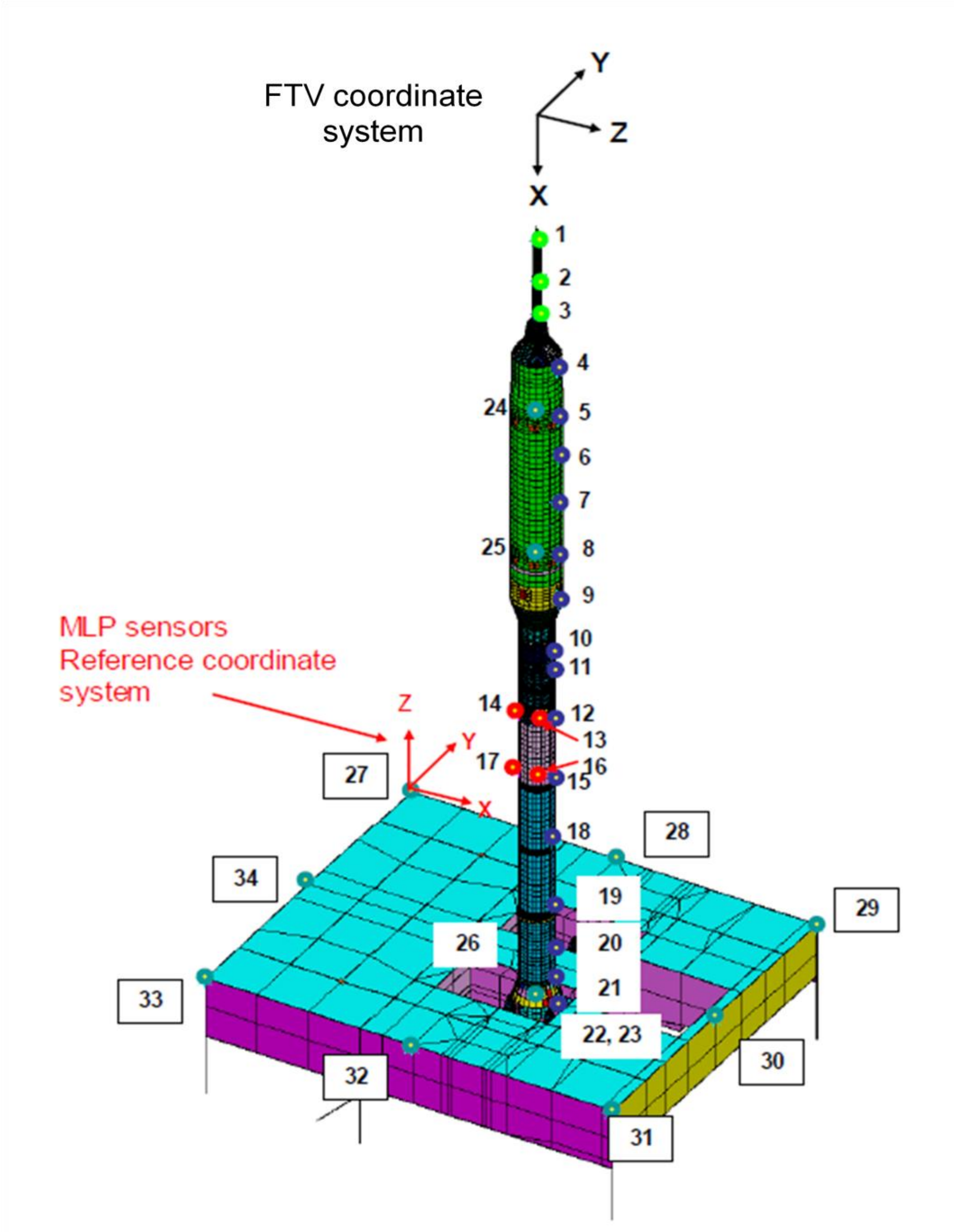

Figure 6. FTV on MLP sensor/shaker locations.

Table 2. Accelerometer/Shaker Locations used in Pre-Test Analysis

Vehicle Sensor	FEM Node	X (FTV) (in)	Angle+ (Degrees)	Description	Measurement Axis (FTV ref cs)
1	4001618	199.4	180.0	LAS	Y, Z
2	4001857	402.5	180.0	LAS	Y, Z
3	4001834	568.3	180.0	LAS	Y, Z
4	6000010	814.0	0.0	Service Module	X, Y, Z
5	6001605	1064.3	0.0	Upper Stage -7	Y, Z
6	6000016	1259.9	0.0	Upper Stage -5	Y, Z
7	6000026	1493.4	0.0	Upper Stage -3	X, Y, Z
8	6003110	1757.3	0.0	Upper Stage -1	Y, Z
9	6001119	1985.2	0.0	Interstage -1	X, Y, Z
10	8903034	2246.6	0.0	Forward Skirt	Y, Z
11	8906012	2333.8	0.0	5th Segment	Y, Z
12	8906444	2567.5	0.0	5th Segment	X, Y, Z
13	8906450	2567.5	45.	E-main shaker 1	Radial (45°)
14	8906468	2567.5	135.	E-main shaker 2	Radial (135°)
15	1011900	2854.5	0.0	Fwd Segment	Y, Z
16	1011903	2854.5	45.	B-deck shaker 1	Radial (45°)
17	1011909	2854.5	135.	B-deck shaker 2	Radial (135°)
18	1022100	3202.5	0.0	Fwd Center Segment	X, Y, Z
19	1032100	3522.5	0.0	Aft Center Segment	Y, Z
20	1051500	3756.6	0.0	Aft Booster	Y, Z
21	1061050	3903.5	0.0	Aft Booster	Y, Z
22	1307540	4007.5	30.0	Hold Down Post #6	X, Y, Z
23	1307255	4007.5	297.75	External -Aft Skirt	X, Y, Z
24	6905698	1023.8	15.	FWD RRGU	X, Y, Z
25	6905699	1770.3	5.0	FTINU	X, Y, Z
26	6905700	3962.9	240.	AFT RRGU	X, Y, Z
MLP sensors	**FEM Node**	**X (MLP ref. cs) (in)**	**Y (MLP ref. cs) (in)**	**Z (MLP ref. cs) (in)**	**Measurement Axis (FTV ref cs)**
27	114087	0.0	0.0	0.0	X, Y, Z
28	114098	958.0	0.0	0.0	X, Y, Z
29	114159	1895.9	0.0	0.0	X, Y, Z
30	114170	1895.5	-798.0	0.0	X, Y, Z
31	114195	1895.9	-1596.0	0.0	X, Y, Z
32	114231	958.0	-1596.0	0.0	X, Y, Z
33	114673	0.0	-1596.0	0.0	X, Y, Z
34	114703	0.0	-798.0	0.0	X, Y, Z

Note+: 0° is aligned with +Z-axis and 270° with +Y-axis of FTV coordinate system.

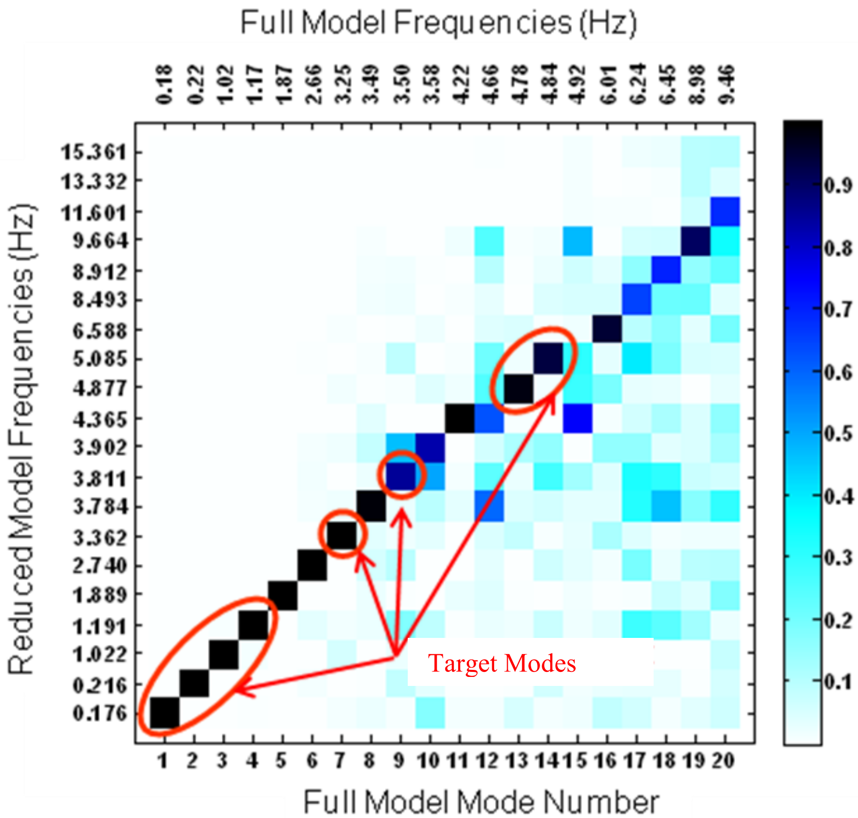

Figure 7. FTV on MLP Cross-Orthogonality

Table 3. FTV on MLP Cross-Orthogonality Values

		Reduced Model Frequency (Hz)												
		0.17568	0.21630	1.02167	1.19124	1.88934	2.73955	3.36247	3.78412	3.81134	3.90187	4.36536	4.87682	5.08534
Full Model Freq. (Hz)	0.1756	1.00	0.00	0.00	0.00	0.00	0.00	0.00	0.00	0.00	0.00	0.00	0.00	0.00
	0.2163	0.00	1.00	0.00	0.00	0.00	0.00	0.00	0.00	0.00	0.00	0.00	0.00	0.00
	1.0171	0.00	0.00	1.00	-0.01	0.00	0.00	0.00	0.00	0.00	0.00	0.00	0.00	0.00
	1.1734	-0.01	0.00	0.02	1.00	0.00	0.00	0.00	0.00	0.00	0.00	0.00	0.00	0.00
	1.8726	0.00	0.00	0.00	0.00	-1.00	0.00	0.00	0.00	0.00	0.00	0.00	0.00	0.00
	2.6611	0.00	-0.01	0.00	0.04	0.00	1.00	0.00	-0.01	-0.02	-0.01	0.00	0.00	0.01
	3.2484	-0.01	0.00	0.06	-0.02	0.00	0.00	-1.00	0.02	0.00	0.02	0.00	0.02	0.00
	3.4899	0.03	0.00	0.00	-0.03	0.03	0.06	0.04	0.99	-0.03	0.09	-0.04	0.00	-0.01
	3.4966	0.01	-0.09	-0.02	0.18	0.01	-0.10	-0.02	0.03	-0.85	-0.47	0.00	-0.01	0.09
	3.5780	0.18	-0.04	0.00	0.09	0.00	0.00	-0.04	0.10	0.50	-0.83	0.00	-0.05	0.00
	4.2195	-0.01	0.00	0.00	0.01	0.03	0.00	0.00	0.04	0.01	0.00	1.00	0.02	0.01
	4.6645	0.01	0.00	-0.01	-0.03	-0.05	-0.04	-0.05	0.60	-0.24	0.06	0.63	-0.25	-0.21
	4.7843	0.06	-0.01	-0.02	0.02	0.01	0.00	-0.08	-0.05	-0.03	0.12	0.01	-0.98	0.02
	4.8417	0.02	0.06	0.00	-0.08	0.00	0.07	-0.01	-0.07	-0.28	-0.16	0.00	-0.02	-0.94

3.0 Test Description

3.1 Test Article

The modal test was performed on the fully assembled 1.8 million-pound 327-foot Ares I-X FTV mounted on the MLP in the Vehicle Assembly Building at NASA's Kennedy Space Center. An overall photograph taken from the MLP is shown in Figure 8. A close up of one of the four hold down posts used to attach the FTV to the MLP is shown in Figure 9. As shown in the photograph in Figure 10, the upper stage of the vehicle was above the facility access platforms. Accelerometer installation in the upper stage required the use of internal access ladders and platforms, shown in Figure 11. Details of the instrumentation, excitation, and data acquisition systems are provided in the following sections.

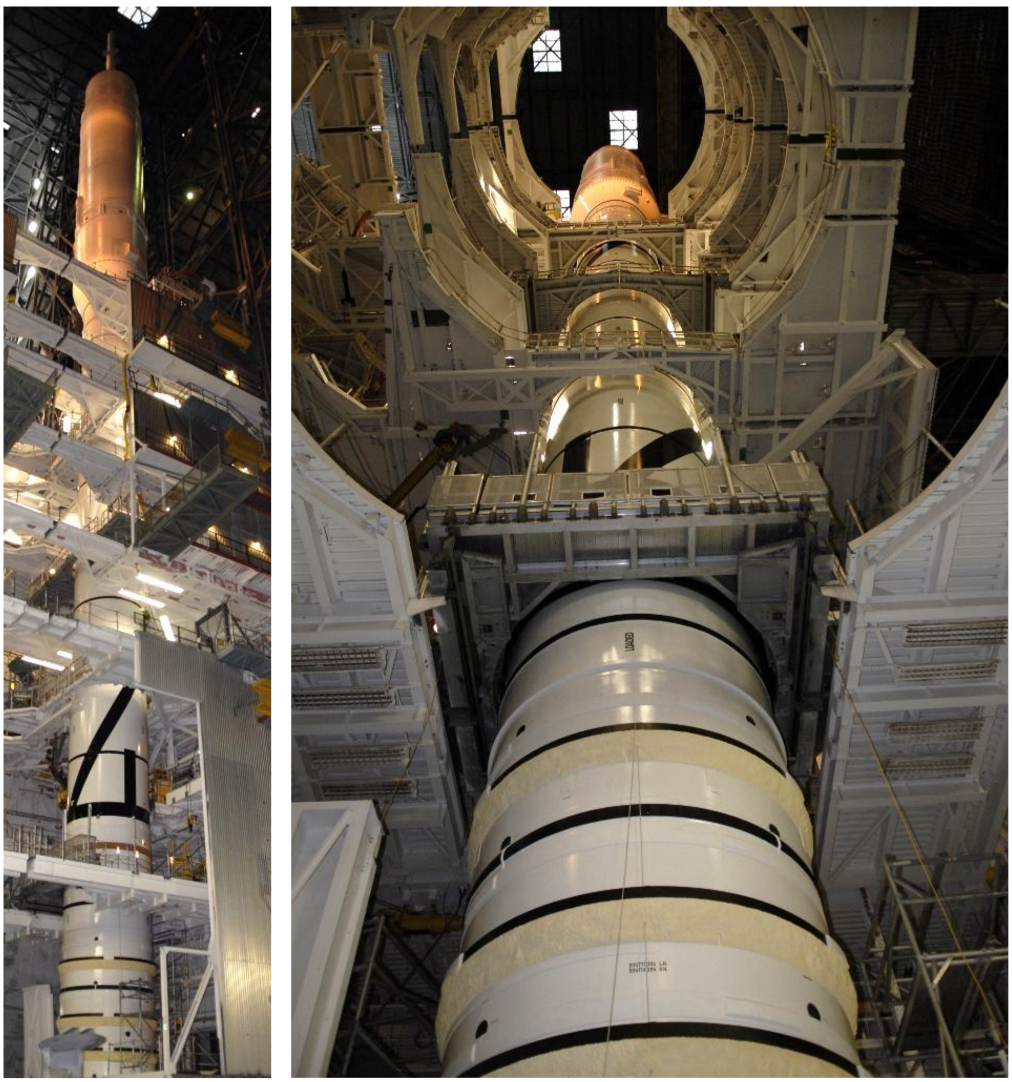

Figure 8. Ares I-X FTV Modal Test Configuration (view from MLP).

Figure 9. FTV to MLP attachment at Hold-down Post #7.

Figure 10. Upper Stage of Ares I-X Vehicle extends above the facility access platforms.

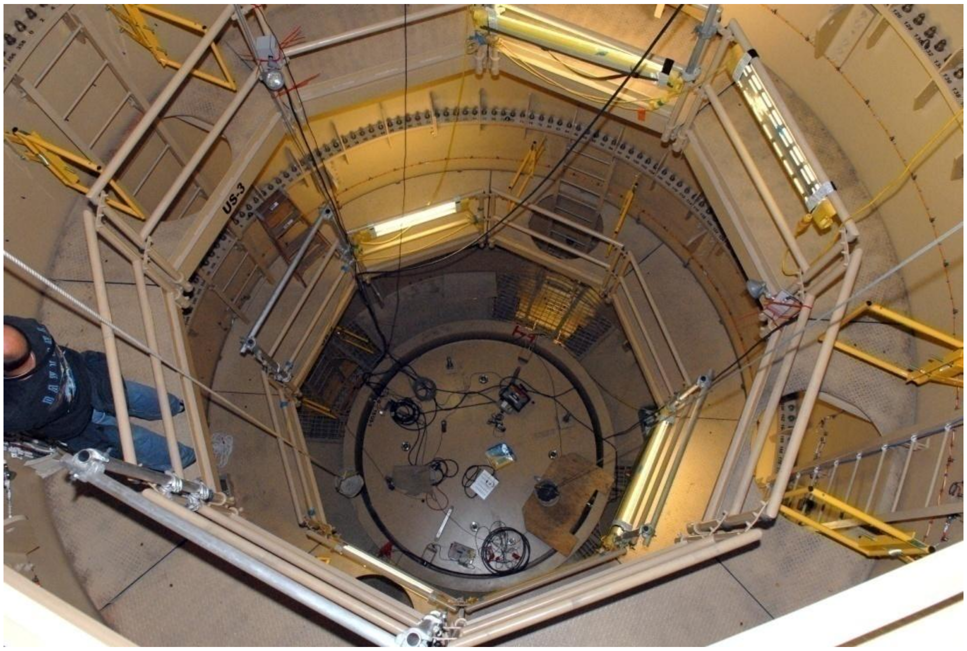

Figure 11. Interior view of Upper Stage showing internal access ladders and platforms.

3.2 Test Instrumentation

The instrumentation used for this modal test consisted of 90 PCB series 3701 capacitive accelerometers with 1 V/g sensitivity that were installed [4] at 40 locations. In addition to the 34 locations defined in the pre-test analysis (see Table 2), 6 locations denoted as locations 39-44 were added during installation to better define the vehicle interface with the MLP and to separate out the torsion mode. This included tangential accelerometers 180 degrees from locations 4, 12, and 21 to help resolve the 3rd bending and torsion modes at approximately 3.5 Hz. Locations and orientations for the as installed accelerometer are listed in Table 4. Items highlighted in yellow were oriented in a local cylindrical coordinate system and require a coordinate transformation to align them with the FTV coordinate system (see Figure 6) as noted in Table 4. All other transducers were oriented in the FTV coordinate system. A typical accelerometer mounting is shown in Figure 12. Over 28000 feet of instrumentation cable was used to connect the accelerometers to the modal data acquisition system for this test. In addition to the accelerometers, a strain gage at each of the four hold down posts (denoted as sensor locations 35-38) where the launch vehicle was bolted to the MLP was recorded with the modal data. A complete set of strain gage bridge measurements at each of the hold down posts was acquired during the modal test on the MLP Critical Data Acquisition System (CDAS).

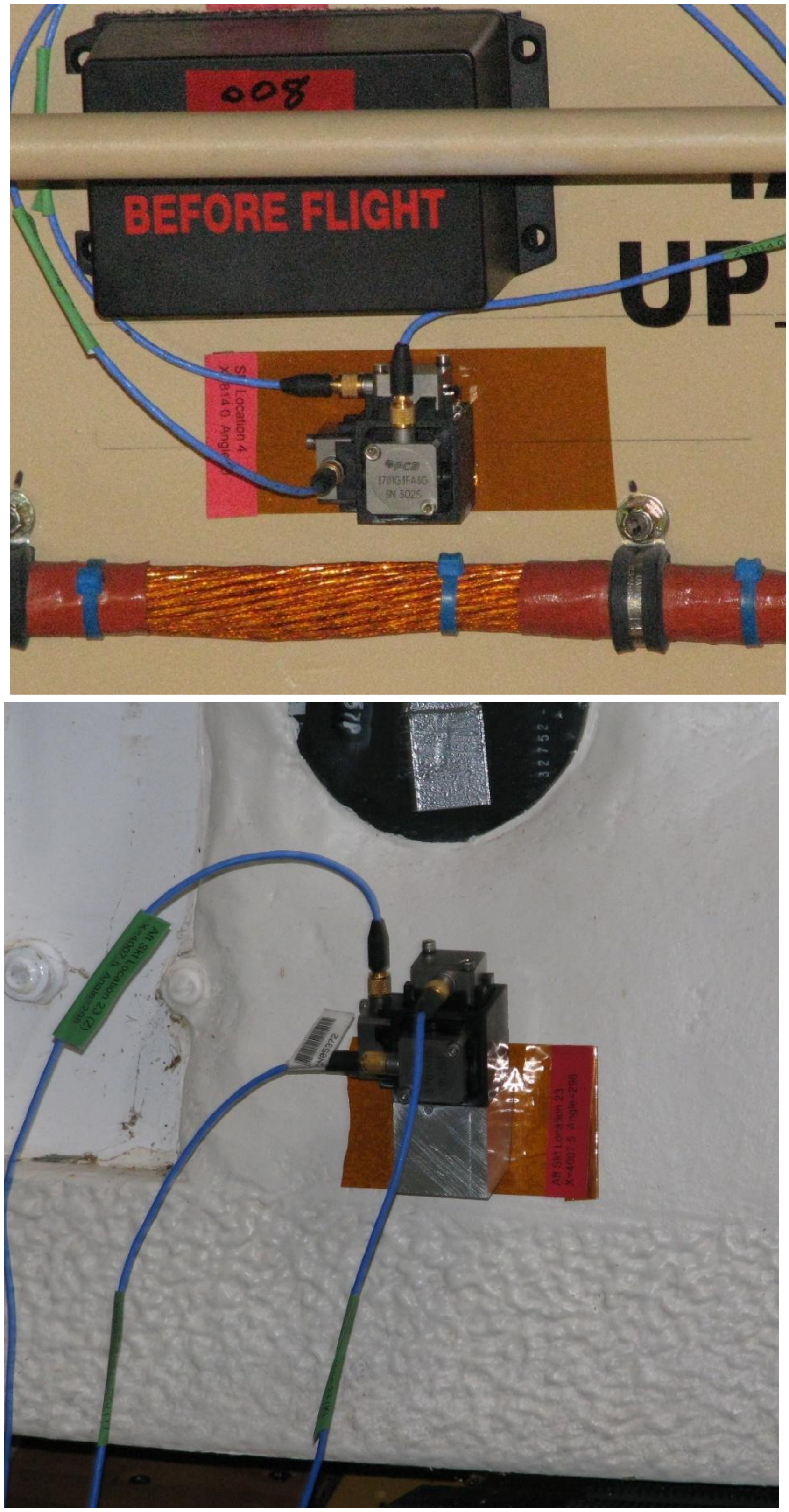

Figure 12. Typical accelerometer installations; (top) service module-location 4 interior and (bottom) aft skirt-location 23 exterior.

Table 4. As-Installed Sensor Locations/Orientations

Sensor Location	Radial+ (in)	Angle+ (Degrees)	X station (in)	Description/Measurement Axis (FTV coordinate system)
1	15.8	180	199.4	LAS Accel. (-Y, Z)
2	17.8	180	402.5	LAS Accel. (-Y, Z)
3	17.8	180	568.3	LAS Accel. (-Y, Z)
4	99.0	0	812.5	Service Module Accel. (-X, Y, -Z)
5	108.2	0	1063.5	US-7 Accel. (Y, -Z)
6	108.2	0	1260.5	US-5 Accel. (Y, -Z)
7	108.2	0	1494	US-3 Accel. (-X, Y, -Z)
8	108.2	0	1757.25	US-1 Accel. (Y, -Z)
9	108.2	0	1985.5	IS-1 Accel. (-X, Y, -Z)
10	72.8	0	2240.4	Forward Skirt Accel. (Y, Z)
11	72.8	0	2232.9	5th Segment Accel. (Y, Z)
12	72.8	0	2557.14	5th Segment Accel. (-X, Y, Z)
13	72.8	45	2557.14	E-main shaker 1; Accel. Z; Force –Z; (45° coordinate rotation about X)
14	72.8	135	2557.14	E-main shaker 2; Accel. Z; Force –Z; (135° coordinate rotation about X)
15	72.8	0	2858.9	Fwd Segment Accel. (Y, Z)
16	72.8	45	2858.9	B-deck shaker 1; Accel. Z; Force –Z; (45° coordinate rotation about X)
17	72.8	135	2858.9	B-deck shaker 2; Accel. Z; Force –Z; (135° coordinate rotation about X)
18	72.8	0	3202.5	Fwd Center Segment Accel. (-X, Y, Z)
19	72.8	0	3524.0	Aft Center Segment Accel. (Y, Z)
20	72.8	0	3756.1	Aft Booster Accel. (Y, Z)
21	72.8	0	3903.9	Aft Booster Accel. (Y, Z)
22	105.2	30	4009.7	Hold down Post #6 Accel. (-X, Y, Z)
23	102.1	270	4003.7	Aft Skirt Accel. (-X, Y, Z)
24	71.8	20	1023.8	Fwd RRGU Accel. (-X, -Y, Z ; 20° coordinate rotation about X)
25	60.9	2	1761.5	FTINU Accel. (X, Y, Z, 2° coordinate rotation about X)
26	67.0	240	3963.7	Aft RRGU Accel. (X, -Y, Z; 330° coordinate rotation about X)
MLP sensors	**X (MLP) (in)**	**Y (MLP) (in)**	**Z (MLP) (in)**	**Description/Measurement Axis (FTV coordinate system)**
27	0.0	0.0	0.0	MLP Corner 3-4 Accel.(-X, Y, Z)
28	958.0	0.0	0.0	MLP Middle of Side 4 Accel. (-X, Y, Z)
29	1895.9	0.0	0.0	MLP Corner 1-4 Accel. (-X, Y, Z)
30	1895.5	-798.0	0.0	MLP Middle of Side 1 Accel. (-X, Y, Z)
31	1895.9	-1596.0	0.0	MLP Corner 1-2 Accel. (-X, Y, Z)
32	958.0	-1596.0	0.0	MLP Middle of Side 2 Accel. (-X, Y, Z)
33	0.0	-1596.0	0.0	MLP Corner 2-3 Accel. (-X, Y, Z)
34	0.0	-798.0	0.0	MLP Middle of Side 3 Accel. (-X, Y, Z)
Sensor Location	**Radial+ (in)**	**Angle+ (Degrees)**	**X station (in)**	**Description/Measurement Axis (FTV coordinate system)**
35				Hold-down Post #5 ; Axial Strain (160 με/V)
36				Hold-down Post #6 ; Axial Strain (160 με/V)
37				Hold-down Post #7; Axial Strain (160 με/V)
38				Hold-down Post #8; Axial Strain (160 με/V)
39	99.0	180	813.5	180° from 4; Service Module Accel. (Y)
40	72.8	180	2557.14	180° from 12; 5th Segment Accel. (Y)
41	72.8	180	3899.85	180° from 21; Aft Booster Accel. (Y)
42	105.2	210	4009.7	Hold-down Post #7 Accel. (-X, Y, Z)
43	105.2	150	4009.7	Hold-down Post #8 Accel. (-X)
44	105.2	330	4009.7	Hold-down Post #5 Accel. (-X)

Note+: 0 degrees is aligned with +Z-axis and 270 degrees with +Y-axis of FTV coordinate system. Nominal radius from vehicle centerline.

3.3 Excitation Systems

The primary excitation system for the FTV modal test used four hydraulic actuator systems manufactured by Team Corporation. The locations of the shakers are specified in Table 4 (Location numbers 13, 14, 16, 17). The shaker systems were located on two Hi-Bay 3 platforms near the 4th and 5th segments of the FTV first stage. Pre-test analysis showed that these locations were able to excite all modes of interest and that the highest chosen platform was an optimal location for exciting the 2nd through 4th bending modes. On each platform, the shakers were oriented at 45° to the preferred direction of travel of the vehicle and 90° relative to each other. This was necessary in order to avoid flight test instrumentation cables and equipment attached to the vehicle while maintaining an orthogonal shaker orientation. Throughout the report the shakers are referred to by the platform and angle of orientation. For example, location 13 is on the E-main platform at 45° and is denoted E45. Similarly, location 14 is denoted E135; location 16 is denoted B45; and location 17 is denoted as B135.

Figures 13-15 show the components of the hydraulic actuator system. Each system consisted of an actuator assembly (Team Part Number 5096500), model HPS-10A hydraulic power supply (Team Part Number 3435000), and model 2240 Moog servo valve driver electronics box (Team Part Number 6151500). Loads were input into the structure through an actuator assembly comprised of the actuator, servo valve, valve mounting manifold, pressure/return accumulators and an internal Linear Variable Differential Transformer (LVDT) position sensor. A hydraulic power supply (HPS), as shown in Figure 14, was located in the vicinity of each actuator assembly and connected to the actuator assembly through a supply, return, and drain hydraulic hose. The system was rated at a peak dynamic load of 1560 lbs, a dynamic stroke of 2-inches peak, and a static load of 2400 lbs. Although the HPS was capable of supplying hydraulic pressure up to 3000 psi, the supply pressure was set at 1000 psi for safety considerations. This reduced the dynamic load capability to 560 lbs peak and 800 lbs static. Other electronic components like the Uninterruptable Power Supply (UPS), the servo valve driver electronic boxes, remote control boxes for the HPS's, oscilloscope, video camera controller, and monitor were all housed in the rack shown in Figure 15. The servo valve driver electronics box was connected to the UPS to assure that control was maintained in case of power outage. In addition, the hydraulic pressure to each shaker could be removed quickly by turning off the HPS at the equipment rack. To control the shaker input level, a servo valve driver electronics box was used that connected the actuator assembly through a position LVDT cable and a servo valve driver cable. An oscilloscope was used for monitoring selected instrumentation, whereas a video camera controller and display provided monitoring for the surveillance cameras that were focused on each of the actuators.

The hydraulic shaker actuators were attached to a mounting frame that allowed the actuator to slide linearly on two reaction hydraulic cylinders with adjustable stiffness as shown in Figure 13. Each platform adapter frame was mounted to two existing holes in Hi-Bay 3 platforms through the front I-beam, and 600 lb of additional weight was added to the rear of the mounting frame to improve the force input to the FTV. Each hydraulic actuator was connected to the vehicle using a ½" threaded rod connected to a PCB series 223 dynamic load cell mounted to an 8" square aluminum plate, which was attached to the vehicle using Tridox F88 dental cement. An additional static load cell was mounted on the actuator side of the threaded rod to monitor static load inputs. Although the reaction hydraulic cylinders were designed to allow linear movement on the mounting frame, they were operated during the modal test with an additional solenoid active to increase the rigidity to the work platform. The hydraulic power supplies and solenoids were controlled remotely at a location near the data acquisition system. Team model 2240 valve drivers were used at this location to control the shakers using a LVDT position feedback loop with each shaker and an input signal from the data acquisition system.

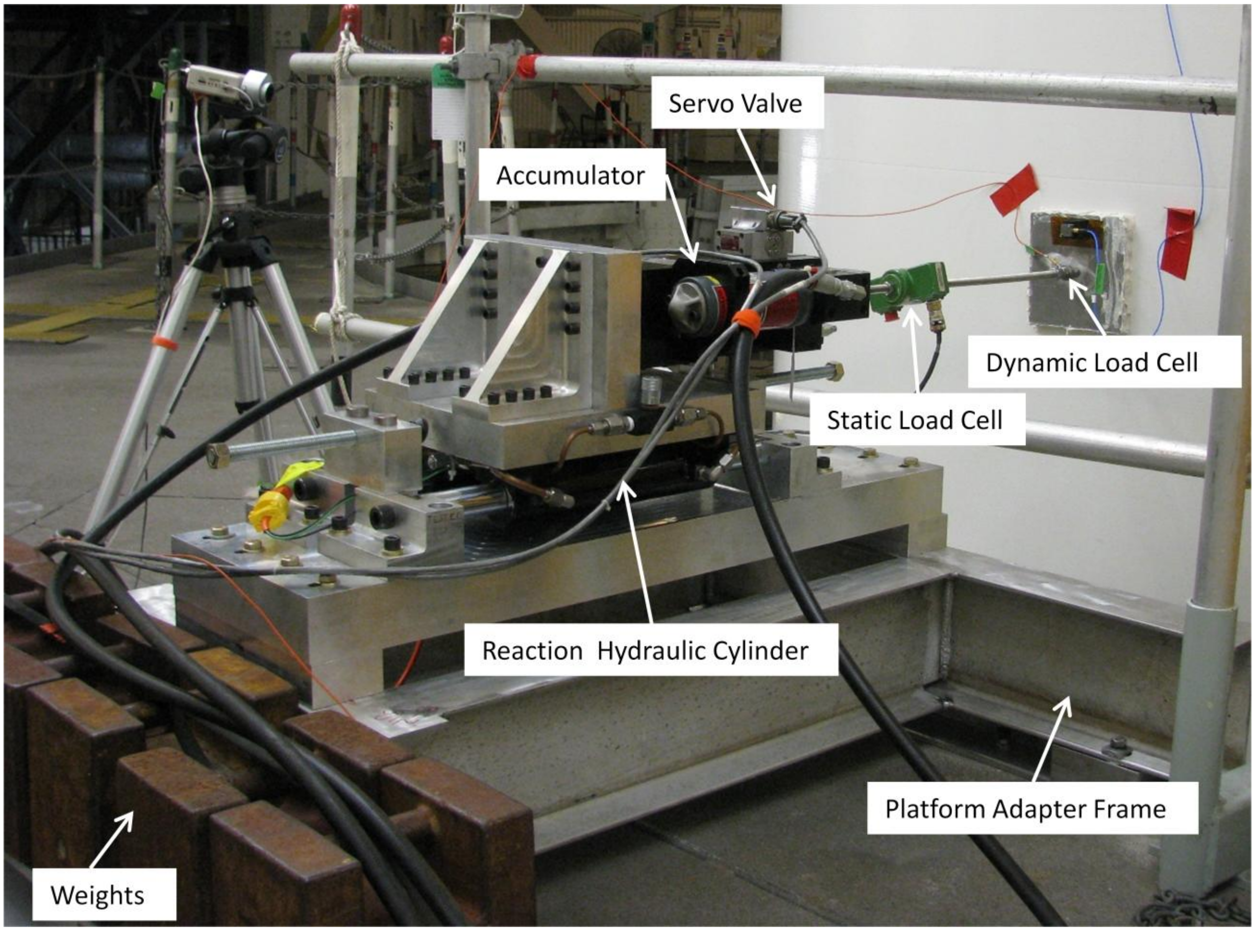

Figure 13. Actuator assembly setup for location 17; B135 (B-Deck 135° orientation).

Figure 14. Hydraulic Power Supply.

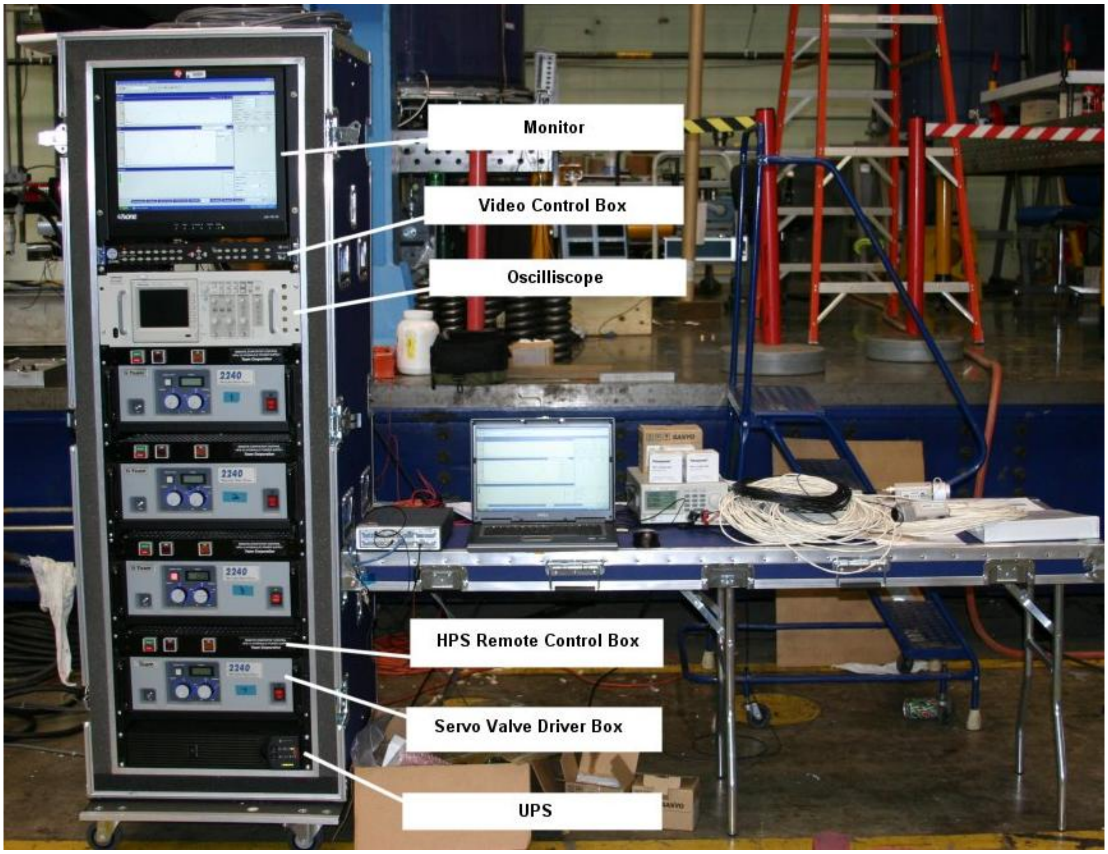

Figure 15. Hydraulic shaker equipment rack.

3.4 Data Acquisition System

The 112 channel data acquisition system (DAS) consisted of seven 16 channel 24-bit VXI data acquisition cards in a single 13-slot VXI mainframe chassis. Sufficient channels were available to simultaneously sample and record all data. A 16-bit VXI source card in the same chassis also provided separate source signals for the excitation system. A firewire interface card allowed the DAS to be controlled by a data acquisition computer running m+p International's Smart Office Analyzer software. During the test, the software calculated the FRFs from the acceleration, strain, and force measurements. Time and FRF data was stored directly to the computer's hard drive as it was acquired. After each test, the FRFs were exported to a universal file format and supplied to the test team for on-site modal parameter estimation. For a complete list of the equipment, see Appendix B.

A picture of the data acquisition rack as it was configured for the modal test is shown in Figure 16. BNC cables from the signal conditioners were routed to patch panels at the top of the rack (black cables). The patch panels were then connected to the data acquisition cards at the bottom of the rack (light gray cables). For more information on the connections from the instrumentation to the data acquisition system, see the channel mapping in Appendix C and KSC Work Plan FA-GIE-0040, Ares IX Full Vehicle Modal Test-Ground Instrumentation Support [4].

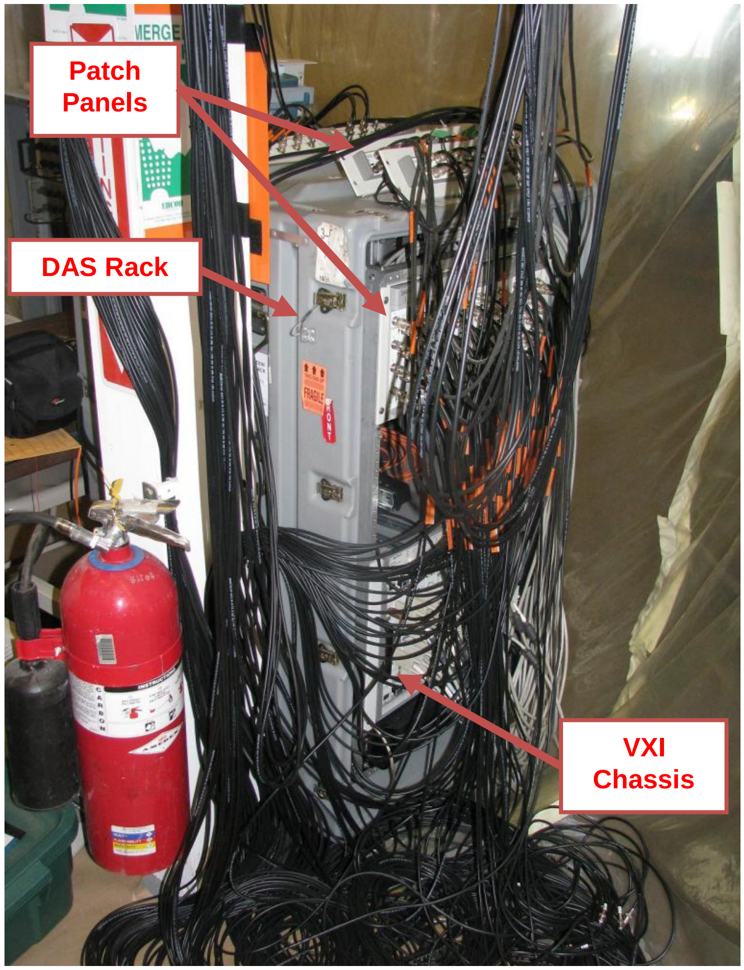

Figure 16. Data acquisition system.

A picture of the signal conditioner rack and the data acquisition computer is shown in Figure 17. The signal conditioner rack contained four Krohn-Hite filters (top of rack, two per box). These filters were used to filter the source signals from the DAS before they were sent to the excitation system. Also shown in this picture is a scope on top of the DAS rack, which allowed the force signals from the load cells to be monitored in real time. Signal conditioners for this test were not located in this rack, but were distributed to several locations around the test article to facilitate cable routing [4].

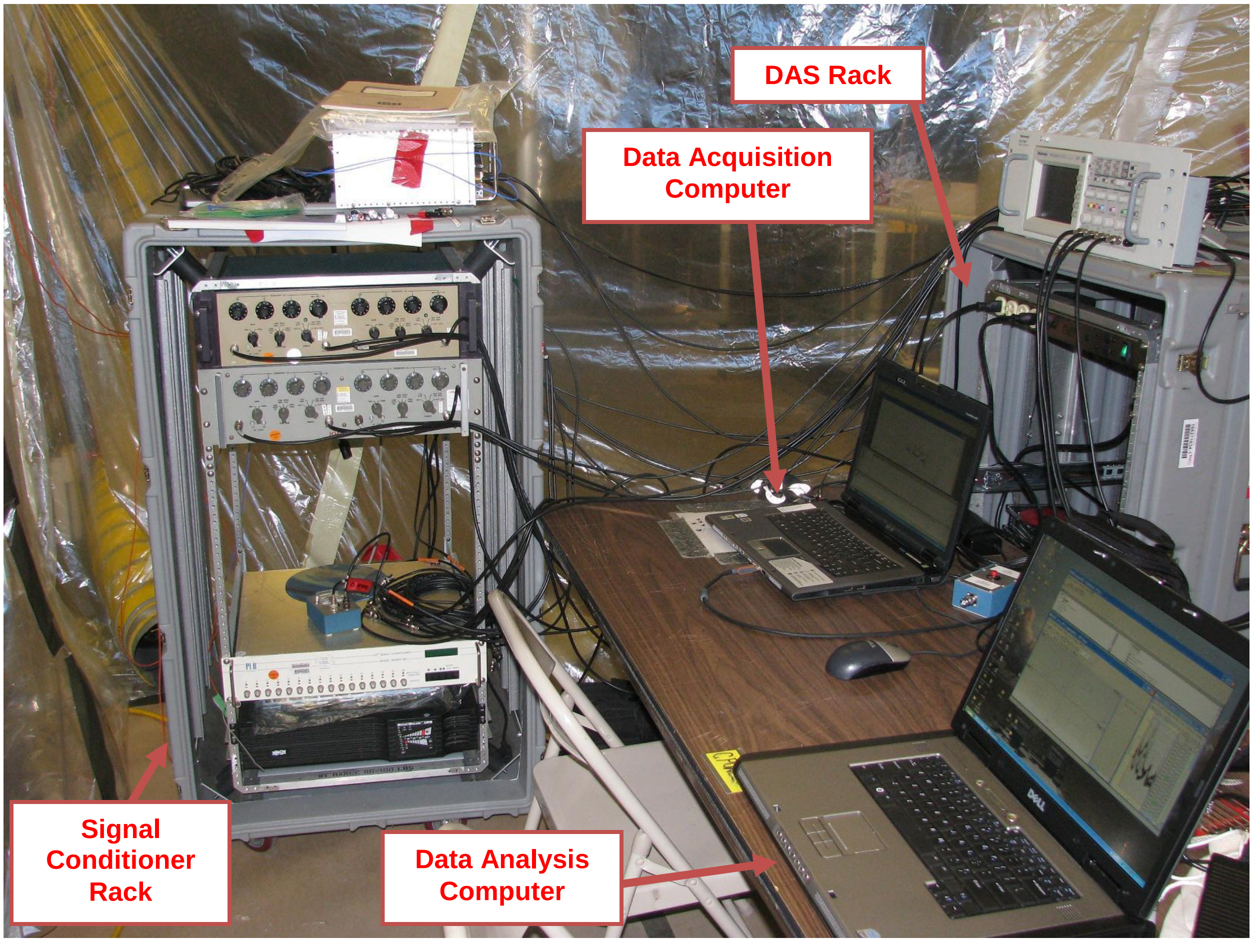

Figure 17. Signal conditioner and filter rack.

4.0 Test Operation and Data Analysis

4.1 Summary of Tests

The modal test was performed by applying a measured excitation force to the test article and measuring the acceleration response at selected locations. The FRFs were calculated as the ratio of the acceleration response to the input force. Modal parameters (natural frequencies, damping factors, and mode shapes) were then estimated from the FRFs. Both the measured FRF data and modal parameter estimates were compared with the pre-test predictions to ensure that sufficient data was acquired to capture the target modes of interest. The primary datasets for modal parameter estimation were FRFs for multi-input random excitation at several force levels. Due to difficulties in exciting the 1st bending mode pair, a manual excitation with free decay data was used. Sine sweeps using a single shaker were used to check for linearity of selected modes with respect to force level. In addition, impact testing was used to evaluate local response near the flight control sensors.

Selection of the resolution for the ambient noise and random datasets was a function of both the desired data quality and the limited test time available [5]. The data was sampled at 16 Hz with a block size of 512 seconds (8.5 minutes) to achieve the desired resolution of 0.0019 Hz. Based on experience with the partial stack tests, 12 blocks were found to provide adequate data quality. This resulted in a 1 hour and 42 minute acquisition period. The data was processed with a Hanning window and 50% overlap resulting in 23 averages.

A summary of all tests conducted on the Ares I-X FTV is given in Table 5. Additional notes are provided in Appendix D. All dataset numbers prefixed by the letter "P" are pretest datasets that were taken during the test setup and prior to the scheduled test days. Data prior to FTV-P7 were only taken for setup and shaker checkout purposes and was not intended to provide quality data. As indicated in the table, two ambient noise datasets were taken prior to the first test day, which means that the vehicle may not have been clear of all personnel. However, analysis of the data has shown that the ambient noise data was sufficient to conduct Operating Deflection Shape analysis. This data gave a rough approximation of the frequencies and shapes of the vehicle.

Four datasets with the FTV excited by random inputs were also taken at various force levels. For the first random dataset (FTV-P9), although it was taken during a pretest day, the vehicle was clear of all personnel because it was acquired during a break in work; however, there was not enough time to acquire more than 7 blocks. For the test day random datasets, 12 blocks were acquired, and the data was processed with a 50% overlap for 23 averages. The final random dataset was initially set up to acquire 20 blocks, but the data did not appear to be changing significantly enough to justify acquiring more than 12 blocks. The random datasets used all four shakers to excite the vehicle with the exception of FTV-11, where an equipment problem with a low pass filter only allowed three shakers to be used. The random datasets contained enough information to identify frequencies, damping, and mode shapes of the 2nd through 4th bending mode pairs. The quality of the data for the 1st bending modes was questionable, which will be discussed in detail later in this report. This led to the use of manual excitation and free decay response test for the 1st bending mode pair.

The first set of sine sweeps corresponding to FTV-3 and 4 revealed that the excitation was difficult to control for the 2nd bending modes. Specifically, the excitation force went unstable soon after sweeping through the peak frequency. A workaround was used for the subsequent sine sweep datasets where the sweep was stopped soon after sweeping through the peak frequency. Therefore, data sets for FTV-5 through FTV-7 are recommended for any sine sweep data analysis efforts. This shaker instability was not a problem for the 3rd bending modes, where a single sweep could be used to excite both modes. A 50, 100, and 200 lb-pk sine sweep from a single shaker was used to excite each of the 2nd and 3rd bending modes. This data was sufficient to identify the natural frequencies of the 2nd and 3rd bending modes and study nonlinearities associated with these modes.

Difficulties in exciting the 1st bending mode pair with the shaker systems led to the use of manual excitation. The modes were excited by pushing the vehicle by hand at the resonant frequency, then allowing the motion to decay. This free-decay data was then used to estimate the frequency, damping and mode shape of the 1st bending mode pair. This test was performed three times for each mode to check repeatability.

In order to investigate local modes near the vehicle control system instrumentation, tap tests were performed at the Forward RRGU, FTINU, and Aft RRGU. The tap tests used a 3 lb hammer with a soft rubber tip in order to excite the surrounding structure with an impulse containing frequencies below 200 Hz. Multiple impulses were recorded and averaged to obtain FRFs for each location and direction. A second set of tap tests was performed approximately one month after the initial FTV modal test to further investigate these local modes with the control sensors operating. Data from these tests is listed with a "T" prefix.

Table 5. FTV Modal Test Summary

Test	Run	Type	Level	Direction(s)	Range	Resolution
FTV-P7	n/a	Ambient Noise	n/a	n/a	0 - 12.5 Hz	0.0019 Hz
FTV-P8	n/a	Tap Test	50-200 lb-pk	24Z, 24X, 25Z-, 25X-	0 - 100 Hz	0.125 Hz
FTV-P9	n/a	Random (7 block, 13 avg)	50 lb-rms	13Z-, 14Z-, 16Z-, 17Z-	0 - 12.5 Hz	0.0019 Hz
FTV-P10	n/a	Ambient Noise	n/a	n/a	0 - 12.5 Hz	0.0019 Hz
FTV-1	n/a	Random (12 block, 23 avg)	50 lb-rms	13Z-, 14Z-, 16Z-, 17Z-	0 - 12.5 Hz	0.0019 Hz
FTV-2	n/a	Random (12 block, 23 avg)	130 lb-rms	13Z-, 14Z-, 16Z-, 17Z-	0 - 12.5 Hz	0.0019 Hz
FTV-3	1	Sine Sweep (0.01 Oct/min)	50 lb-pk	17Z-	1.01 - 1.26 Hz	n/a
	2		100 lb-pk			
	3	Open Loop Sine Sweep (0.01 Oct/min)	100 lb-pk			
FTV-4	n/a	Sine Sweep (0.01 Oct/min)	50 lb-pk	17Z-	1.01 - 1.26 Hz	n/a
FTV-5	1	Sine Sweep (0.01 Oct/min)	50 lb-pk	17Z-	1.00 - 1.07 Hz	n/a
	2		100 lb-pk			
	3		200 lb-pk			
FTV-6	1	Sine Sweep (0.01 Oct/min)	50 lb-pk	17Z-	1.14 - 1.26 Hz	n/a
	2		100 lb-pk			
	3		200 lb-pk			
FTV-7	1	Sine Sweep (0.01 Oct/min)	50 lb-pk	13Z-	3.29 - 3.88 Hz	n/a
	2		100 lb-pk			
	3		200 lb-pk			
FTV-8	n/a	Free Decay Test, 1st Bending Modes	n/a	Y, Z	n/a	n/a
FTV-9	n/a	Free Decay Test, 2nd Bending Mode	n/a	Y	n/a	n/a
FTV-10	n/a	Tap Test	50-200 lb-pk	24Z, 24X, 25Z-, 25X	0 - 200 Hz	0.125 Hz
FTV-11	n/a	Random (12 block, 23 avg)	200 lb-rms	13Z-, 14Z-, 17Z-	0 - 6.0 Hz	0.0019 Hz
FTV-12	n/a	Free Decay Test, 1st Bending Modes	n/a	Y, Z	n/a	n/a
FTV-13	n/a	Sine Dwell, 2nd Bending Mode	Unstable	Y	n/a	n/a
FTV-14	n/a	Tap Test	50-200 lb-pk	26X-, 26Y, Aft Skirt (5 Locations)	0 - 200 Hz	0.125 Hz
FTV-T1	n/a	Tap Test	250-500 lb-pk	24X, 24Z	0 - 200 Hz	0.125 Hz
FTV-T2	n/a	Tap Test	400-800 lb-pk	25X, 25Z-	0 - 200 Hz	0.125 Hz
FTV-T3	n/a	Tap Test	100-400 lb-pk	26X-, 26Y	0 - 200 Hz	0.125 Hz

4.2 Ambient Noise Measurements

Peak frequencies corresponding to the target modes were initially identified using the ambient noise data. A sample data set is shown in Figure 18 from FTV-P10, where the first 2000+ seconds were acquired while the High Bay 3 doors were open. This excited the vehicle to larger amplitudes than was normally achieved with the doors closed. The high bay was also in the process of being cleared, so the data are not likely to include any effects from personnel being inside the vehicle.

The resulting autospectra from the ambient noise test is shown in Figure 19. The peak frequencies associated with the target modes were easy to identify from the autospectra. These peak frequencies are listed in Table 6, and can be seen to correspond to the frequencies identified from the pre-test analysis. Operating deflection shapes were also found to be consistent with the pre-test mode shapes.

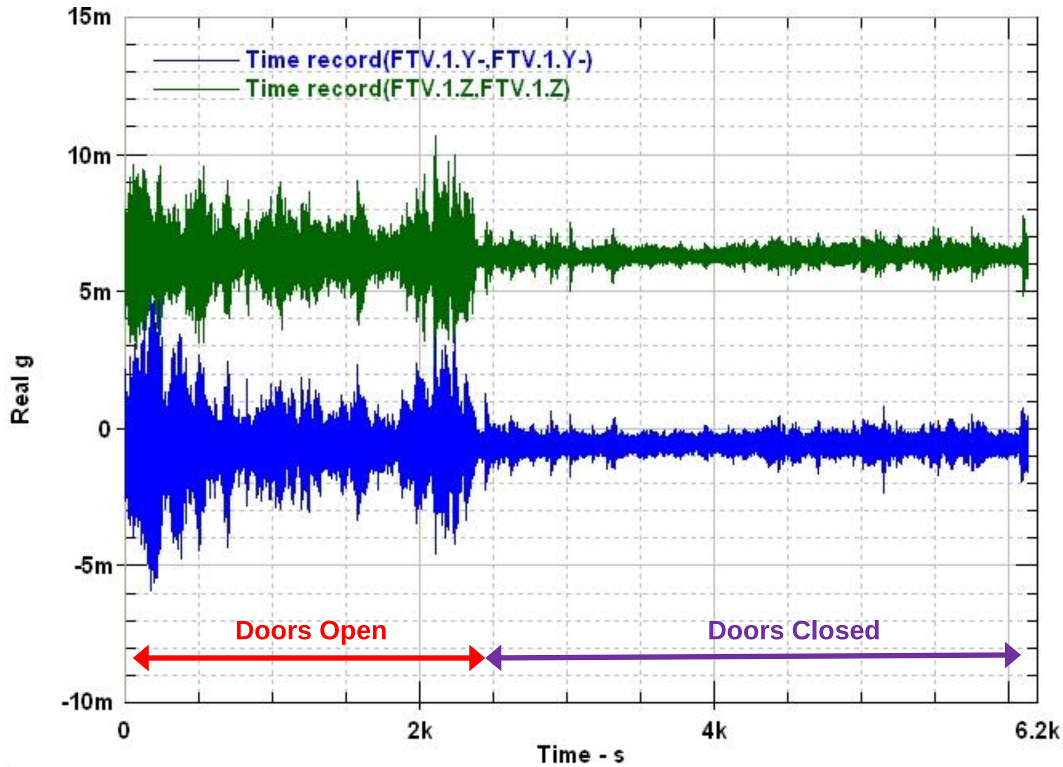

Figure 18. Time history from FTV-P10 ambient noise test.

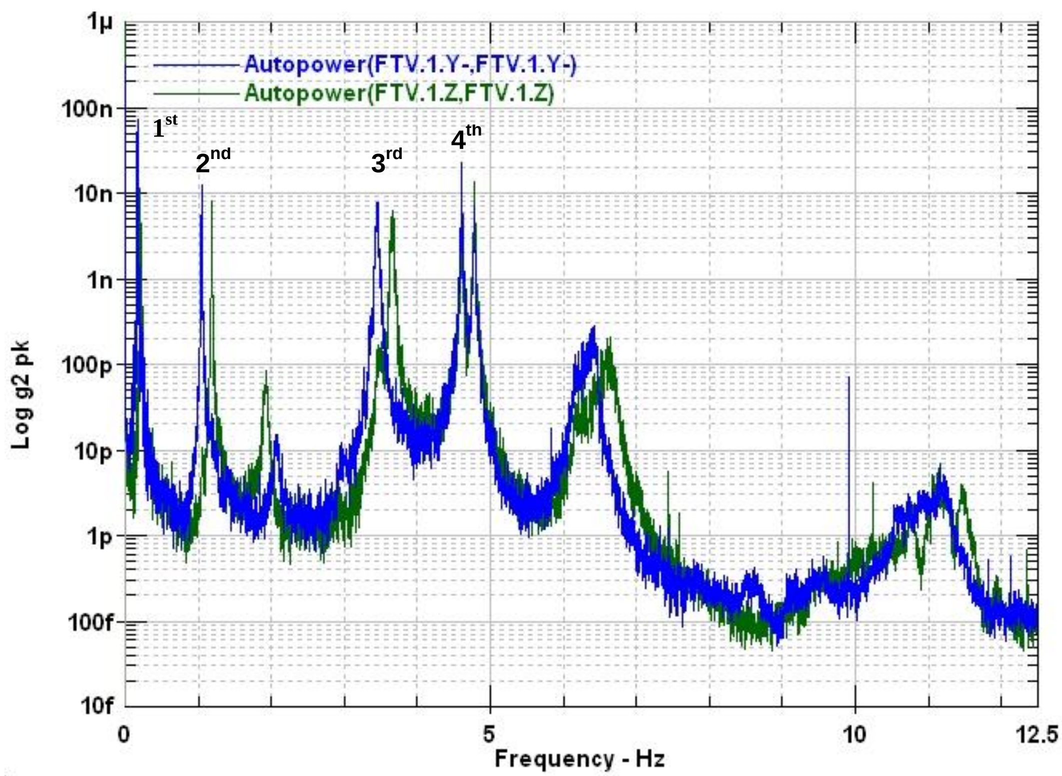

Figure 19. Autospectra from FTV-P10 ambient noise test with bending mode pairs labeled.

Table 6. Peak Frequencies Identified in Ambient Noise Test FTV-P10

Pre-Test Analysis Mode	Ambient (FTV-P10) Peak Frequency (Hz)	Pre-Test Analysis Frequency (Hz)
1st Bending Y	0.18	0.18
1st Bending Z	0.22	0.22
2nd Bending Y	1.05	1.02
2nd Bending Z	1.19	1.17
3rd Bending Y	3.45	3.25
3rd Bending Z	3.68	3.50
4th Bending Y	4.62	4.78
4th Bending Z	4.79	4.84

4.3 Random Excitation Tests

The random excitation data sets were the primary data for mode shape estimation and model calibration. In this section, the data quality from these tests is evaluated based on the FRF, coherence, reciprocity, and input force characteristics. Measurement linearity with force amplitude is also examined for the three random input test levels.

Figure 20 shows a typical FRF that was computed by the H_1 estimator during random excitation. The FRF shown relates the response at the top of the LAS structure to the excitations due to shaker E45 (location 13). After reviewing Figure 20, it should be clear that the data acquired for frequencies greater than 0.25 Hz was very clean with well defined peaks. Furthermore, the coherence in this frequency band is adequate, with only minor drops near the peak frequencies. However, for frequencies below 0.25 Hz, the coherence dropped significantly, as shown in Figure 21. This greatly affected the data for the 1st bending mode pair. Part of the problem is attributed to the exogenous high ambient excitation input relative to the shaker inputs in this low frequency range. Attempts to improve the low frequency coherence for the random datasets included increasing the force level, reducing the bandwidth of the excitation, using signal conditioners with a lower frequency response, and acquiring raw ICP signals from the load cells. None of these techniques was able to improve the quality of the random data below 0.25 Hz.

Because the data from the FTV-2 random test used four excitations, reciprocity can be assessed using Figures 22-27. All figures show that the Multi-Input Multi-Output (MIMO) tests have good reciprocity, particularly near the peak frequencies.

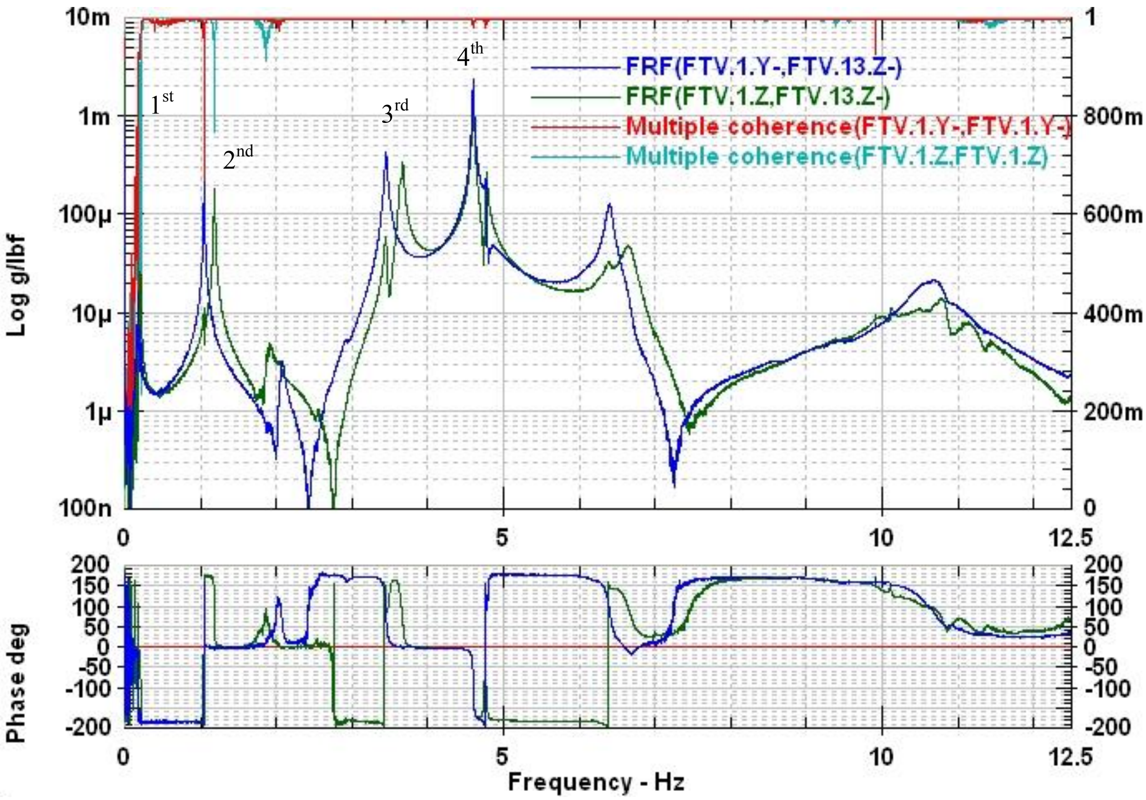

Figure 20. Shaker 13Z- reference FRFs from FTV-2 random test.

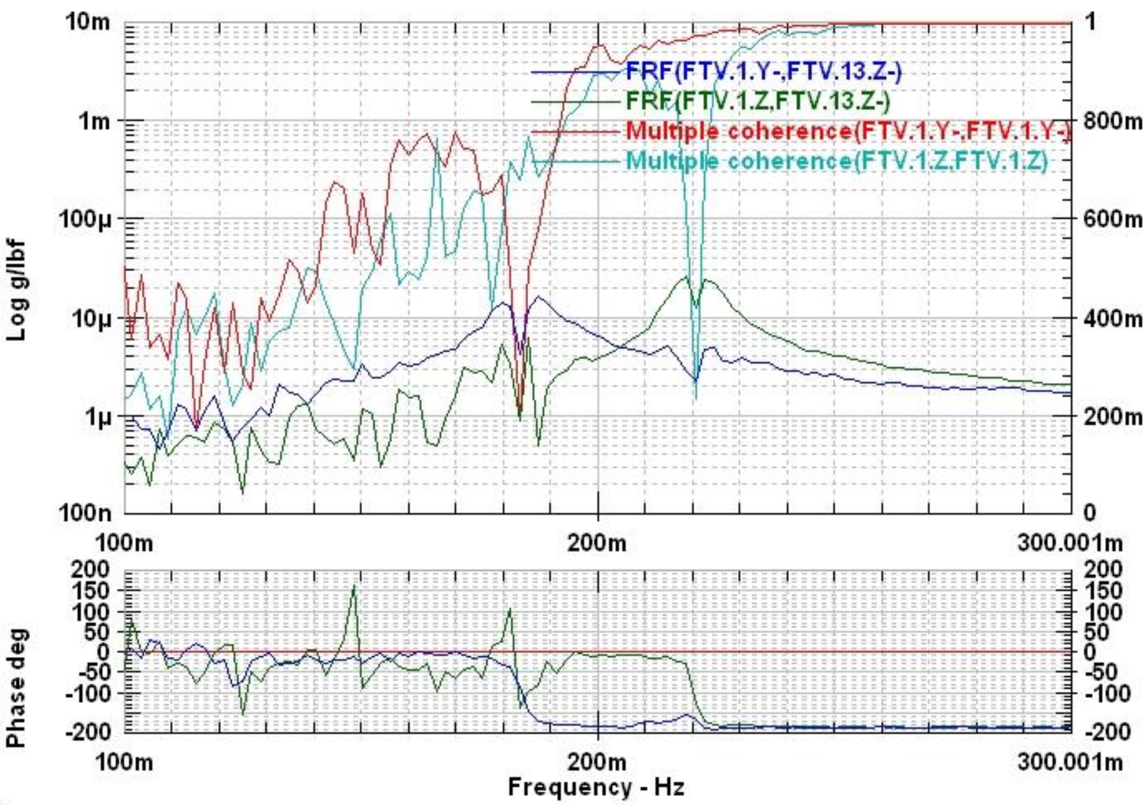

Figure 21. Shaker 13Z- low frequency for reference FRFs from FTV-2 random test.

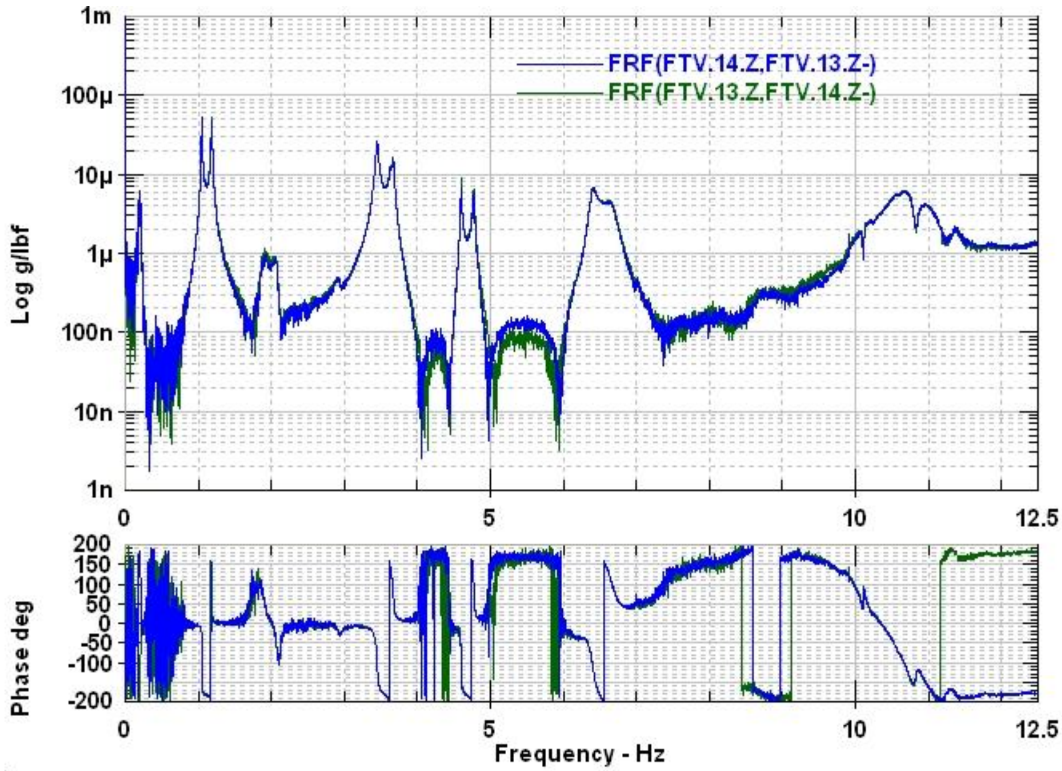

Figure 22. E-level shaker reciprocity from FTV-2 random test.

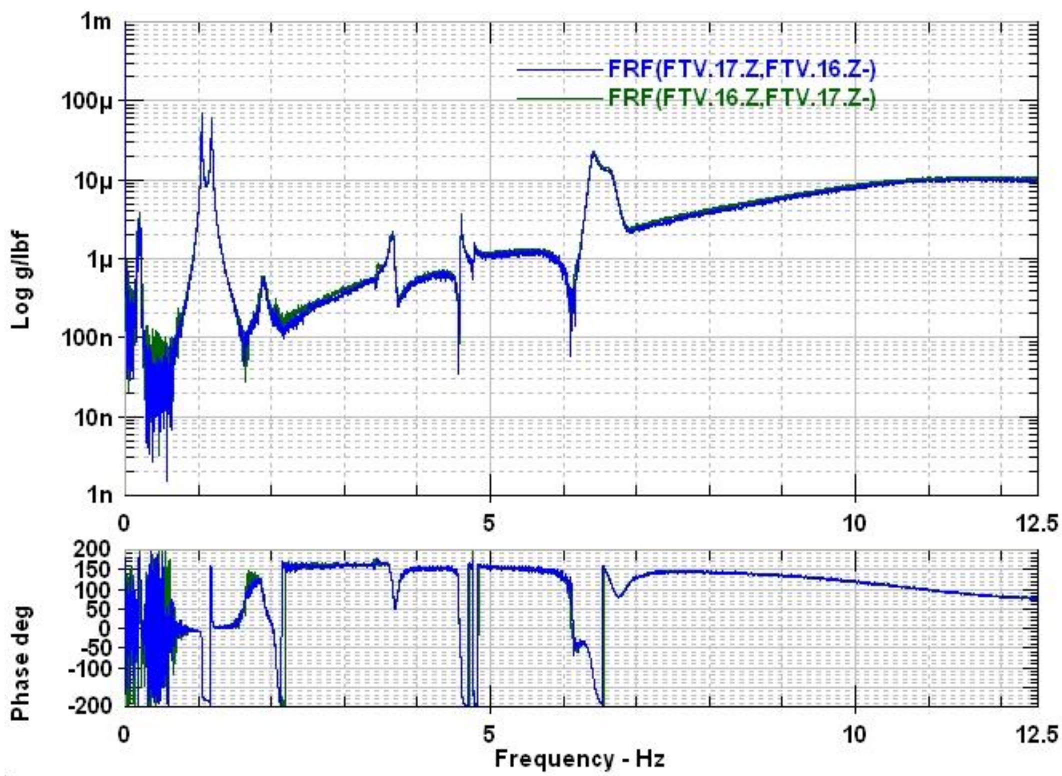

Figure 23. B-level shaker reciprocity from FTV-2 random test.

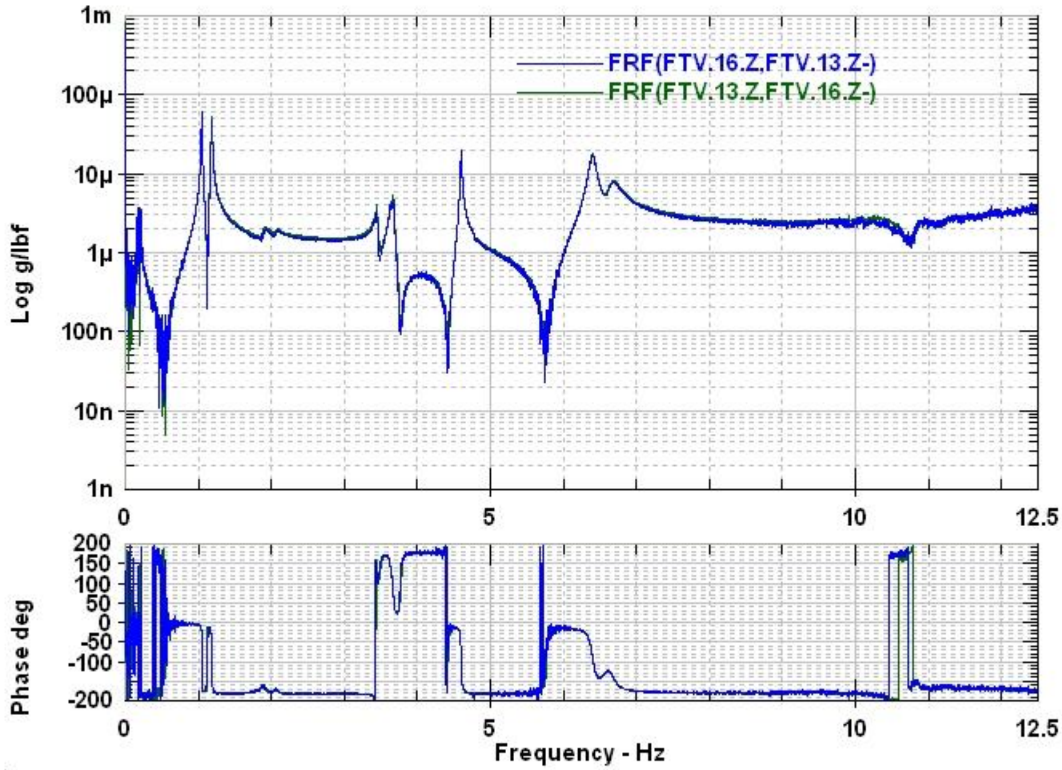

Figure 24. 45° shaker reciprocity from FTV-2 random test.

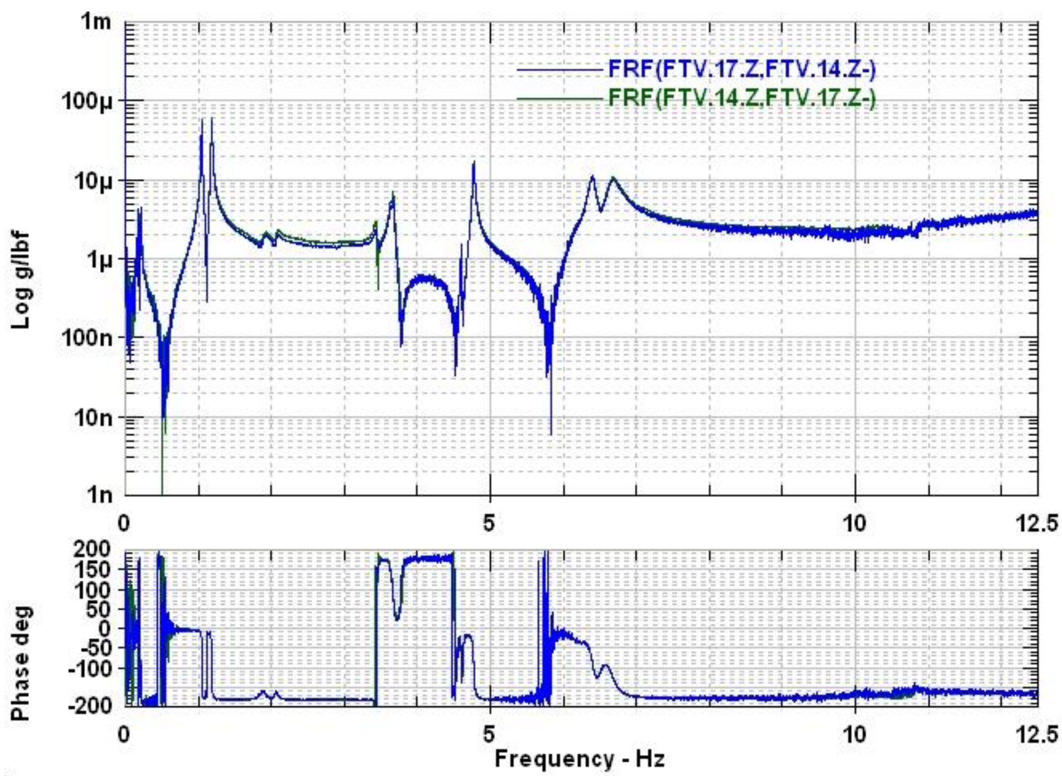

Figure 25. 135° shaker reciprocity from FTV-2 random test

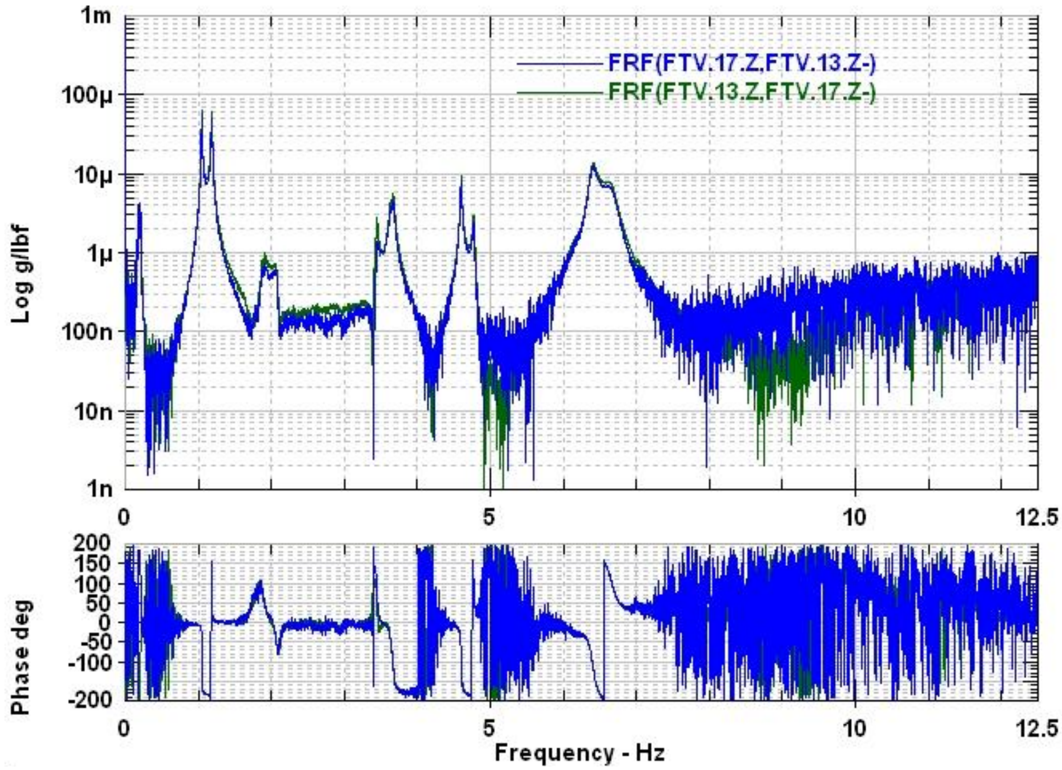

Figure 26. E45/B135 shaker reciprocity from FTV-2 random test

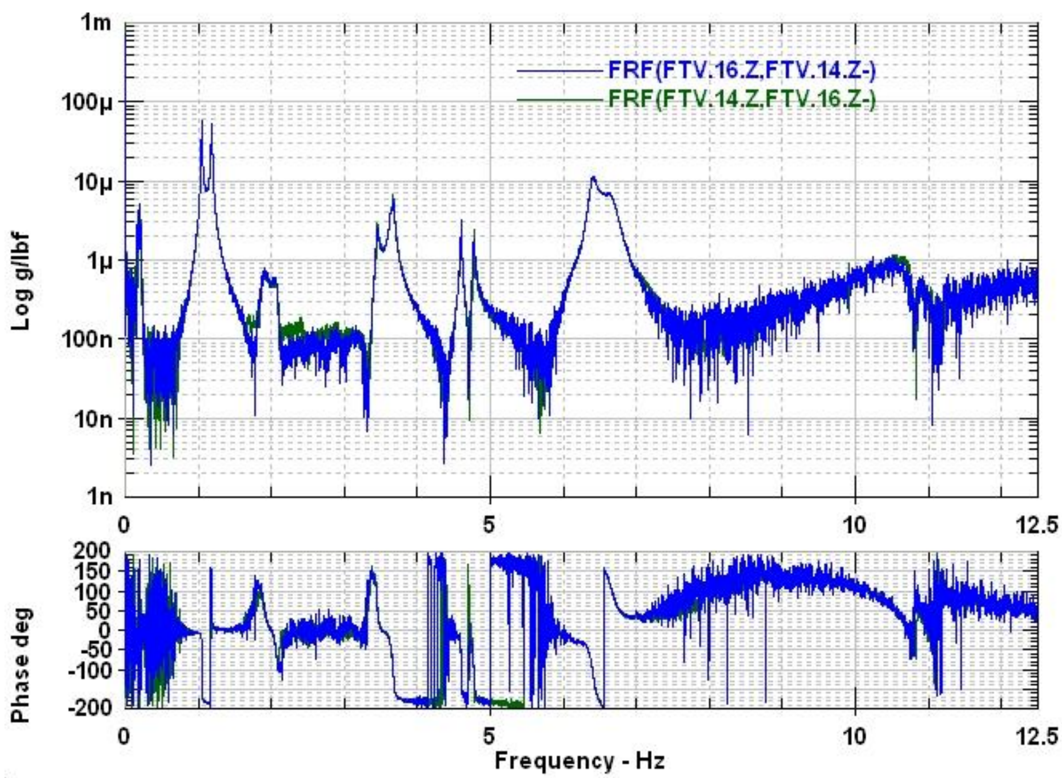

Figure 27. E135/B45 reciprocity from FTV-2 random test

The average autopower of the excitations for the 130-lbs force level is shown in Figure 28 with several peaks in the ranges of 0.25 to 0.30 Hz, 1.10 to 1.30 Hz, and 2.00 to 2.25 Hz. Although this is an indication of interaction between the vehicle and the shakers, force levels were relatively flat across the excitation bandwidth for frequencies greater than 2.25 Hz. Between peaks, there were some minor drops in the force level, with the most significant drops occurring below 0.25 Hz.

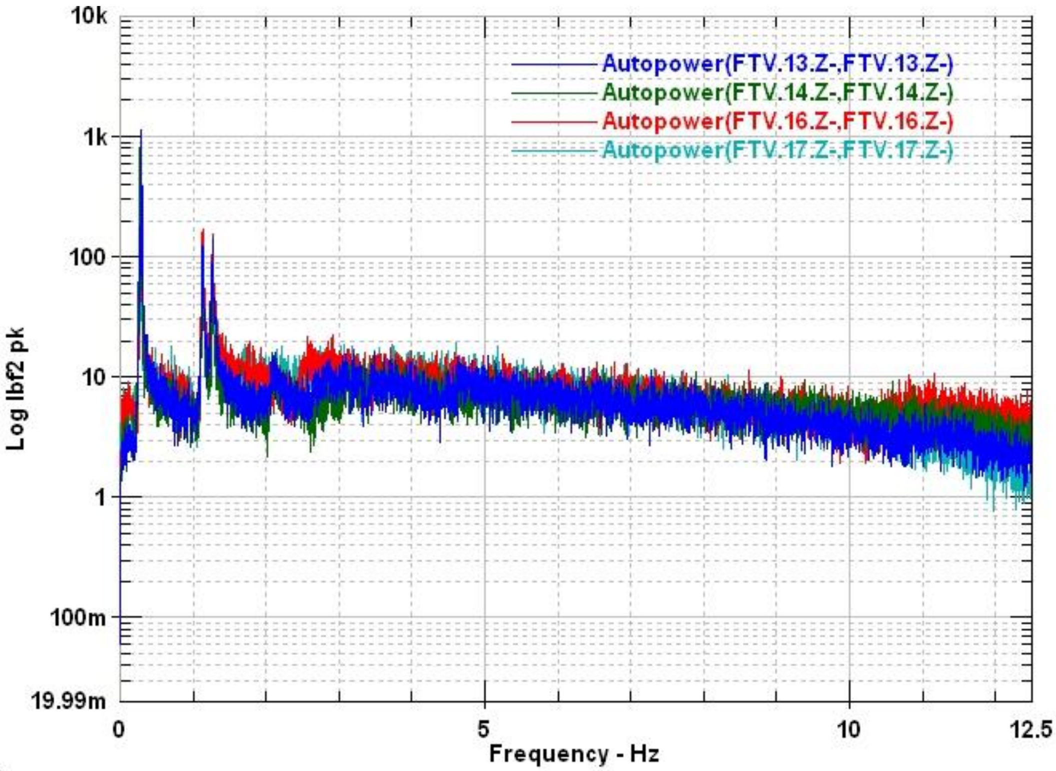

Figure 28. Excitation autopower from FTV-2 random test (12.5 Hz bandwidth)

The force principal auto power spectra for the FTV-2 random test are shown in Figure 29. The differences between the principal values indicate that there was correlation among the inputs in the vicinity of the first two bending mode pairs and near the peaks observed in the input autopower. An examination of the coherence between these inputs (Figure 30 and 31) shows that correlated inputs associated with first bending mode pair only showed up between shakers in the same directions, which could indicate coupling through the structure due to the shaker platforms being located relatively close to one another. A similar coupling could also explain the correlated inputs present near the 2nd bending mode pair. Correlation between the inputs occurred at the peaks in the autopower, which are still unexplained. Although these findings may suggest that the test setup could have been updated to improve the random data, schedule and platform access constraints did not allow for modifications in the shaker setup. Nonetheless, consistency of modal parameter estimates derived from the random data and other test methods demonstrates that the setup was sufficient. Details about the consistency of the modal parameters will be discussed later in this report.

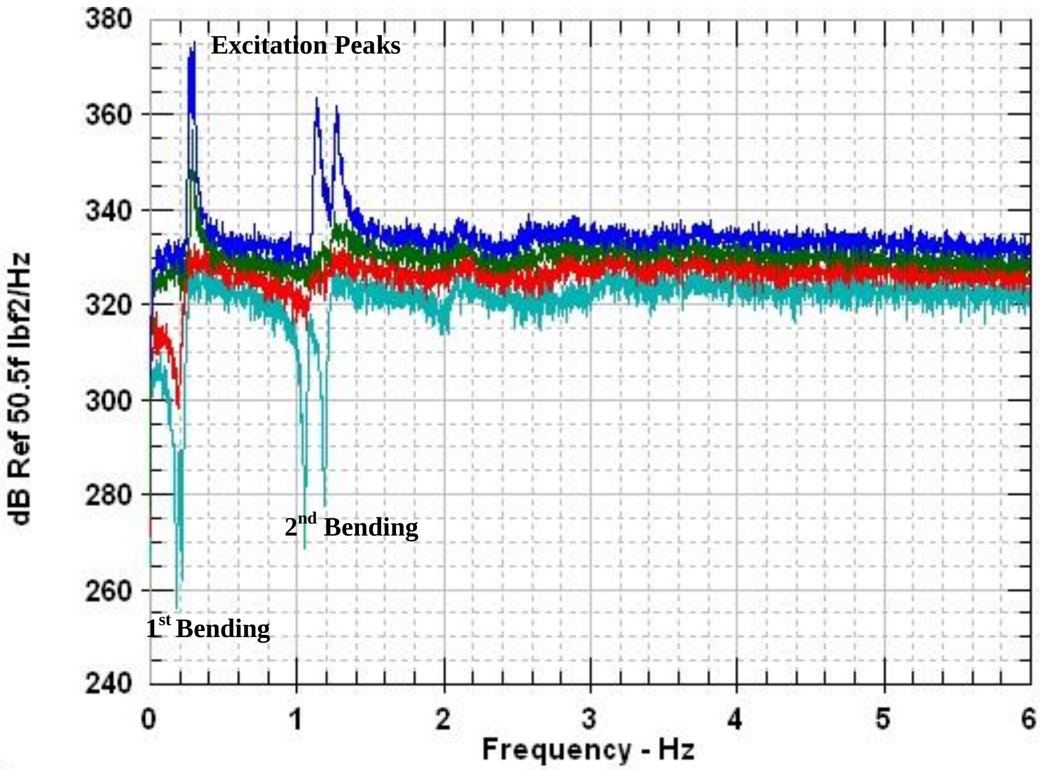

Figure 29. Principal input spectra from FTV-2 test

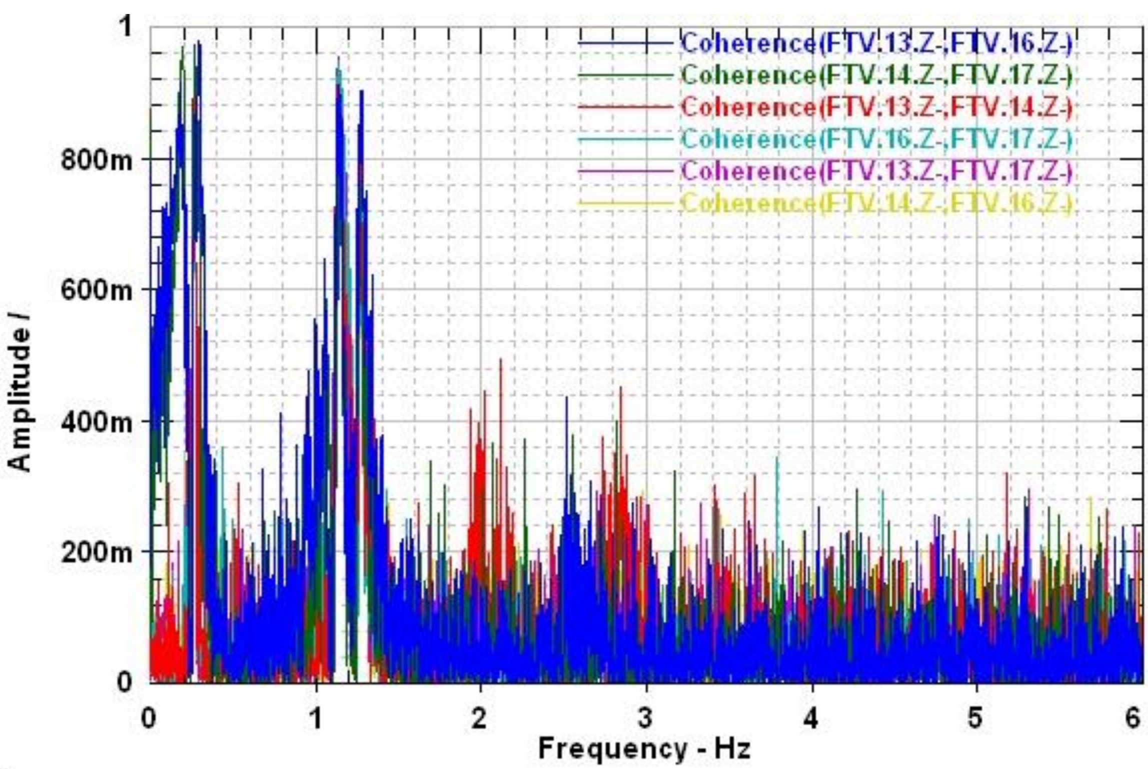

Figure 30. Coherence between input forces

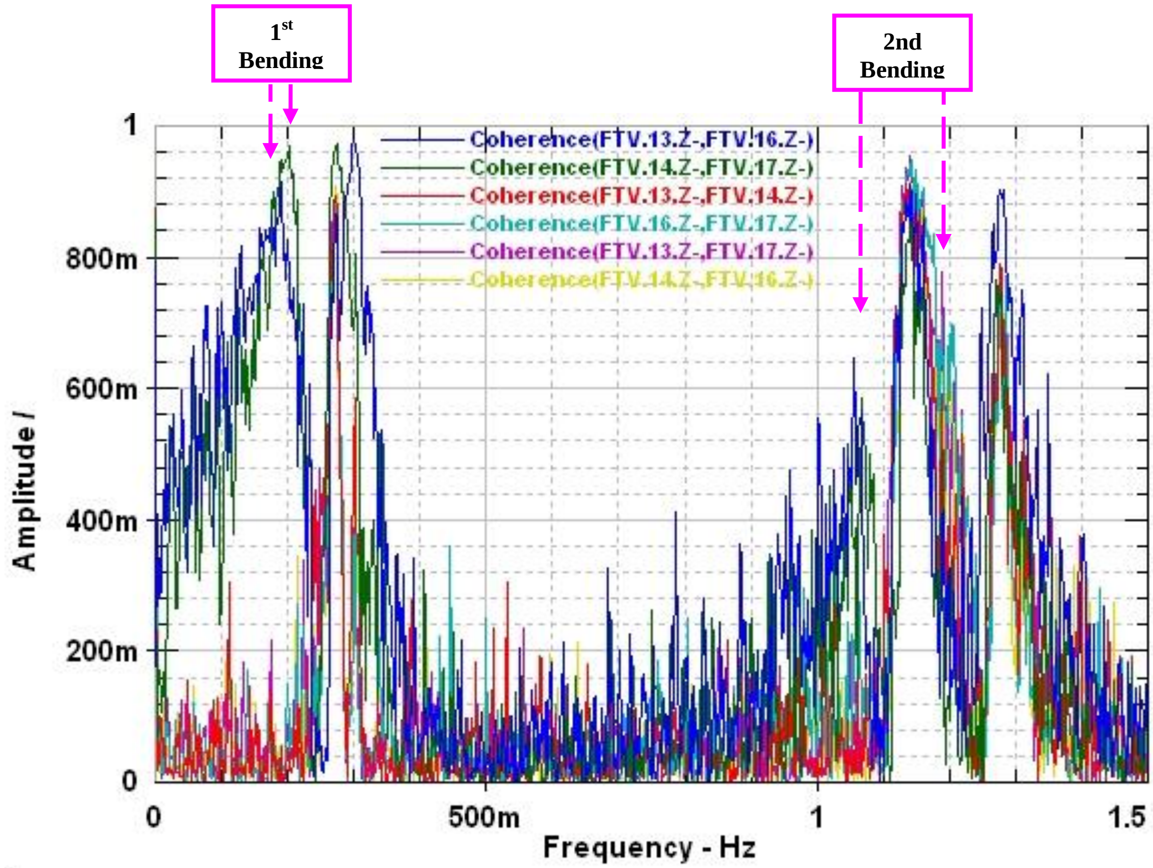

Figure 31. Low frequency view of coherence between input forces

The linearity of the vehicle is studied by comparing FRFs using three force level inputs, as shown in Figures 32 and 33. The Y-direction FRFs are practically identical for all three load cases, indicating that the vehicle was linear in that direction. Likewise, the Z-direction FRFs are also nearly on top of each other, with the exception of the mode near 2.0 Hz, which was not a target mode and involved lateral movement of the vehicle and MLP.

Variations in the resonant frequencies due to input load levels for the 2nd through 4th bending modes are shown in Table 7. Using only FRFs 1Y:-13Z and 1Z:-13Z from the random tests, the peak frequencies for several input levels are compared. Note that none of these modes varied by more than 0.82% in frequency. Because the damping value for these modes is low, the peak frequency is nearly identical to the natural frequency.

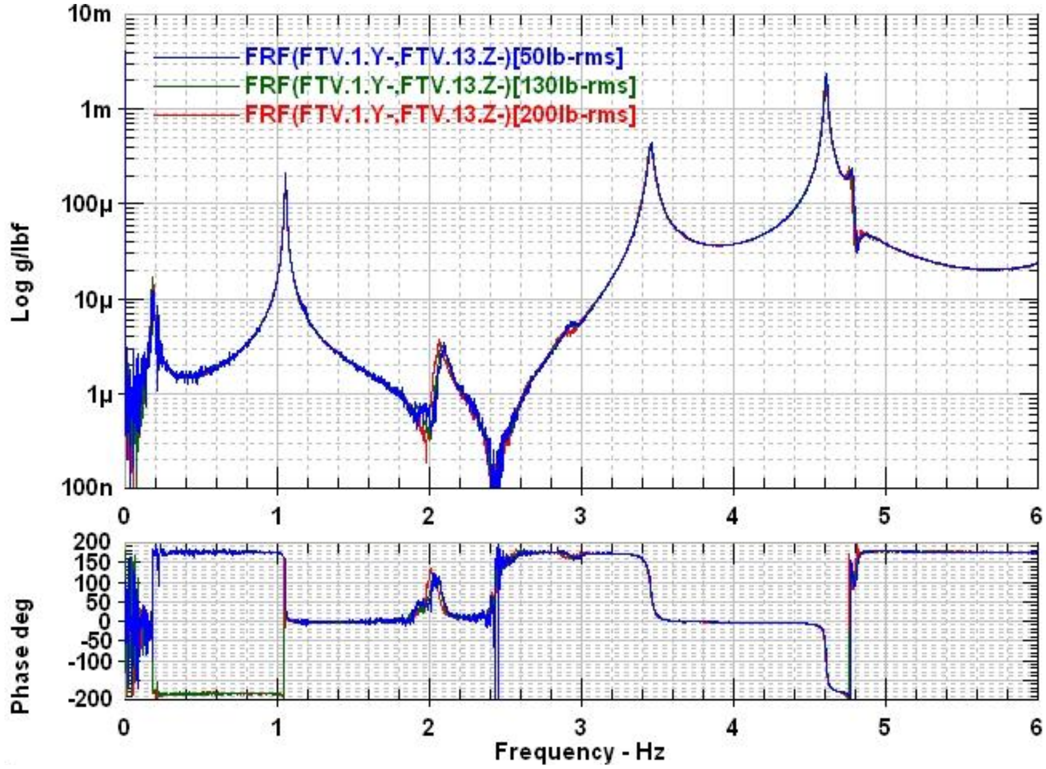

Figure 32. Y-direction random test linearity

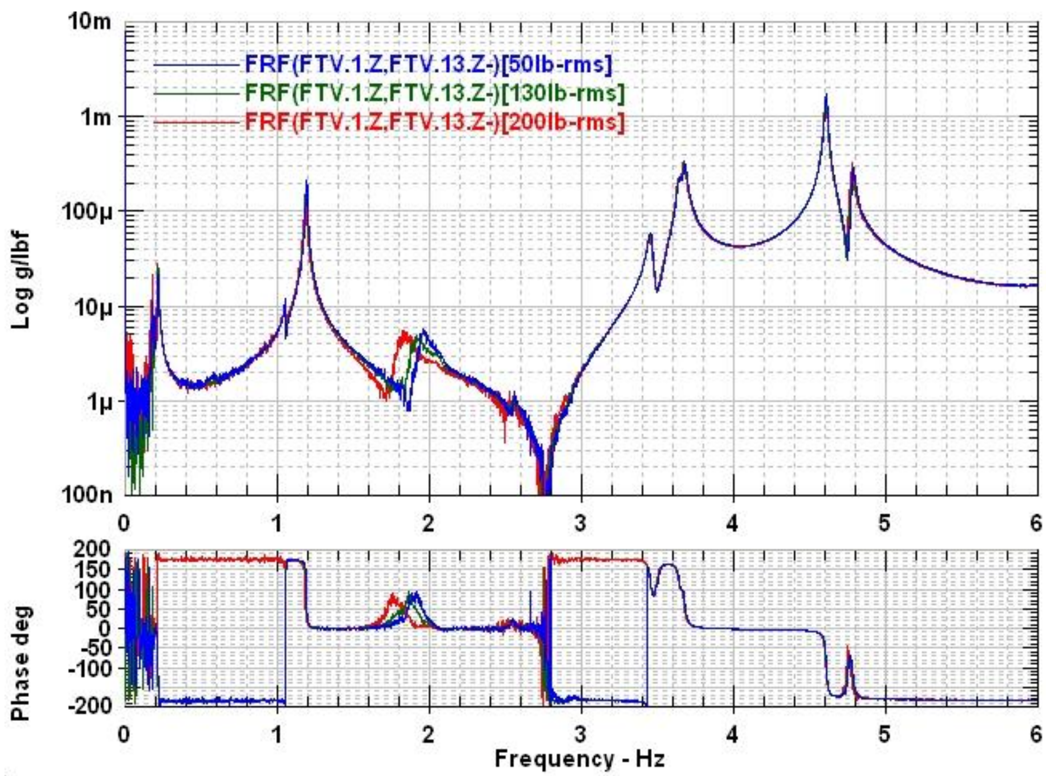

Figure 33. Z-direction random test linearity

Table 7. Peak Frequency Variation Due to Random Excitation

Mode	Random 50 lb-rms Peak Frequency (Hz)	Random 130 lb-rms Peak Frequency (Hz)	Random 200 lb-rms Peak Frequency (Hz)	50 vs. 200 lb-rms Percent Difference (%)
2Y	1.0605	1.0586	1.0586	-0.18
2Z	1.1953	1.1953	1.1855	-0.82
3Y	3.4649	3.4590	3.4531	-0.34
3Z	3.6856	3.6816	3.6738	-0.32
4Y	4.6133	4.6113	4.6074	-0.13
4Z	4.7910	4.7832	4.7832	-0.16

4.4 Free Decay Tests

As illustrated in Figure 21, the random excitation techniques did not provide quality data for estimating the modal parameters for the 1st bending mode pair. There was also concern with the 1st mode frequency and damping at high amplitudes. In order to determine the frequency and damping of the 1st bending modes at high amplitude levels, the modes were excited by hand at the resonant frequency, then allowing the motion to decay. Figure 34 shows the manual excitation of the vehicle in the Y-direction from the E-roof platform. Because the shakers were detached, they did not have an influence on the damping of the vehicle, which allowed a logarithmic decrement approach to be used to compute the damping associated with the 1st bending modes directly from the time history data. A time history of the acceleration at the tip of the LAS during one of these tests is shown in Figure 35. The data in the figure is low pass filtered with a Bessel filter at 1.0 Hz in order to reduce the influence of higher frequency modes on the peak amplitudes. The red lines in the figure indicate the beginning and end of the data used in the logarithmic decrement damping estimate and for calculation of the damped natural frequency. As was the case with the peak frequency, the damped natural frequency is assumed equal to the natural frequency of the mode due to low damping.

Data for the logarithmic decrement damping estimate in terms of log of peak amplitude versus peak number is shown in Figure 36, where the slope is proportional to damping. Because the slope is linear with amplitude, one should expect the damping to be constant over the tested amplitude range. A similar trend can be seen for the Z-direction in Figures 37 and 38.

Figure 34. Manual excitation for 1st bending mode in Y-direction.

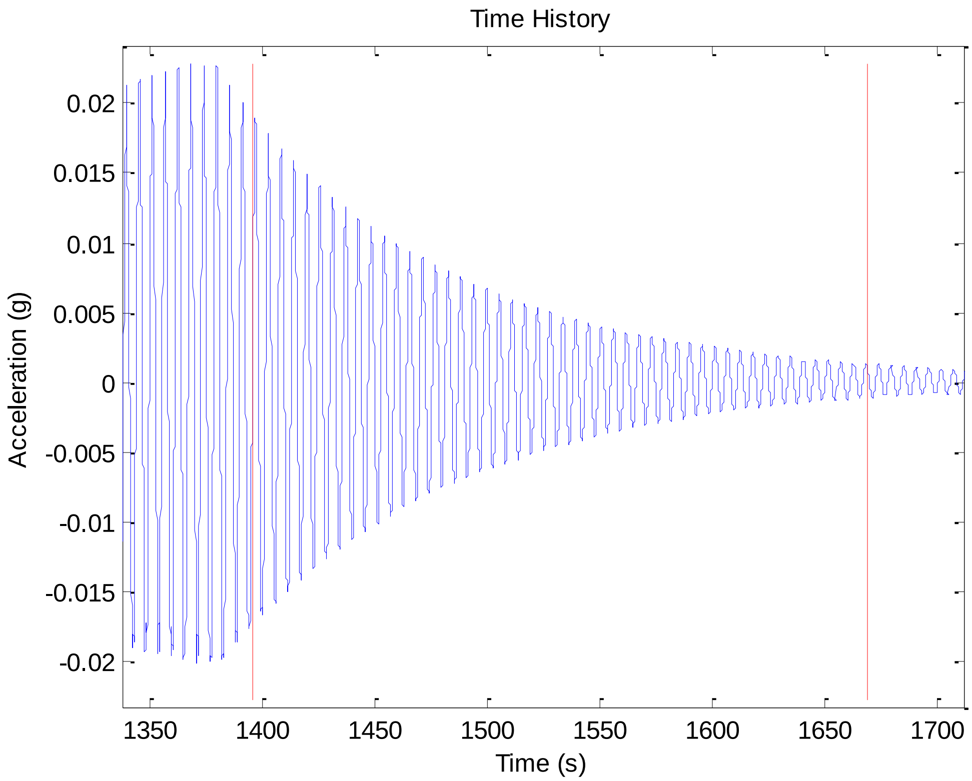

Figure 35. Third Y-direction free decay test time history (location 1Y)

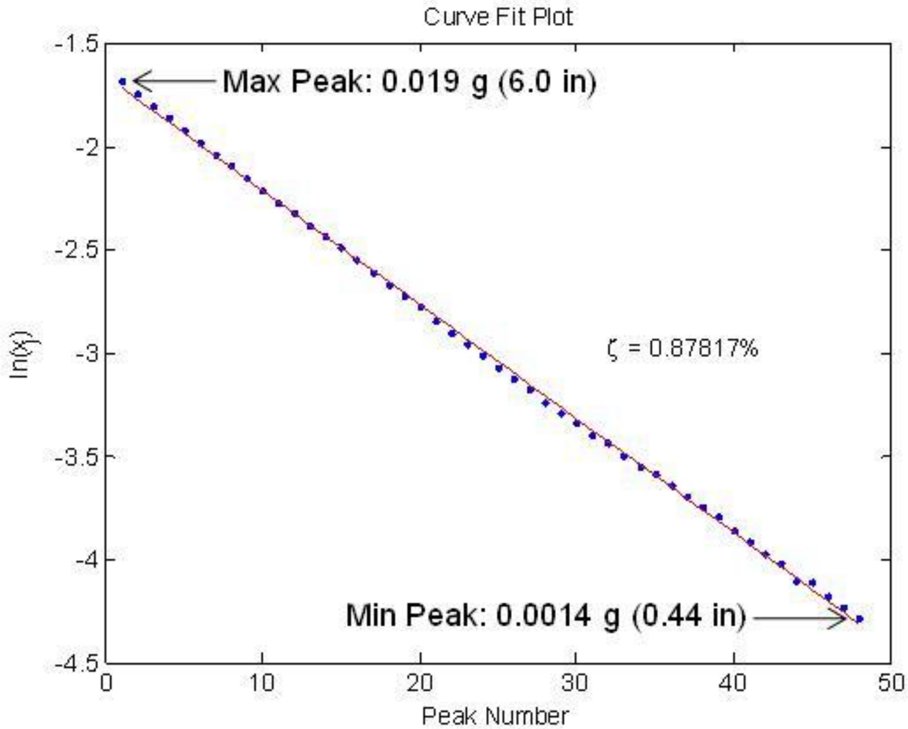

Figure 36. Fit of damping from third Y-direction free decay test (location 1Y)

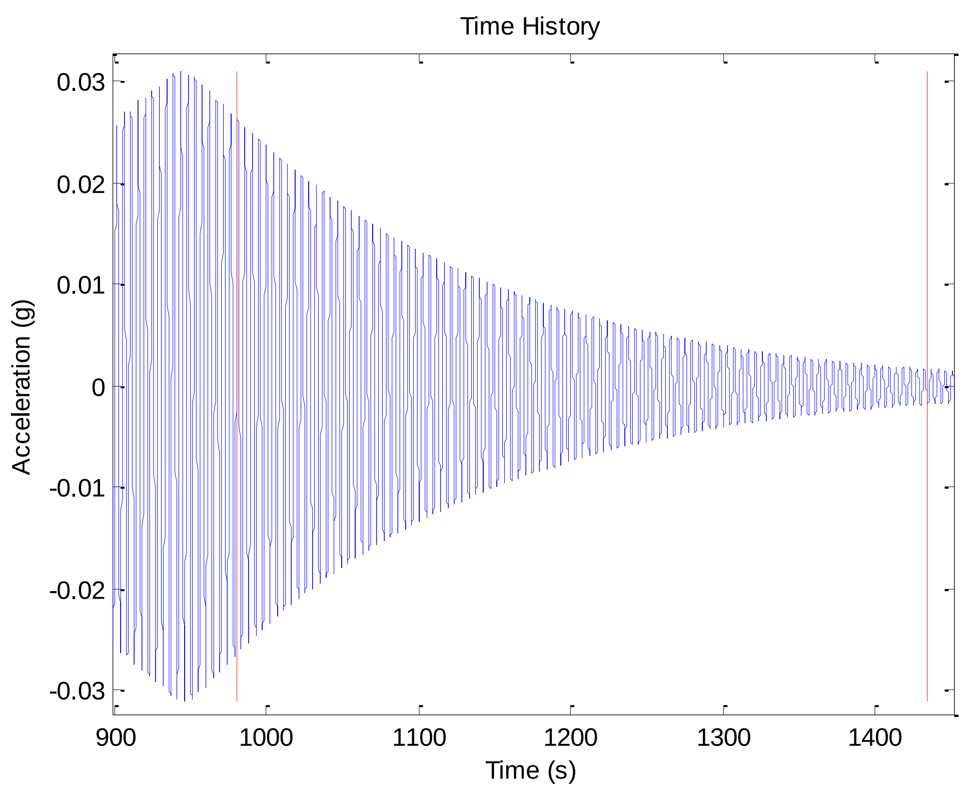

Figure 37. First Z-direction free decay test time history (location 1Z)

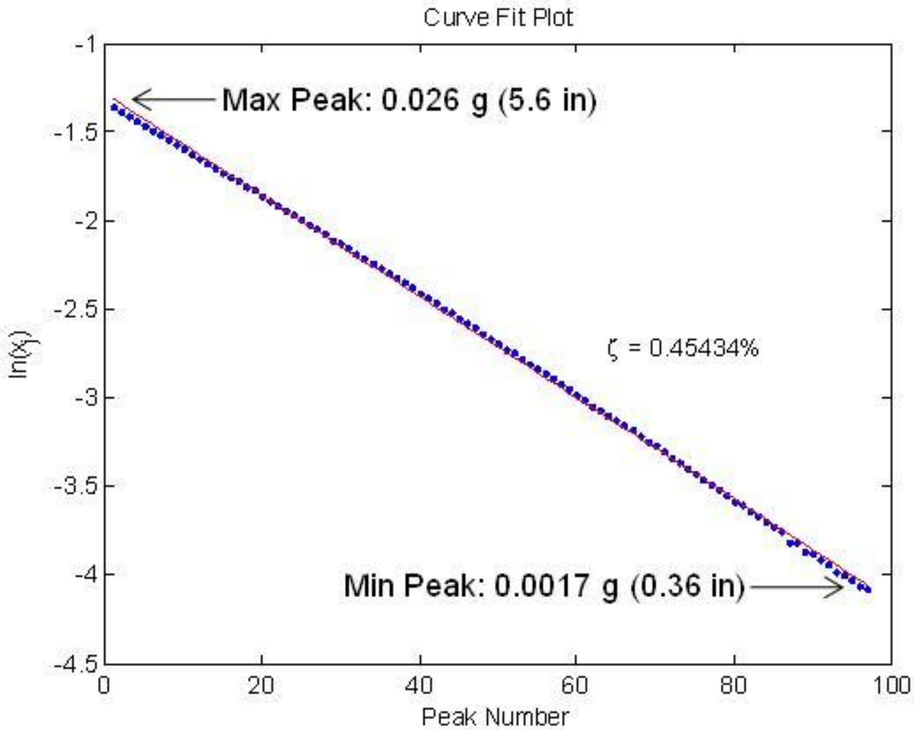

Figure 38. Fit of damping from first Z-direction free decay test (location 1Z)

A summary of the results from the logarithmic decrement damping estimates from all free decay tests is shown in Table 8. The amplitudes listed in the table were integrated by dividing the acceleration amplitudes by the square of the estimated frequency. This allowed the amplitude dependence of the damping to be studied for the first bending mode pair. Also shown in the table is a single estimate for the second bending mode in the Y-direction. This was estimated from dataset FTV-9, which was band-pass filtered with a Bessel filter from 0.7 to 1.3 Hz.

Table 8. Damping Estimates from All Free Decay Tests

Mode	Decay #	Maximum Unfiltered Amplitude During Push (in)	Maximum Unfiltered Amplitude at Start of Decay (in)	Maximum Fit Amplitude (in)	Free Decay Frequency (Hz)	Damping (%)
1Y	1	5.40	4.90	4.75	0.1776	0.81
1Y	2	7.80	7.80	6.78	0.1764	0.88
1Y	3	8.28	8.28	5.98	0.1764	0.88
1Z	1	6.85	6.85	5.55	0.2149	0.45
1Z	2	8.29	8.29	6.45	0.2142	0.43
1Z	3	7.82	7.82	6.97	0.2145	0.44
2Y	1	0.0908	0.0793	0.0392	1.0561	0.23

Note: Mode 1Y=1st Bending Y-direction; 1Z=1st Bending Z-direction; 2Y=2nd Bending Y-direction

4.5 Sine Sweep Tests

In order to test the linearity of the 2^{nd} through 3^{rd} bending modes due to input force levels, sine sweep tests were performed at 50, 100, and 200 lb-pk force levels at a sweep rate of 0.01 Oct/min. For the force controlled sine sweeps, the 0.01 Oct/min sweep rate was the slowest rate that could be selected in the software. This was an optimum sweep rate to reach steady state response for the 3^{rd} bending modes, but for the 2^{nd} bending modes, the optimum sweep rate was 0.003 Oct/min. Recall that the optimum logarithmic sweep rate through a resonance is less than $310(f_n)(\zeta_n)^2$ Oct/min [6], where f_n is the natural frequency (Hz) and ζ_n is the percent critical damping. Because these sweeps were not performed at the optimum rate for the 2^{nd} bending modes, certain processing approaches are not applicable to the data, although the FRF estimates are still valid.

The force controlled sine sweeps of the 2^{nd} bending mode pair went unstable after the excitation frequency passed through resonance. Figures 39 and 40 show a sample set of data depicting the instability. In this case, the 100 lb-pk force input increased to 190 lb-pk after passing the peak acceleration amplitude, then dropped to 60 lb-pk before the excitation was shut off at approximately 540 seconds.

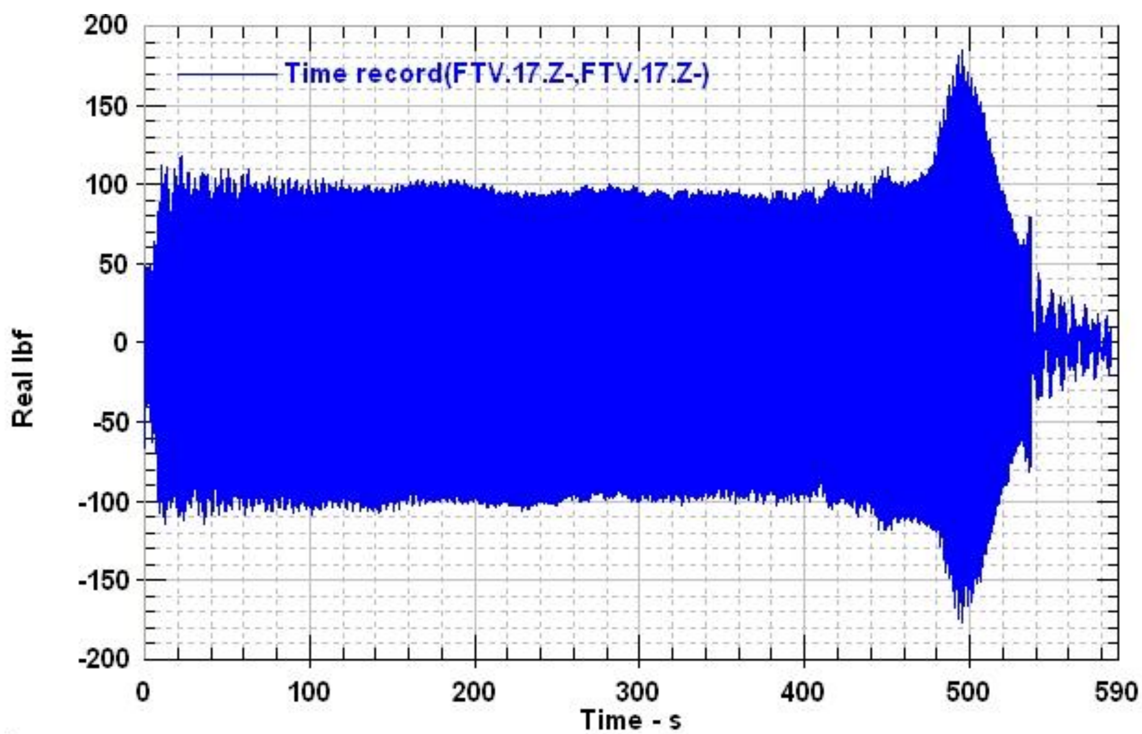

Figure 39. Force control instability for 100 lb-pk sine sweep of mode 2Y

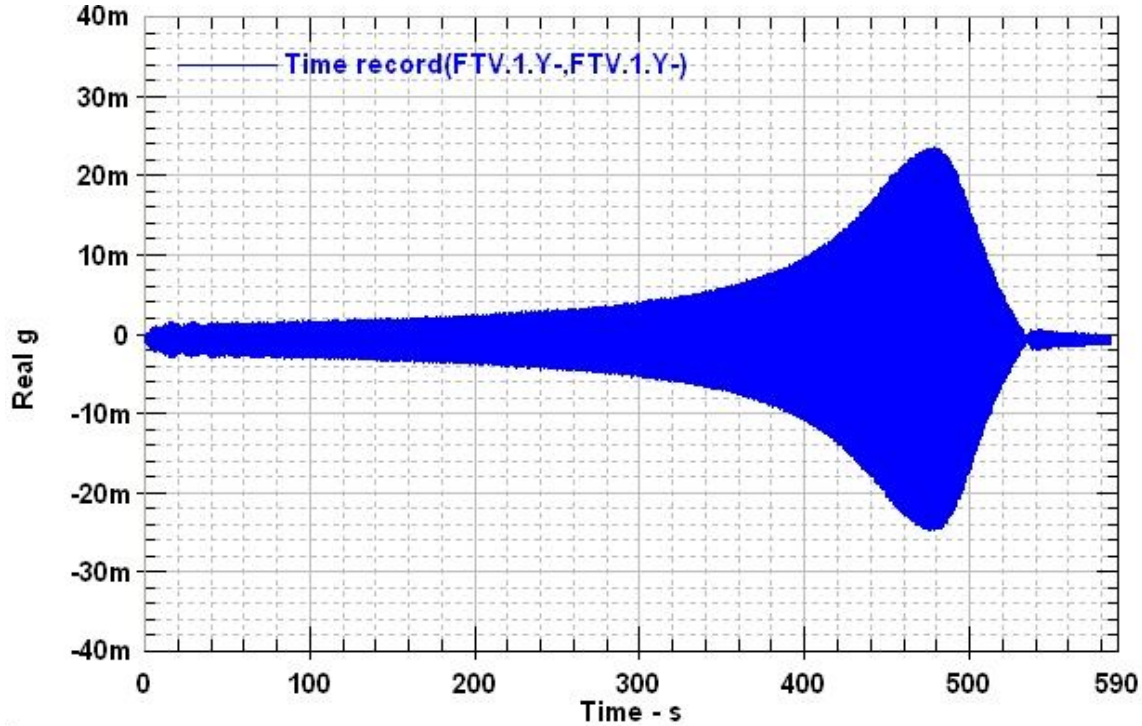

Figure 40. LAS Tip Acceleration for 100 lb-pk sine sweep of mode 2Y

Figures 41-44 show FRFs from sine sweep tests with three input force levels (FTV-5 through FTV-7) and the 200 lb-rms random test. To estimate the FRF data from sine sweeps, a single Discrete Fourier Transform (DFT) of the entire time history for each channel is used. Because a single DFT block was used to process the data, the FRFs could then be estimated by a simple ratio of the acceleration spectra divided by the force spectrum. For the sine sweeps of the 3rd bending modes, a Hanning window was applied to the block in order to reduce leakage while having a minimal effect on the damping estimates. This Hanning window technique could not be applied to the 2nd bending mode sine sweeps because it had too much effect on the damping estimates. The resulting FRF data from the sweeps show that the sine sweep excitation slightly changes the characteristics of the 2nd bending modes, but that the 3rd bending modes remain essentially unchanged.

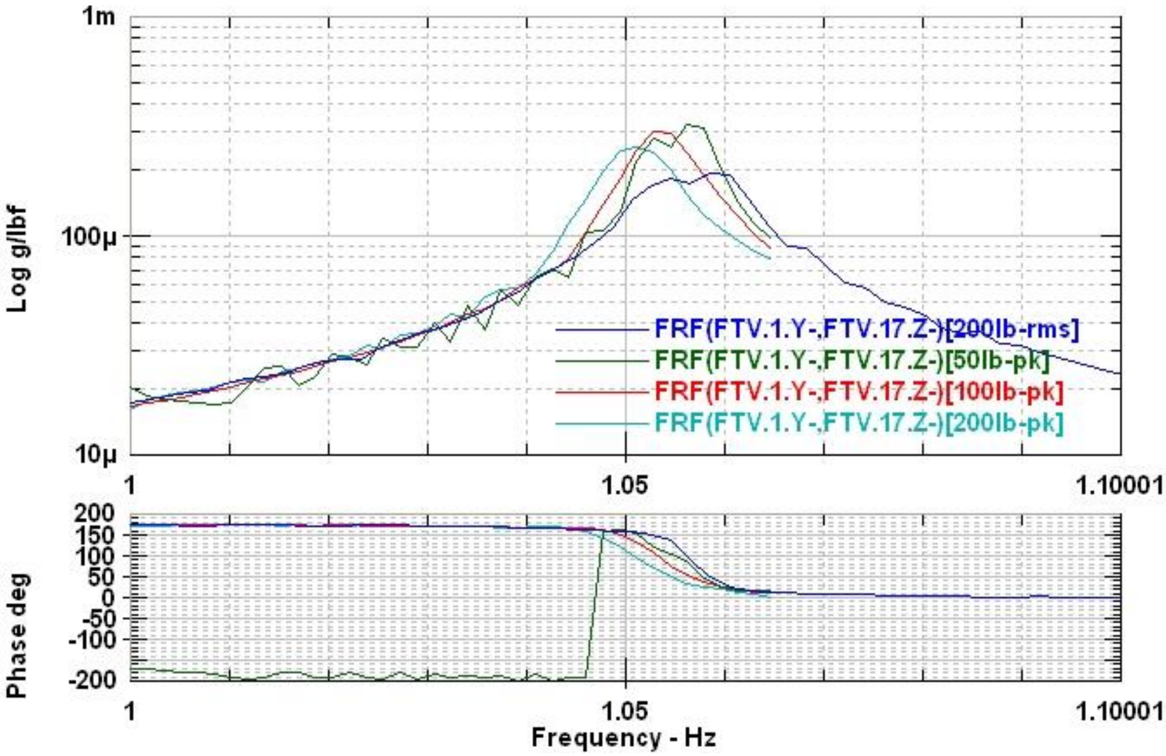

Figure 41. Nonlinearity in mode 2Y due to varying sine sweep levels

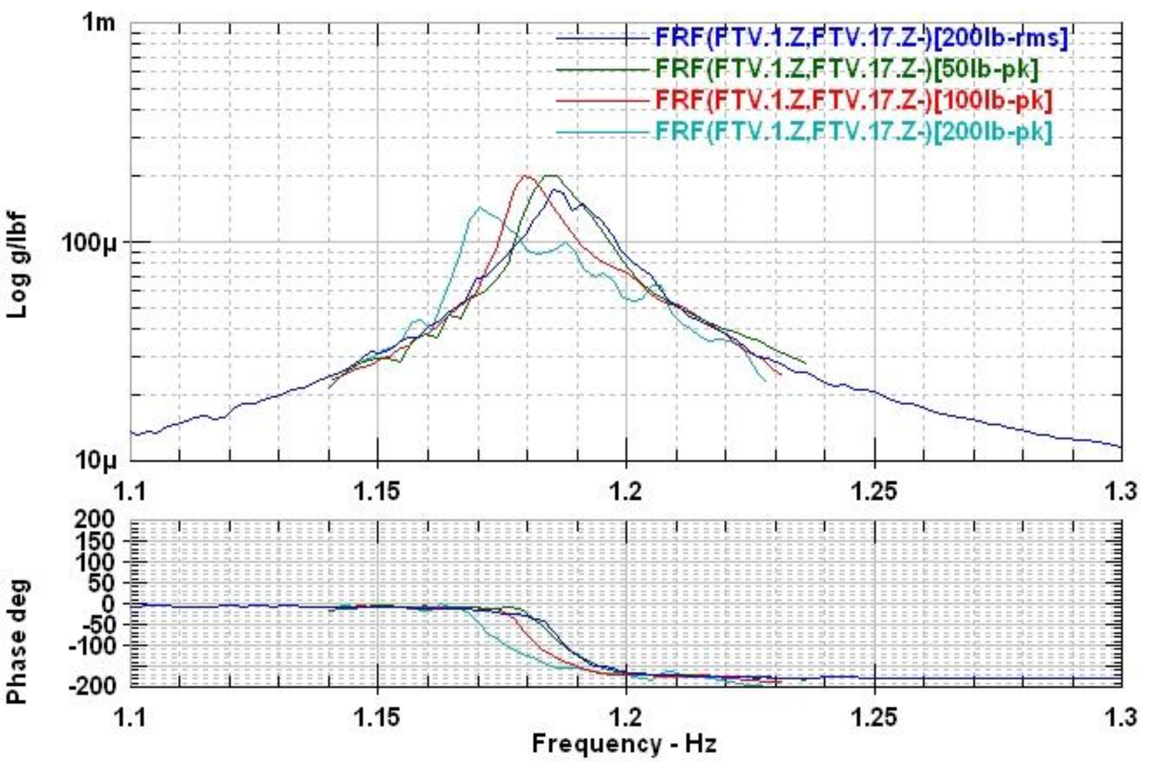

Figure 42. Nonlinearity in mode 2Z due to varying sine sweep levels

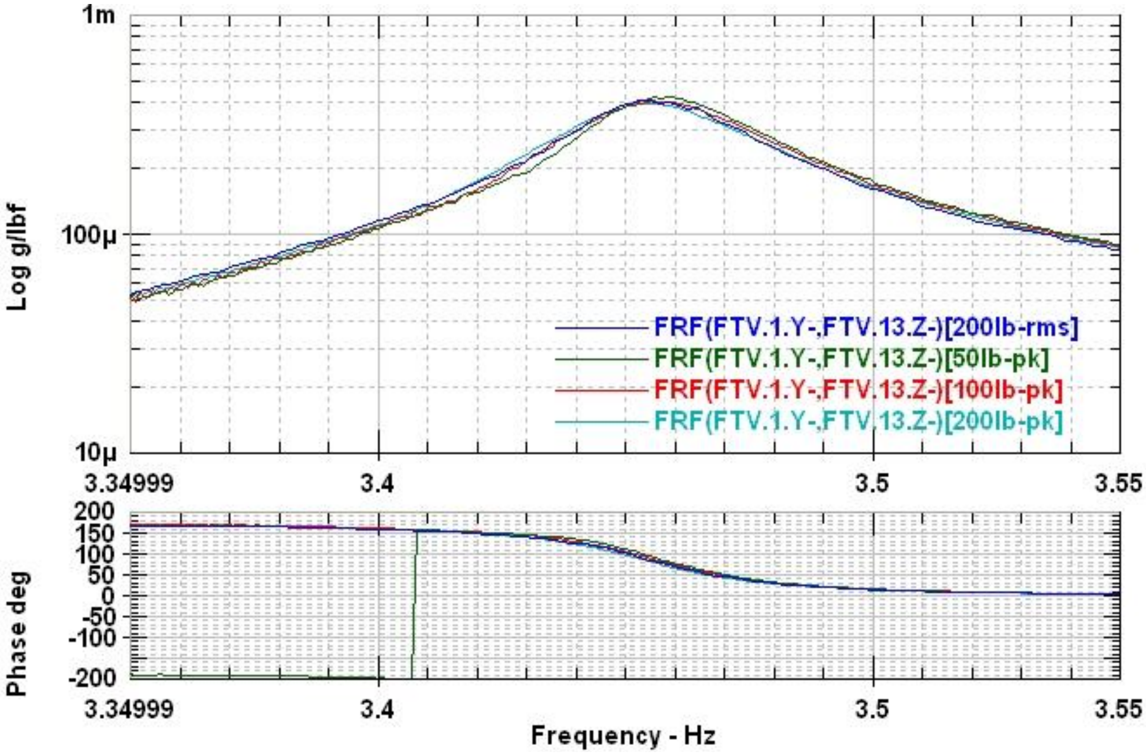

Figure 43. Nonlinearity in mode 3Y due to varying sine sweep levels

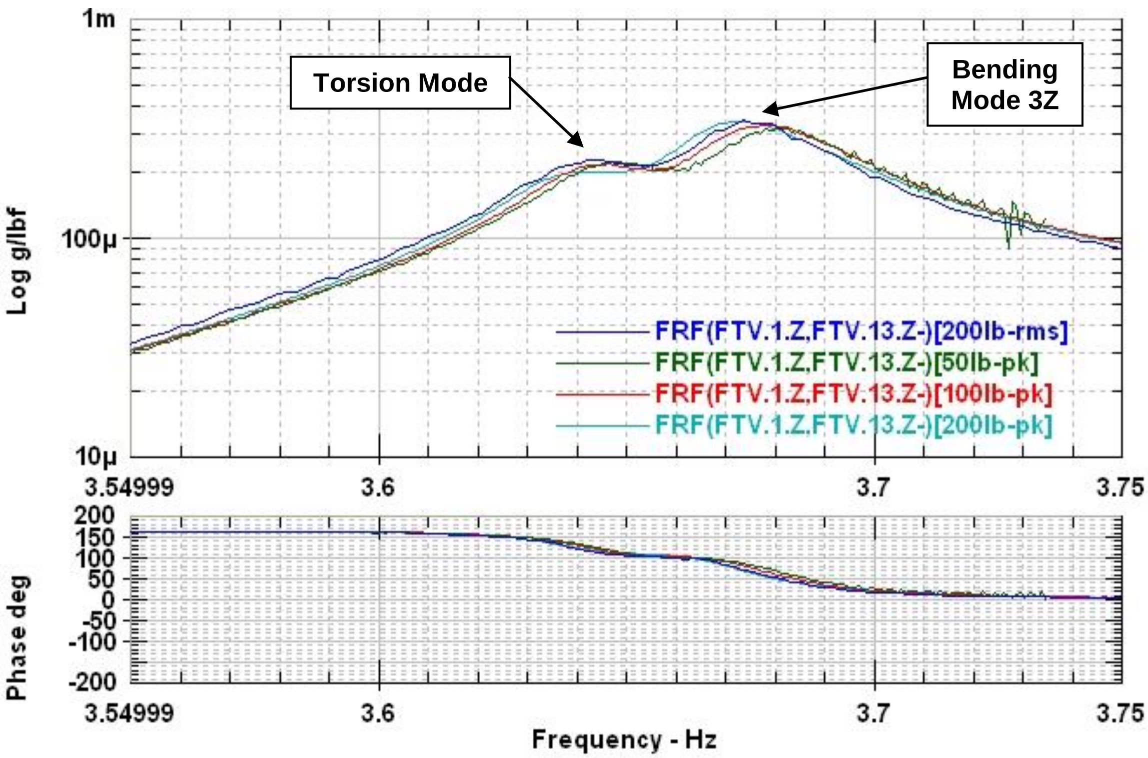

Figure 44. Nonlinearity in mode 3Z due to varying sine sweep levels

Changes in the peak frequency when using sine sweep excitation are shown in Table 9. The natural frequency of the 2nd bending mode in the Z-direction changed -1.2% from 50 to 200 lb-pk. However, other modes changed less than 0.2% due to the different force levels.

Table 9. Peak Frequency Nonlinearity Due to Sine Sweep Excitation

Mode	Sweep Up 50 lb-pk Peak Frequency (Hz)	Sweep Up 100 lb-pk Peak Frequency (Hz)	Sweep Up 200 lb-pk Peak Frequency (Hz)	50 vs. 200 lb-pk Percent Difference (%)
2Y	1.0527	1.0527	1.0508	-0.18
2Z	1.1836	1.1797	1.1699	-1.16
3Y	3.4600	3.4590	3.4590	-0.03
3Z	3.6777	3.6797	3.6729	-0.13

4.6 Impact Tests

Figures 45-50 show results from the impact (Tap) test. The impact tests were initially performed at the time of the modal test with the GNC instrumentation inactive and later repeated with the GNC sensors powered on. The first impact test, performed on August 30, 2009 (FTV-14), used capacitive accelerometers [CAP], whereas the second test performed on September 23, 2009, used ICP® accelerometers [ICP]. ICP accelerometers have an acceleration range of 10 g versus 3 g for the capacitive accelerometers, which allowed for higher impact loads at the input location without saturation of the sensor. This could explain why the ICP measurements appear to be cleaner than the capacitive ones. In addition, the vehicle control system instrumentation was mounted in its flight configuration for the second set of tap tests. During the second set of tap tests, the control sensors were powered and data was recorded in the control bandwidth. No problems were identified based on the control sensor measurements. The drive point measurements for the forward RRGU show that the first major responses occur above 100 Hz. A similar trend was observed for the FTINU location in the X-direction, but the radial direction did not show a significant response in the measured bandwidth due to significant local stiffness in that direction. However, the aft RRGU measurement in the radial direction showed that the first major response at that location occurred near 60 Hz. Additionally, a series of tap tests around the aft skirt, shown in Figure 51, revealed that the first major response of the aft skirt was also around 60 Hz. It is important to bear in mind that this is the response of the aft skirt while the FTV is fastened to the MLP hold down posts, which is not expected to be the same as the response during flight.

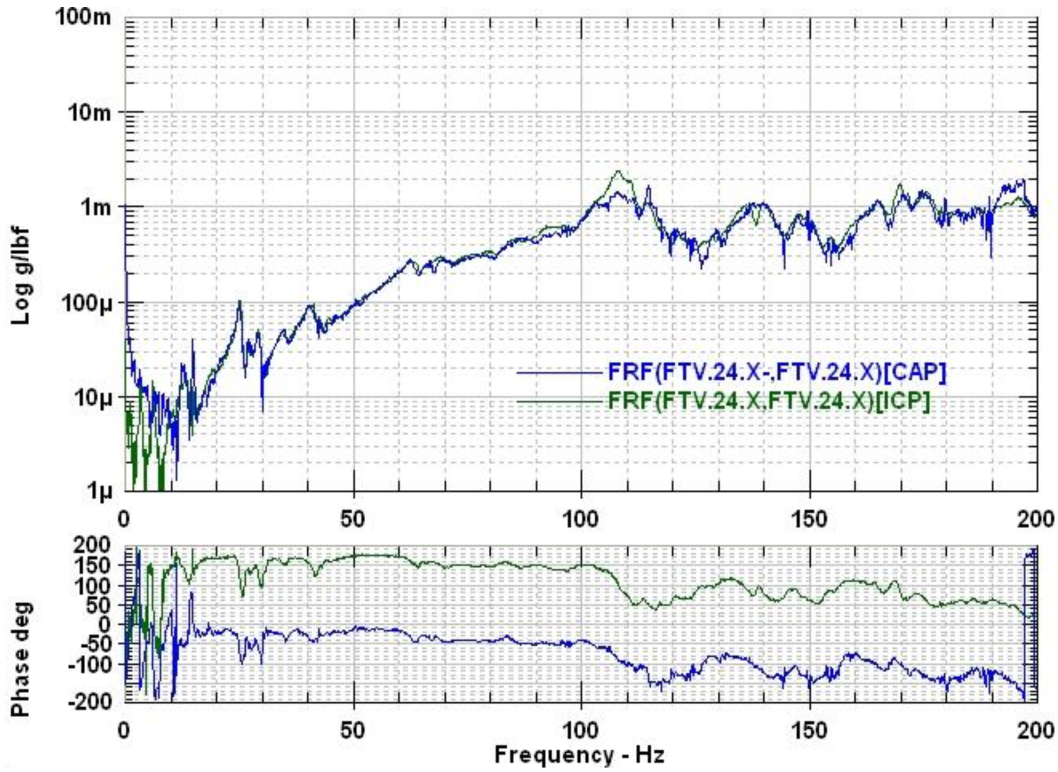

Figure 45. Drive point FRFs from tap tests at forward RRGU in X-direction

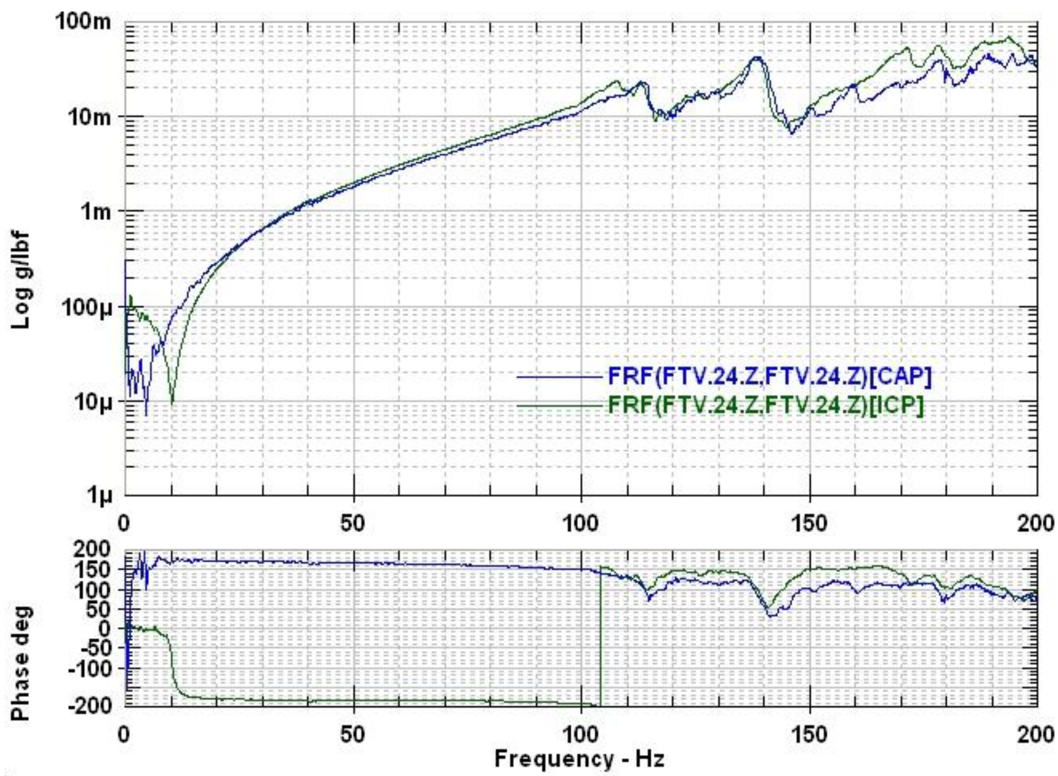

Figure 46. Drive point FRFs from tap tests at forward RRGU in radial direction

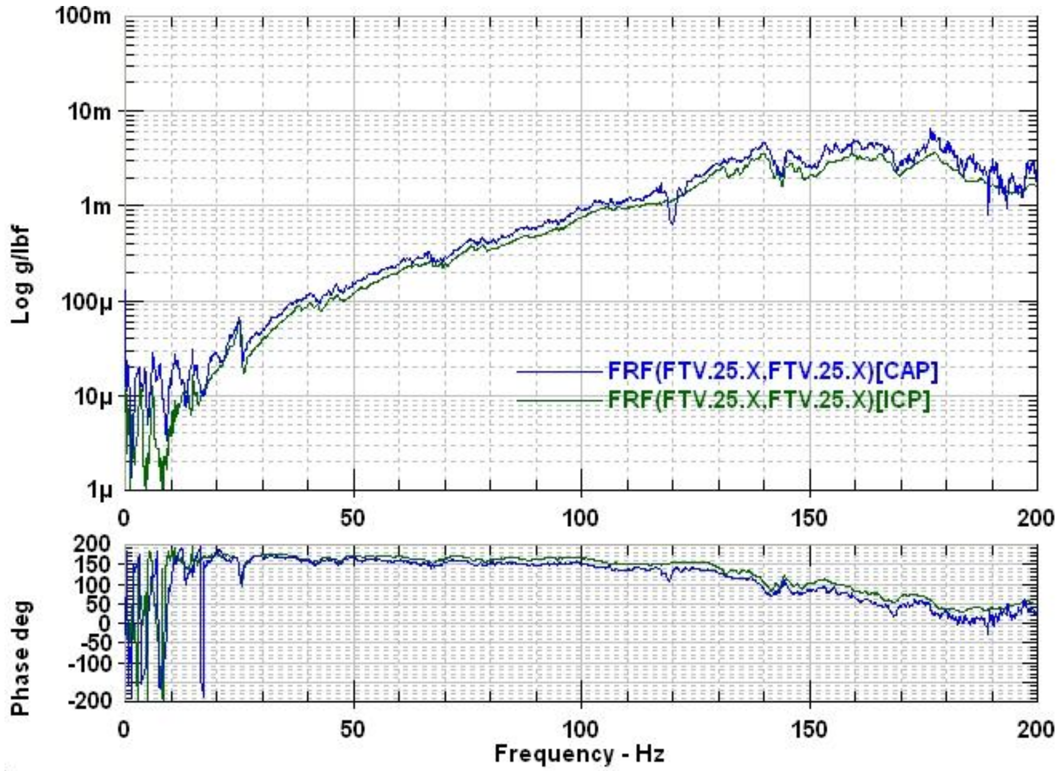

Figure 47. Drive point FRFs from tap tests at FTINU in X-direction

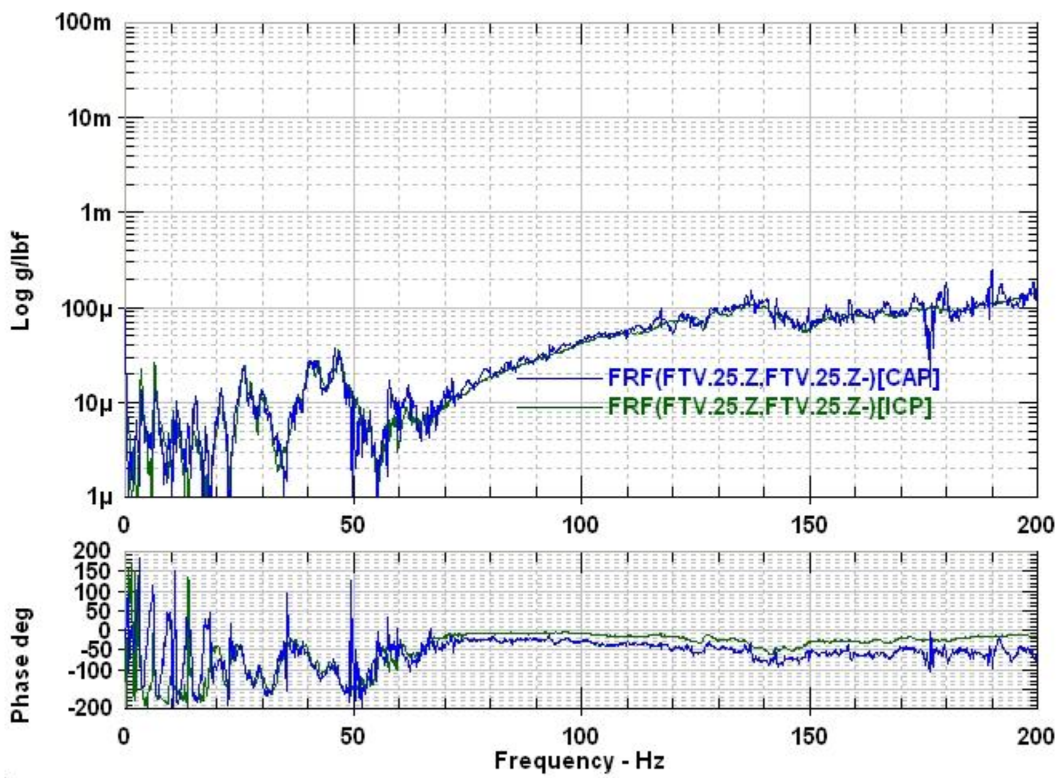

Figure 48. Drive point FRFs from tap tests at FTINU in radial direction

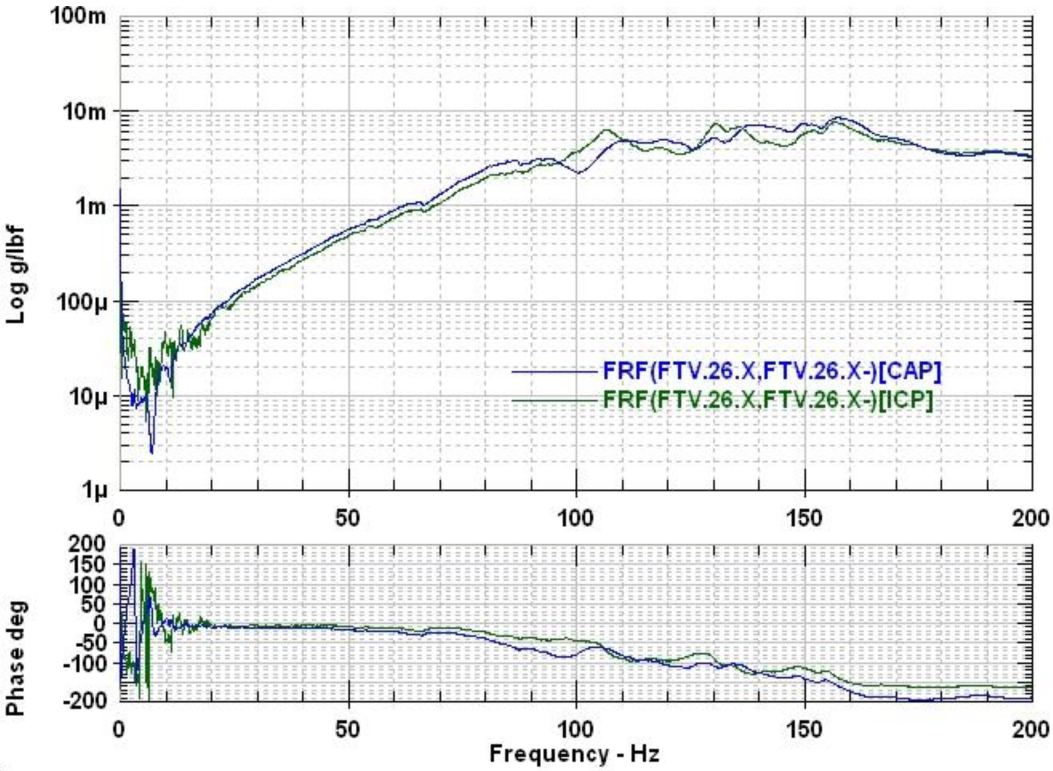

Figure 49. Drive point FRFs from tap tests at aft RRGU in X-direction

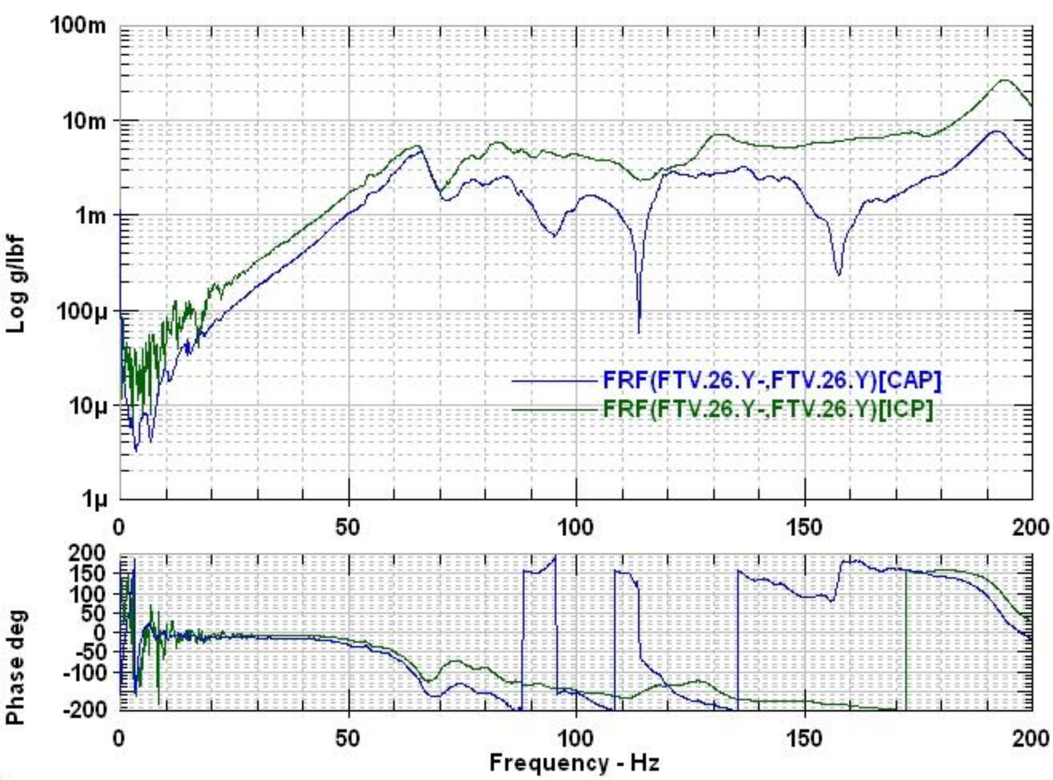

Figure 50. Drive point FRFs from tap tests at aft RRGU in radial direction

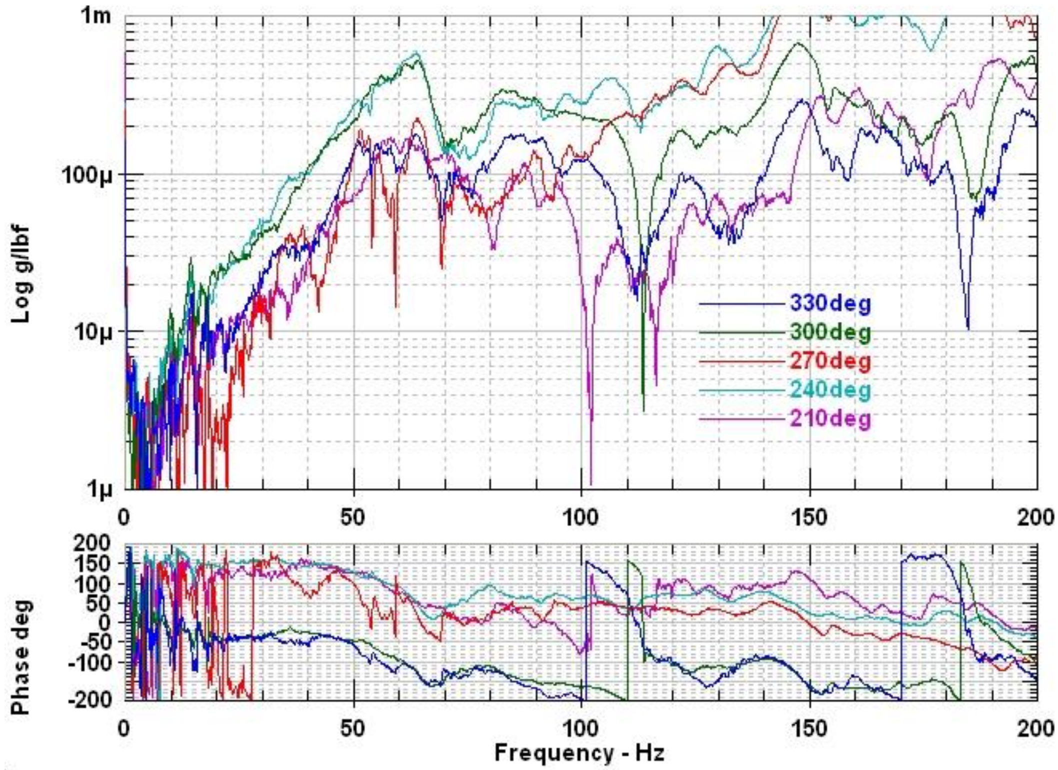

Figure 51. FRFs from tap tests on aft skirt in radial direction (reference: 23Z, 270°)

5.0 Experimental Modal Analysis Results

Modal parameters were estimated using different estimation algorithms by several analysts. Most analysts used the H_1 FRF estimates from random excitation data with industry standard parameter estimation routines. A more rigorous approach was used to improve the 1st bending mode estimates using data from the 200 lb-rms random test. In this case, time history data from the accelerometers and Integrated Electronics Piezo Electric (IEPE) load cell signals were processed (after removing biases) by taking cyclic averages, then applying a Hanning window, and processing the blocks with a 75% overlap. An H_v estimator is then applied to compute the FRF. The curve fit used the PolyMAX algorithm [7], and only the Y and Z-axis measurements were included during the pole estimation process.

Parameter estimation results for the Ares I-X FTV on the MLP are summarized in Table 10 with the target modes highlighted. Because of the difficulties estimating the 1st bending mode pair, the frequency and damping estimates for these modes are from the free decay data. Free decay data was also used in addition to the random data to estimate the frequency and damping of the 2nd bending modes. Overall, the results compiled from different analysts, parameter estimation routines, and datasets is very consistent. Furthermore, the peak frequencies identified in the ambient data sets without the shakers attached are also consistent with the estimated modal frequencies (see Table 6). A test geometry file and final set of modes is included on the data archival DVD. The archived modal parameter estimates are from the FTV-11 (200 lb-rms) test and the free-decay tests. The corresponding mode shapes are shown in Appendix E.

Frequency and damping variations with amplitude were also of interest. It was shown in Section 4 that the frequencies of the target modes changed by 1.2% or less over the tested force range. Likewise, the damping for the 1st bending mode pair was examined using the free-decay data (see Section 4.3) and shown to have linear response. To gain additional insight into the damping behavior for the 2nd and 3rd bending modes, parameter estimates for the random and sine sweep data were used to investigate the damping linearity. Table 11 shows the damping values for the 200 lb-rms random test along with estimated peak displacements. To estimate the peak displacements at location 1, the rms acceleration between the half power points of each mode from the autospectra measurements is multiplied by 3 to estimate a 3-sigma peak, and then integrated to compute the displacement by dividing by the frequency squared.

Table 10. Summary of Modal Parameter Estimates for Ares I-X FTV

Mode No. & Description	Average Freq (Hz)	STDev Freq (Hz)	Average Damp (%)	STDev Damp (%)	Min Damp (%)	Max Damp (%)	Data Source
1-1st Bending Y	0.178	0.002	0.848	0.038	0.81	0.88	free-decay data
2-1st Bending Z	0.213	0.002	0.433	0.017	0.41	0.45	free-decay data
3-2nd Bending Y	1.06	0.001	0.290	0.034	0.23	0.31	free-decay / random
4-2nd Bending Z	1.19	0.004	0.372	0.081	0.25	0.46	free-decay / random
5-System Lateral Z	1.87	0.004	2.48	0.335	2.24	2.95	random
6- System Lateral Y	2.07	0.010	1.25	0.057	1.17	1.30	random
7-System Torsion	2.92	0.029	1.20	0.222	0.96	1.40	random
8-System Vertical	3.42	-	1.66	-	-	-	random :FTV-2
9-3rd Bending Y	3.46	0.003	0.483	0.036	0.43	0.51	random
10-3rd Bending Z & Torsion	3.65	0.002	0.388	0.015	0.37	0.40	random
11-3rd Bending Z	3.68	0.003	0.385	0.006	0.38	0.39	random
12-4th Bending LAS dominated (45°)	4.61	0.001	0.175	0.006	0.17	0.18	random
13-4th Bending LAS dominated (135°)	4.78	0.003	0.243	0.01	0.23	0.25	random
14-System Lateral	6.18	0.001	1.36	0.017	1.35	1.38	random
15-5th Bending Y	6.41	0.003	0.673	0.015	0.66	0.69	random
16-5th Bending Z	6.66	0.004	1.35	0.056	1.29	1.40	random

Table 11. Damping and Displacement Estimates from Random Tests

Mode	Force (lb-rms)	Location 1 Displacement (in-pk)	Curve Fit Damping (%)
2nd Bending Y	200	0.00618	0.31
2nd Bending Z	200	0.00809	0.43
3rd Bending Y	200	0.0199	0.49
3rd Bending Z	200	0.0204	0.39
4th Bending (45°)	200	0.0251	0.18
4th Bending (135°)	200	0.0228	0.25

Listed in Table 12 are the sine sweep damping and displacement values. The peak displacements were determined by finding the peak acceleration value from the time histories, then integrating by dividing by the frequency squared. In contrast, the damping values were determined by curve fitting the FRFs from the sine sweeps.

Table 12. Damping and Displacement Estimates from Sine Sweep Tests

Mode	Force (lb-pk)	Location 1 Displacement (in-pk)	Curve Fit Damping (%)
2nd Bending Y	50	0.111	0.272
	100	0.213	0.283
	200	0.389	0.302
2nd Bending Z	50	0.073	0.386
	100	0.127	0.335
	200	0.199	0.343
3rd Bending Y	50	0.0178	0.470
	100	0.0338	0.507
	200	0.0655	0.537
3rd Bending Z	50	0.0128	0.395
	100	0.0251	0.388
	200	0.0524	0.410

The sine sweep and random damping estimates from Tables 11 and 12 are plotted in Figures 52 and 53. Recall that free-decay damping estimates for the 2nd bending mode in the Y-direction were shown in Table 8. There is no clear trend in the damping with respect to displacement amplitude. The damping for the 2nd and 3rd bending modes in the Y-direction appear to increase slightly with amplitude, while the damping for the 2nd bending mode in the Z-direction appears to decrease with amplitude over the range tested. Nonetheless, the 3rd bending mode in the Z-direction appears to have an approximately constant damping value across the tested range. In all cases, the variation in damping is relatively small for the tested amplitude range.

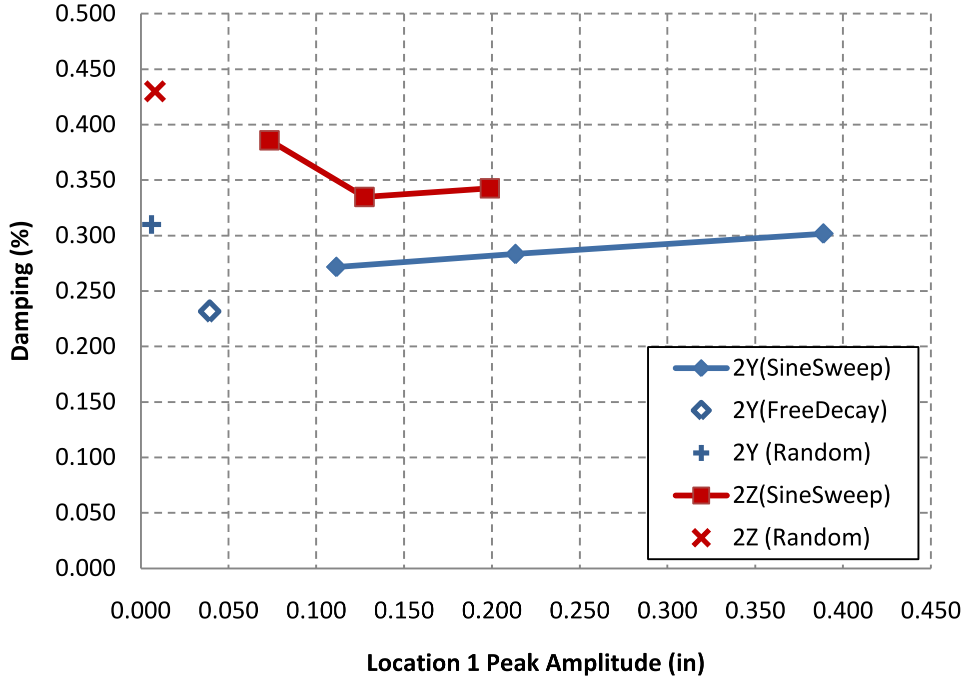

Figure 52. Amplitude dependence of 2nd bending mode damping estimates

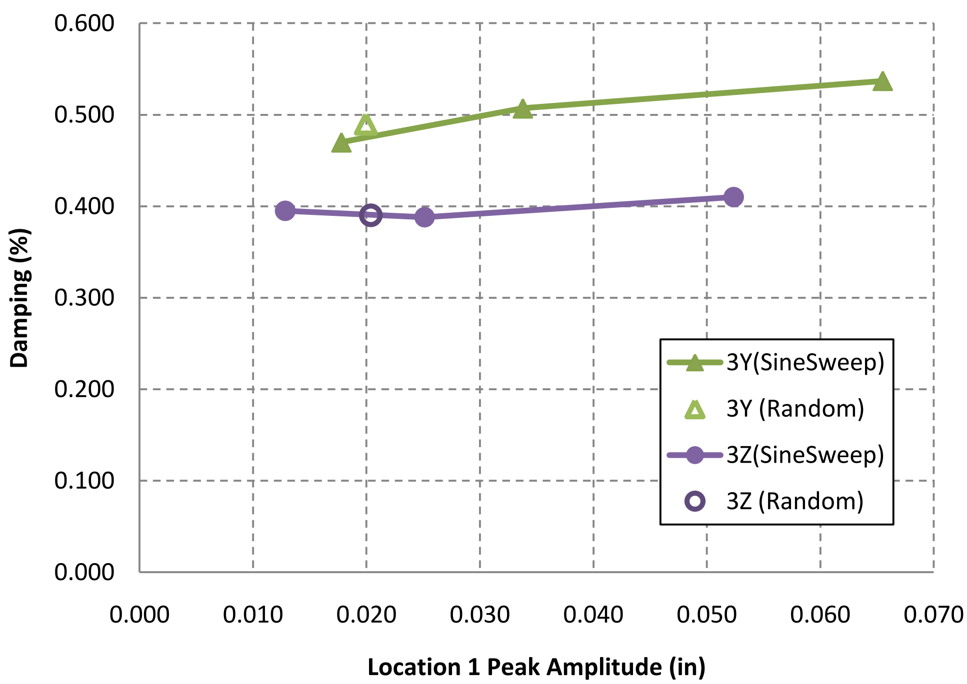

Figure 53. Amplitude dependence of 3rd bending mode damping estimates

The Ares I-X FTV and MLP were transported to the launch pad using the Crawler Transporter on October 20, 2009. Figure 54 shows the rollout configuration. There were two sets of triaxial accelerometers recorded during rollout, one on the crew module (X=785”) and one on the IS-1 segment (X=1966”). After setting the Ares I-X and MLP system down on the support stands, ambient data was acquired at the pad to confirm that the modal response behavior did not change due to rollout. A comparison of the pre-modal test ambient response in the Vehicle Assembly Building and the on-pad ambient response is shown in Figure 55. No significant changes in the frequency response are noted. The peak frequencies for the target modes are in excellent agreement. The higher on-pad response is attributed to wind loading.

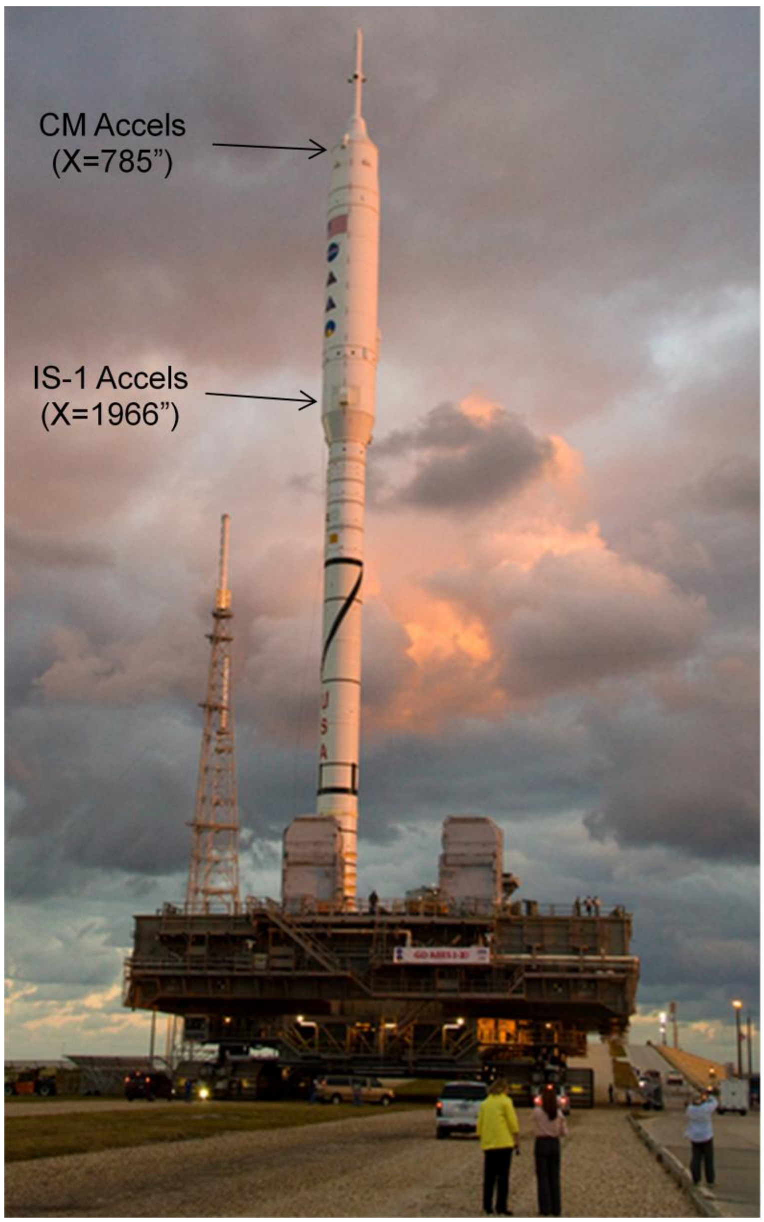

Figure 54. Rollout Configuration: Ares I-X on the MLP and Crawler Transporter.

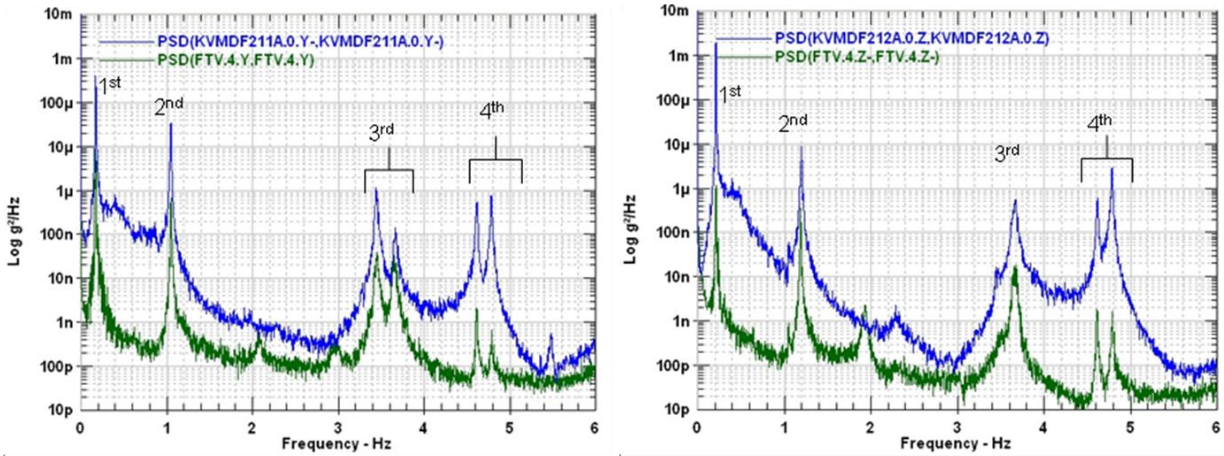

Figure 55. Comparison of pre-modal test (green) and on-pad (blue) ambient response for crew module accelerometers. Y-axis response (Left) and Z-axis response (Right).

6.0 Comparison of Analysis and Test

This section provides a summary of the comparisons between the pre-test analysis and test data. Details of the model calibration process can be found in Horta [8]. Evaluation with respect to the guidance and control requirements outlined in section 2.0 will also be summarized. The guidance and control metrics for the first three free-free bending modes were: 10% for 1st bending mode frequency and 20% for higher modes; node locations within +/- 100 inches; and modal deformations within 20% of nominal for the 1st bending mode pair and 50% for higher modes. While these requirements could not be verified on the free-free configuration, the calibration of the model was done for comparable modes (2nd through 4th bending) for the FTV on the MLP. The predictions of the free-free modes were then assumed to have similar test/analysis variances as determined for the FTV on MLP configuration.

The Y-Axis bending modes for test and analysis are overlaid in Figure 56 (courtesy of Aerospace Corporation). Similar behavior for the Z-axis bending modes was observed. For display purposes, the test data was expanded back to the full finite element model. Mode shapes and node locations are consistent between test and analysis. Primary response directions for the 4th bending mode for the test data is aligned with the 45-degree plane and 135-degree plane, whereas the analysis shows a primarily Y-axis and Z-axis response. The 4th bending mode pair is dominated by the LAS motion and varies from the Y- and Z-axis response directions observed for the 1st through 3rd bending mode pairs. Although the measured fourth bending modes are not on the Y- and Z-axis, they still provide an orthogonal set that adequately describes the modal space.

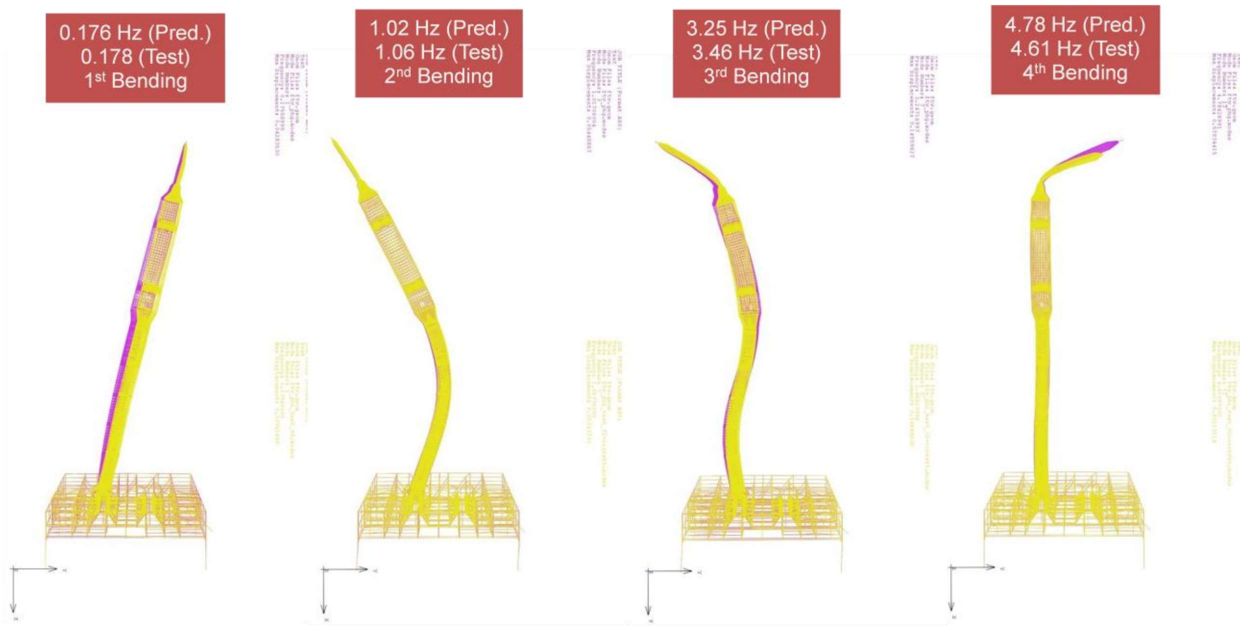

Figure 56. Overlay of pre-test analysis (purple) and test (yellow) mode shapes in Y-axis.

A comparison of the average measured frequencies to the pre-test analysis frequencies for the target modes is provided in Table 13. The comparison shows that the majority of the measured frequencies were within 5% of predictions, with one exception at 6.1% for the 3rd bending mode in the Y-direction. These results are within the guidance and control requirements on frequency.

Table 13. Comparison of Test/Analysis Frequencies

Mode	Pre-Test Analysis Frequency (Hz)	Modal Test Frequency[1] (Hz)	% Difference $(f_{test}-f_{analysis})/f_{test}*100$
1st Bending Y	0.176	0.178	1.1
1st Bending Z	0.216	0.213	-1.4
2nd Bending Y	1.02	1.06	3.8
2nd Bending Z	1.17	1.19	1.7
3rd Bending Y	3.25	3.46	6.1
3rd Bending Z	3.50	3.68	4.9
4th Bending LAS Y (45°)	4.78	4.61	-3.7
4th Bending LAS Z (135°)	4.84	4.78	-1.2

Note: ([1]) Average frequency from Table 10.

The cross-orthogonality metric compares test mode shapes extracted from measured FRFs with mode shape predictions weighted using the analytical mass matrix. The cross-orthogonality is shown in Figure 57. Since the project constrained the amount of instrumentation, no threshold values were set for this metric. Strong correlation for the target modes is found with values ≥0.98 for the first five target modes. However, the 3rd bending mode had a low value of 0.72 due to difficulty in separating this mode from the closely spaced torsion mode. Lastly, orthogonality values for the 4th bending mode pair are greater than 0.78 but have high off-diagonal terms due to the test modes being aligned with the 45- and 135-degree orientations.

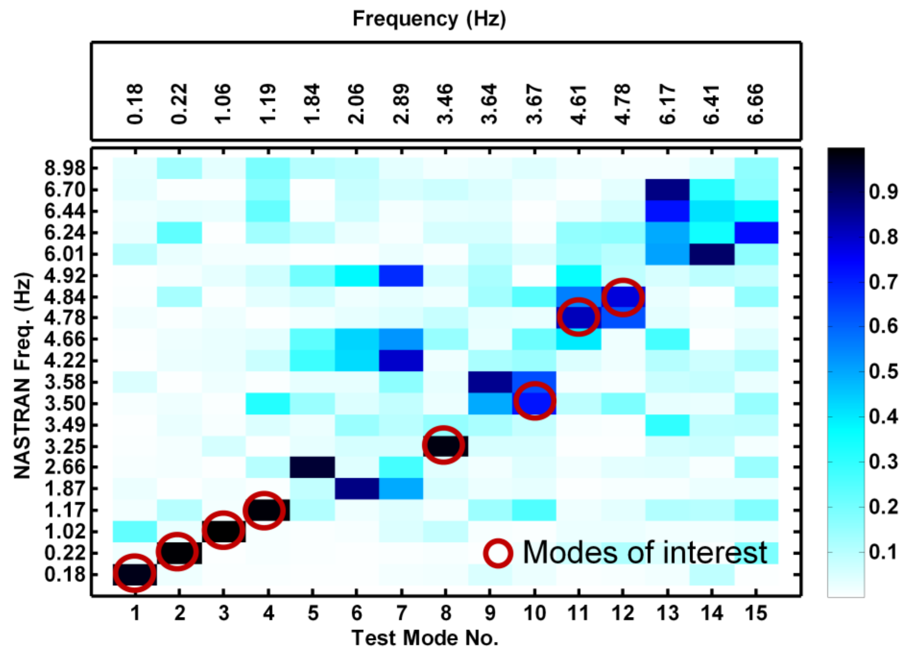

		IVM13b Frequencies (Hz)																			
		0.18	0.22	1.02	1.17	1.87	2.66	3.25	3.49	3.50	3.58	4.22	4.66	4.78	4.84	4.92	6.01	6.24	6.44	6.70	8.98
Test Freq. (Hz)	0.18	-0.97	-0.02	0.23	-0.02	-0.03	0.01	0.00	0.00	-0.01	0.05	0.00	-0.01	0.02	0.00	0.00	-0.10	0.03	0.02	0.04	0.03
	0.22	-0.02	0.99	0.03	-0.10	0.00	0.02	-0.01	-0.03	-0.02	0.00	-0.03	0.02	0.01	-0.13	-0.01	-0.03	-0.23	0.03	-0.01	-0.13
	1.06	-0.01	0.00	-1.00	-0.01	0.02	0.00	-0.06	0.01	-0.01	0.02	-0.03	0.03	0.02	0.00	0.03	-0.02	0.00	0.03	0.01	0.04
	1.19	0.00	0.01	-0.01	0.99	-0.01	0.10	0.00	0.05	0.32	0.01	0.08	-0.04	0.00	-0.04	-0.07	-0.01	-0.13	0.22	0.16	-0.19
	1.84	0.00	0.01	0.00	0.11	0.09	-0.95	0.03	-0.02	-0.15	-0.03	-0.28	0.24	0.02	0.06	0.21	0.00	0.09	-0.01	0.00	0.11
	2.06	0.00	0.00	0.01	-0.02	0.87	-0.04	-0.06	-0.15	-0.05	0.03	0.42	-0.44	-0.03	-0.02	-0.38	-0.01	-0.03	-0.07	-0.08	-0.09
	2.89	-0.01	-0.01	0.05	-0.05	0.50	0.27	0.06	0.10	0.09	-0.17	-0.80	0.53	0.05	0.03	0.68	-0.03	0.01	-0.01	-0.06	0.04
	3.46	-0.02	-0.01	-0.08	-0.01	-0.06	-0.04	-0.98	0.15	-0.03	0.03	0.02	0.15	-0.08	-0.02	-0.06	-0.01	0.06	0.03	0.07	0.02
	3.64	0.05	0.00	0.01	-0.14	-0.03	0.02	0.06	0.12	-0.50	-0.86	0.12	-0.03	0.03	-0.14	-0.12	-0.09	0.06	0.04	0.05	-0.02
	3.67	0.02	0.02	0.00	0.26	-0.03	-0.04	-0.06	0.09	0.72	-0.63	0.15	-0.21	0.03	0.24	0.01	-0.05	-0.01	0.00	-0.02	0.05
	4.61	-0.01	-0.07	-0.03	-0.02	0.00	-0.02	0.00	0.01	0.10	-0.01	0.05	-0.40	0.81	0.56	0.36	0.14	-0.16	0.03	-0.01	-0.02
	4.78	-0.01	0.12	-0.02	0.04	-0.01	0.04	0.00	-0.01	-0.19	-0.01	0.02	0.02	0.63	-0.78	-0.09	0.10	0.17	-0.07	-0.04	0.01
	6.17	-0.02	0.05	0.02	-0.11	-0.01	0.04	0.06	-0.30	0.03	-0.07	-0.11	-0.27	-0.04	0.03	0.06	-0.51	-0.50	-0.72	-0.87	0.01
	6.41	-0.09	-0.01	-0.02	0.10	-0.02	0.01	0.08	0.09	-0.03	-0.08	0.07	0.00	-0.01	0.00	-0.10	-0.90	0.35	0.41	0.31	-0.04
	6.66	0.00	0.19	-0.02	0.18	-0.02	0.15	0.01	0.09	-0.15	0.03	0.11	0.05	-0.02	0.16	0.08	-0.17	-0.73	0.37	0.17	0.16

Figure 57. Cross-orthogonality matrix in graphical and table format.

Data for test and analysis are compared in terms of the Principal Value (PV) bounds of the FRFs. These PVs are computed as the singular value decomposition of the FRF matrix at each frequency. To compute the PV bounds, the maximum of all maxima and minimum of all minima are collected from multiple NASTRAN runs. For cases with multiple singular values (i.e., multiple input shakers), only the maximum and minimum are compared. For the flight vehicle, the pre-test analysis PV uncertainty bounds were estimated using 200 NASTRAN runs with uncertainty in the FEM properties as defined in Reference [8]. Pre-test uncertainty studies included variations in the ballast mass of the upper stage, LAS modulus, upper stage joint stiffness, forward skirt modulus, and the FTV to MLP interface stiffness. Figure 58 shows the PV bounds for the analysis (solid) and test (dashed). Using 200 NASTRAN models, the probability of observing test data outside the analysis bounds is < 1/200, assuming that the parameter uncertainty model is adequate. To be consistent with the guidance and control studies the FEM used a nominal damping value of 0.5%. For the most part the test data is within the analysis uncertainty bounds, which indicates good agreement between the test and analysis. For additional information on the model calibration process, see Horta [8].

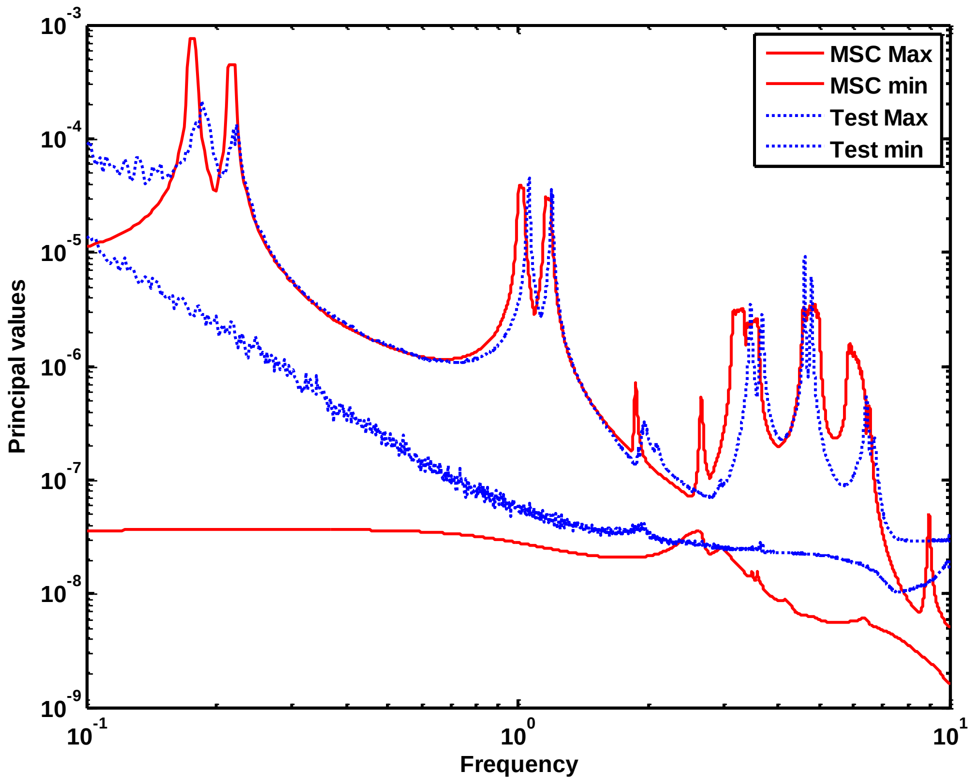

Figure 58. Comparison of principal values of the frequency response functions.

Aside from comparing mode shapes using orthogonality, the guidance and control group requested a comparison of node line locations and modal deformation for the 2nd through 4th bending modes, which are modes similar to the free-free modes of interest (see Figure 5). In order to estimate node line locations without the effects of the MLP, the base motion at the interface was removed from both the FEM and the measured mode shapes and the resulting shapes plotted along the sensor line in Figures 59-61. Superimposed on the figures are shapes with amplitudes that have been perturbed by 20% and/or 50%. It was difficult to assess the 4th bending mode due to the dominant LAS motion shown for X≤500 inches in Figure 61 (Top). Lower amplitude response data with the LAS points removed are shown in Figure 61 (Bottom). Node locations were estimated along the sensor line and along the vehicle centerline. Worst-case variance between analysis and test for three independent estimates along the sensor line are provided in Table 14. The only violation of the +/-100 inch requirement was at one node point for the LAS dominated 4th bending mode. After review by the guidance and control group prior to flight, this violation was deemed non-critical for the flight control system.

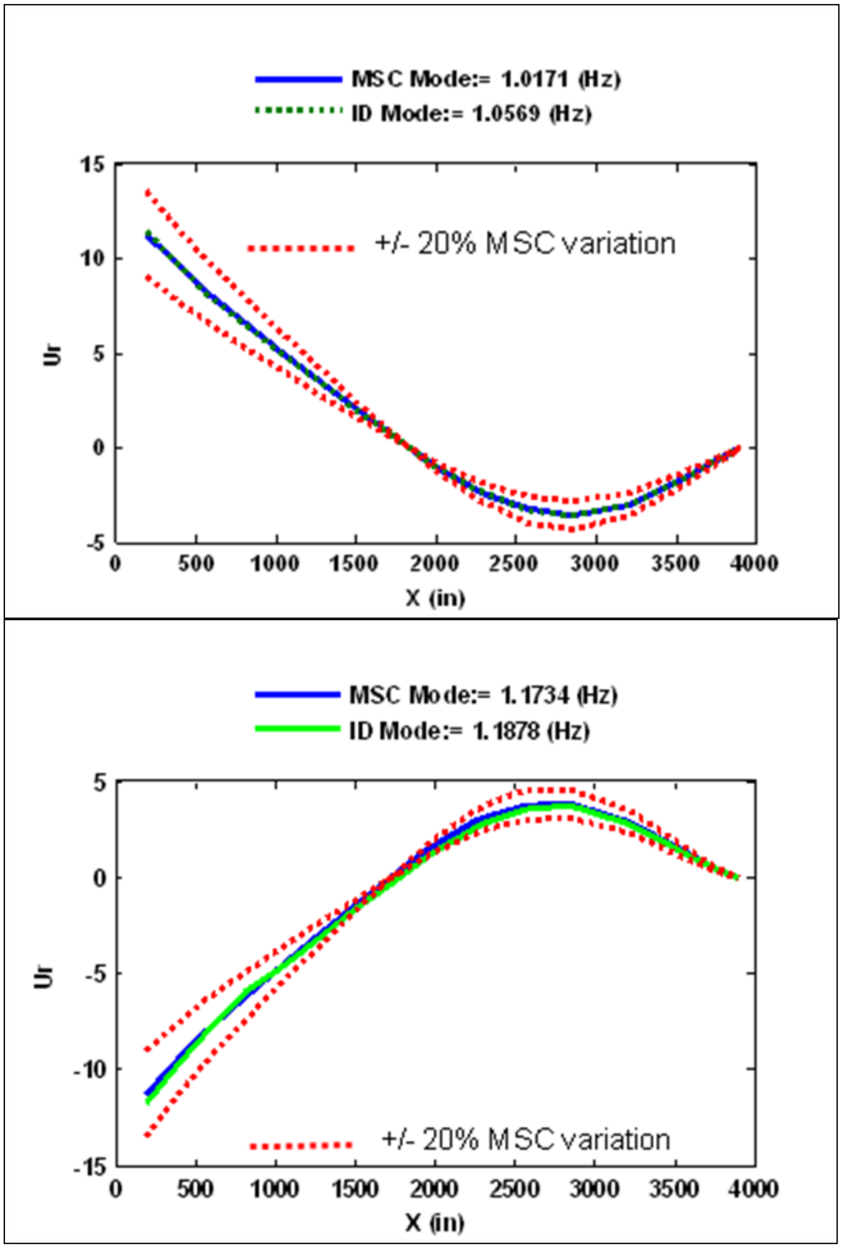

Figure 59. Comparison of mode shape deformation and nodal lines along sensor line for 2nd Bending Mode Y-Axis (Top) and Z-Axis (Bottom).

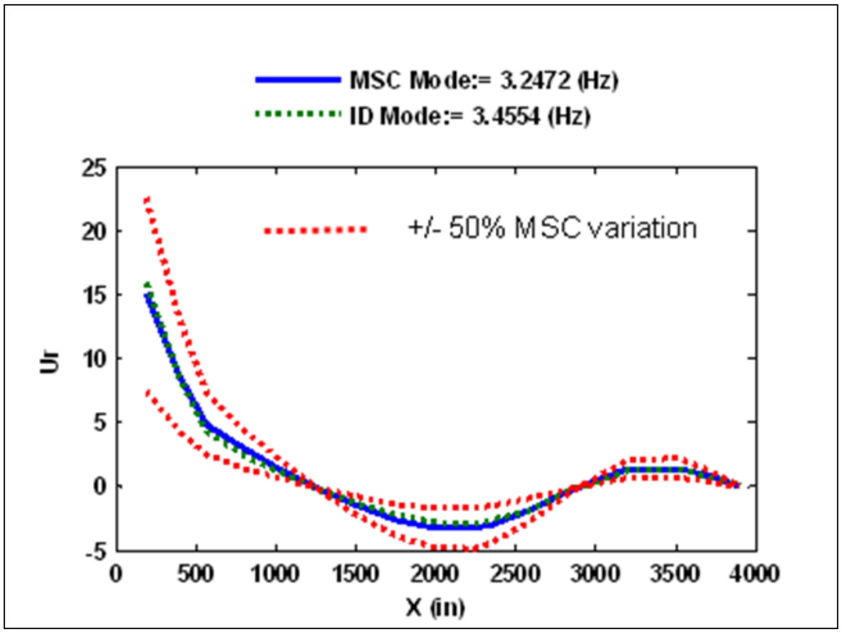

Figure 60. Comparison of mode shape deformation and nodal lines along sensor line for 3rd Bending mode.

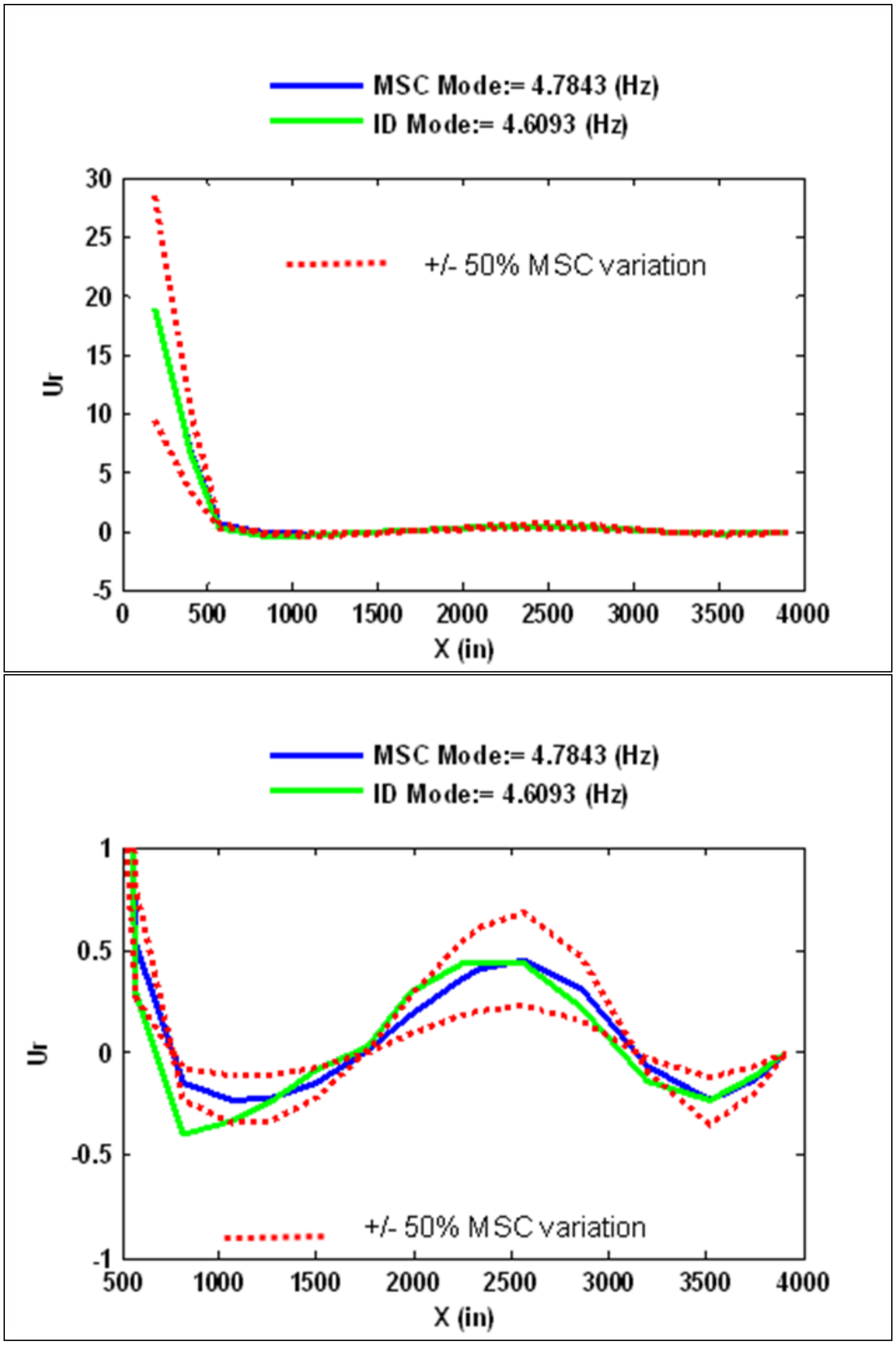

Figure 61. Comparison of mode shape deformation and nodal lines along sensor line for 4th Bending mode. Full vehicle (Top) and with LAS measurement points removed (Bottom).

Table 14. Node Location Estimates

Mode	Node 1		Node 2		Node 3	
	Centerline Location (in)	Max Variation +/- (in)	Centerline Location (in)	Max Variation +/- (in)	Centerline Location (in)	Max Variation +/- (in)
2nd Bending Y: 1.02 Hz	1814	3				
2nd Bending Z: 1.17 Hz	1702	39				
3rd Bending Y: 3.25 Hz	1289	3	2873	9		
4th Bending LAS Y (45°): 4.78 Hz	637	74	1789	109	3124	82

Notes: Listed max variation is from three independent assessments about sensor line; for mode pairs not shown use the listed variation.

7.0 Conclusions

The modal test successfully identified all of the targeted bending modes for the Ares I-X FTV on the MLP. Modal parameters were obtained using both multi-input random and free decay tests. Although the 1st bending mode pair was difficult to measure with the random shaker input, due to low coherence and split-peaks in the FRFs, manual excitation and free-decay response provided adequate data to estimate the 1st bending mode parameters. The 2nd through 4th bending modes were well identified using the multi-input random data. Additionally, sine sweep tests were performed on the 2nd and 3rd bending modes to investigate frequency nonlinearities. Results from multiple levels of random and sine sweep testing indicated linear response behavior of the modes, with maximum frequency shifts of 1.2% for quadruple the force levels. Comparisons of pre-test analysis and test data showed good agreement based on cross-orthogonality and principal value metrics.

It was shown that the measured modal parameters fell within the assumed Monte Carlo variance used in the control system studies, with the exception of the 4th bending mode node line for the FTV on the MLP. The LAS motion dominated this mode and errors in the relatively low amplitude response along the rest of the vehicle may have contributed to this exception. Measured modal frequencies were in good agreement with pre-test analysis having a worst-case error of 6.1%. With this information and the requirements initially provided by the guidance and navigation team, the nominal Ares I-X model was found to be adequate for evaluation of the flight control system without need for additional parameter adjustments.

References:

[1] NASA Fact Sheet, Constellation Program: Ares I-X Flight Test Vehicle, FS-2009-03-007-JSC, 2009. http://www.nasa.gov/pdf/354470main_aresIX_fs_may09.pdf

[2] Tuttle, R., and Lollock, J. A.; Modal Test Data Adjustment for Interface Compliance, Proceedings of IMAC XXVIII, Jacksonville, Florida, February 1-4, 2010.

[3] Kammer, D. C.; Sensor Placement for On-Orbit Modal Identification and Correlation of Large Space Structures, Journal of Guidance, Volume 14, No. 2, March-April 1991.

[4] Walker, Frank; KSC Work Plan FA-GIE-0040, Ares IX Full Vehicle Modal Test-Ground Instrumentation Support, NASA KSC, August 2009.

[5] Templeton, J. D., Buehrle, R. D., Parks, R. A., Lazor, D. R., and Gaspar, J. L.; Ares I-X Launch Vehicle Modal Test Measurements and Data Quality Assessments, Proceedings of IMAC XXVIII, Jacksonville, Florida, February 1-4, 2010.

[6] Ewins, D.J., Modal Testing: Theory, Practice and Application, 2nd Edition, Research Studies Press Ltd., pp. 231-234, 2000.

[7] Peeters, B, et. al., “The PolyMAX Frequency Domain Method: A New Standard for Modal Parameter Estimation?” Journal of Shock and Vibration, Vol. 11, pp. 395 – 409, 2004.

[8] Horta, L. H., Reaves, M. C., Buehrle, R. D., Templeton, J. D., Lazor, D. R., Gaspar, J. L., Parks, R. A., and Bartolotta, P. A..; Finite Element Model Calibration Approach for Ares I-X, Proceedings of IMAC XXVIII, Jacksonville, Florida, February 1-4, 2010.

Appendix A: Acronyms and Abbreviations

BNC	(Bayonet Neill Concelman) coaxial cable connector
CM	Crew Module
CS	Coordinate System
CDAS	Critical Data Acquisition System
DAS	Data Acquisition System
DFT	Discrete Fourier Transform
DOF	Degree of Freedom
FEM	Finite Element Model
FTINU	Fault Tolerant Inertial Navigation Unit
FRF	Frequency Response Function
FTV	Flight Test Vehicle
GRC	Glenn Research Center
GSE	Ground Support Equipment
HPS	Hydraulic Power Supply
Hz	Hertz
IEEE	Institute of Electrical and Electronics Engineers
IEPE	Integrated Electronics Piezo Electric
IPT’s	Integrated Product Teams
IS	Interstage
IVM	Integrated Vehicle Model
HB	High Bay
KSC	Kennedy Space Center
LaRC	Langley Research Center
LAS	Launch Abort System
lb	Pound
LVDT	Linear Variable Displacement Transducer
MIMO	Multi-Input Multi-Output

MLP	Mobile Launcher Platform
MSFC	Marshall Space Flight Center
pk	Peak
psi	Pounds per square inch
PV	Principal Value
rms	Root Mean Square
RRGU	Redundant Rate Gyro Unit
SA	Spacecraft Adapter
SE&I	Systems Engineering & Integration
SM	Service Module
SSAS	Super-Segment Assembly Stand
STDev	Standard Deviation
STI	Scientific and Technical Information
TBD	To Be Determined
TBR	To Be Resolved
UPS	Uninterrupted Power Supply
USS	Upper Stage Simulator
VAB	Vehicle Assembly Building
VXI	VME eXtensions for Instrumentation

Appendix B: Equipment List

Table B.1. FTV Equipment List (1 of 3)

	DATA ACQUISITION SYSTEM (DAS) RACK								
NAME	**MANUFACTURER**	**MODEL**	**SERIAL**	**OWNER**	**QTY**	**CAL DATE**	**CAL DUE**	**MISC**	
VXI MAINFRAME	AGILENT TECHNOLOGIES	E8403A	US38001676	LaRC	1	n/a	n/a		
SLOT-0 INTERFACE	AGILENT TECHNOLOGIES	E8491A	US39007039	LaRC	1	n/a	n/a	VXI 0	
16 CHANNEL DIGITIZER	VXI TECHNOLOGY INC	VT1432B	US45004211	LaRC	1	6/26/2009	6/26/2011	VXI 1	
16 CHANNEL DIGITIZER	VXI TECHNOLOGY INC	VT1432B	US45004212	LaRC	1	6/26/2009	6/26/2011	VXI 2	
16 CHANNEL DIGITIZER	VXI TECHNOLOGY INC	VT1432B	US45004209	LaRC	1	6/26/2009	6/26/2011	VXI 3	
16 CHANNEL DIGITIZER	VXI TECHNOLOGY INC	VT1432B	US45004210	LaRC	1	6/26/2009	6/26/2011	VXI 4	
16 CHANNEL DIGITIZER	VXI TECHNOLOGY INC	VT1432B	US45004537	LaRC	1	1/22/2008	1/22/2010	VXI 5	
16 CHANNEL DIGITIZER	VXI TECHNOLOGY INC	VT1432B	US45004538	LaRC	1	1/22/2008	1/22/2010	VXI 6	
4 CHANNEL SOURCE MODULE	HEWLETT-PACKARD CO	E1434A	US37260104	LaRC	1	n/a	n/a	VXI 7	
16 CHANNEL DIGITIZER WITH SOURCE	VXI TECHNOLOGY INC	VT1432B	US45004540	LaRC	1	1/22/2008	1/22/2010	VXI 8	
DIGITAL OSCILLOSCOPE	TEKTRONIX	TDS2014	C014678	LaRC	1	n/a	n/a		
ICP/VOLTAGE 8CH INPUT BOX	AGILENT TECHNOLOGIES	3241A	n/a	LaRC	4	n/a	n/a		
VOLTAGE 8CH INPUT BOX	HEWLETT-PACKARD CO	3240A	n/a	LaRC	4	n/a	n/a		
ICP/VOLTAGE 8CH INPUT BOX	HEWLETT-PACKARD CO	E1432-61600	US35371483, 88	LaRC	2	n/a	n/a		
VOLTAGE 8CH INPUT BOX	HEWLETT-PACKARD CO	E1432-61602	US35370238, 44	LaRC	2	n/a	n/a		
	SIGNAL CONDITIONER (S/C) Rack								
NAME	**MANUFACTURER**	**MODEL**	**SERIAL**	**OWNER**	**QTY**	**CAL DATE**	**CAL DUE**	**MISC**	
CAPACITIVE SIGNAL CONDITIONER	PCB PIEZOTRONICS	478A16	157	MSFC	1	1/12/2009	1/12/2010	S/C 1	
CAPACITIVE SIGNAL CONDITIONER	PCB PIEZOTRONICS	478A16	154	MSFC	1	3/10/2009	3/10/2010	S/C 2	
CAPACITIVE SIGNAL CONDITIONER	PCB PIEZOTRONICS	478A16	151	LaRC	1	11/7/2008	11/7/2009	S/C 3	
CAPACITIVE SIGNAL CONDITIONER	PCB PIEZOTRONICS	478A16	311	MSFC	1	1/12/2009	1/12/2010	S/C 4	
CAPACITIVE SIGNAL CONDITIONER	PCB PIEZOTRONICS	478A16	290	MSFC	1	6/24/2009	12/24/2009	S/C 5	
CAPACITIVE SIGNAL CONDITIONER	PCB PIEZOTRONICS	478A16	312	MSFC	1	1/12/2009	1/12/2010	S/C 6	
ICP SIGNAL CONDITIONER	PCB PIEZOTRONICS	483B07	729	MSFC	1	5/11/2009	11/11/2009	S/C 7	
CAPACITIVE SIGNAL CONDITIONER	PCB PIEZOTRONICS	445A101	327-328	LaRC	2	2/20/2009	2/20/2010	S/C 8	
POWER SUPPLY	PCB PIEZOTRONICS	441A101	1364	LaRC	1	n/a	n/a	S/C 8	
BANDPASS FILTER	KROHN-HITE	3343	2080	LaRC	1	4/20/2009	4/20/2011	E Shakers	
BANDPASS FILTER	KROHN-HITE	3343R	479	LaRC	1	3/11/2009	3/11/2011	B Shakers	
ICP SIGNAL CONDITIONER	PCB PIEZOTRONICS	480C02	5512	MSFC	1	12/28/1998	12/28/1999	E45 (13Z-) Load Cell	
ICP SIGNAL CONDITIONER	PCB PIEZOTRONICS	480C02	5509	MSFC	1	12/28/1998	12/28/1999	E135 (14Z-) Load Cell	
ICP SIGNAL CONDITIONER	PCB PIEZOTRONICS	480C02	5507	MSFC	1	12/28/1998	12/28/1999	B45 (16Z-) Load Cell	
ICP SIGNAL CONDITIONER	PCB PIEZOTRONICS	480C02	5505	MSFC	1	12/28/1998	12/28/1999	B135 (17Z-) Load Cell	
	ICP INSTRUMENTATION								
NAME	**MANUFACTURER**	**MODEL**	**SERIAL**	**OWNER**	**QTY**	**CAL DATE**	**CAL DUE**	**SENS**	**MISC**
IMPACT HAMMER	PCB PIEZOTRONICS	086B20	4095	LaRC	1	4/9/2009	4/9/2010	1.08 mV/lbf	
LOAD CELL	PCB PIEZOTRONICS	223M13	1614	MSFC	1	6/26/2009	6/26/2010	5.410 mV/lbf	Shaker B45
LOAD CELL	PCB PIEZOTRONICS	223M13	1615	MSFC	1	12/10/2008	12/10/2009	5.148 mV/lbf	Shaker B135
LOAD CELL	PCB PIEZOTRONICS	223M13	1616	MSFC	1	12/10/2008	12/10/2009	5.549 mV/lbf	Shaker E45
LOAD CELL	PCB PIEZOTRONICS	223M13	1618	MSFC	1	12/10/2008	12/10/2009	5.528 mV/lbf	Shaker E135

Table B.1. FTV Equipment List (2 of 3)

	MSFC ACCELEROMETERS								
NAME	MANUFACTURER	MODEL	SERIAL	OWNER	QTY	CAL DATE	CAL DUE	159.2Hz SENS (mV/g)	DC SENS (mV/g)
CAPACITIVE ACCELEROMETER	PCB PIEZOTRONICS	3701M15	2562	MSFC	1	1/21/2009	1/21/2010	998	975
CAPACITIVE ACCELEROMETER	PCB PIEZOTRONICS	3701M15	2563	MSFC	1	1/21/2009	1/21/2010	1050	988
CAPACITIVE ACCELEROMETER	PCB PIEZOTRONICS	3701M15	2567	MSFC	1	1/22/2009	1/22/2010	1020	989
CAPACITIVE ACCELEROMETER	PCB PIEZOTRONICS	3701M15	2569	MSFC	1	1/21/2009	1/21/2010	1000	991
CAPACITIVE ACCELEROMETER	PCB PIEZOTRONICS	3701M15	2570	MSFC	1	1/21/2009	1/21/2010	964	980
CAPACITIVE ACCELEROMETER	PCB PIEZOTRONICS	3701M15	2571	MSFC	1	1/21/2009	1/21/2010	975	982
CAPACITIVE ACCELEROMETER	PCB PIEZOTRONICS	3701M15	2576	MSFC	1	1/21/2009	1/21/2010	991	975
CAPACITIVE ACCELEROMETER	PCB PIEZOTRONICS	3701M15	2577	MSFC	1	1/21/2009	1/21/2010	1050	989
CAPACITIVE ACCELEROMETER	PCB PIEZOTRONICS	3701M15	2578	MSFC	1	1/22/2009	1/22/2010	983	984
CAPACITIVE ACCELEROMETER	PCB PIEZOTRONICS	3701M15	2579	MSFC	1	1/21/2009	1/21/2010	1020	984
CAPACITIVE ACCELEROMETER	PCB PIEZOTRONICS	3701M15	2580	MSFC	1	1/21/2009	1/21/2010	1040	990
CAPACITIVE ACCELEROMETER	PCB PIEZOTRONICS	3701M15	2581	MSFC	1	1/21/2009	1/21/2010	1040	988
CAPACITIVE ACCELEROMETER	PCB PIEZOTRONICS	3701M15	2582	MSFC	1	1/21/2009	1/21/2010	1040	997
CAPACITIVE ACCELEROMETER	PCB PIEZOTRONICS	3701M15	2583	MSFC	1	1/21/2009	1/21/2010	1040	986
CAPACITIVE ACCELEROMETER	PCB PIEZOTRONICS	3701M15	2584	MSFC	1	1/22/2009	1/22/2010	1030	983
CAPACITIVE ACCELEROMETER	PCB PIEZOTRONICS	3701M15	2585	MSFC	1	1/22/2009	1/22/2010	996	992
CAPACITIVE ACCELEROMETER	PCB PIEZOTRONICS	3701M15	2586	MSFC	1	1/22/2009	1/22/2010	999	981
CAPACITIVE ACCELEROMETER	PCB PIEZOTRONICS	3701M15	2587	MSFC	1	1/21/2009	1/21/2010	1030	991
CAPACITIVE ACCELEROMETER	PCB PIEZOTRONICS	3701M15	2588	MSFC	1	1/22/2009	1/22/2010	1020	978
CAPACITIVE ACCELEROMETER	PCB PIEZOTRONICS	3701M15	2589	MSFC	1	1/21/2009	1/21/2010	979	983
CAPACITIVE ACCELEROMETER	PCB PIEZOTRONICS	3701M15	2591	MSFC	1	1/22/2009	1/22/2010	1040	990
CAPACITIVE ACCELEROMETER	PCB PIEZOTRONICS	3701M15	2592	MSFC	1	1/21/2009	1/21/2010	1040	986
CAPACITIVE ACCELEROMETER	PCB PIEZOTRONICS	3701M15	2595	MSFC	1	1/22/2009	1/22/2010	1010	995
CAPACITIVE ACCELEROMETER	PCB PIEZOTRONICS	3701M15	2596	MSFC	1	1/22/2009	1/22/2010	1040	988
CAPACITIVE ACCELEROMETER	PCB PIEZOTRONICS	3701M15	2597	MSFC	1	1/21/2009	1/21/2010	1040	997
CAPACITIVE ACCELEROMETER	PCB PIEZOTRONICS	3701M15	2598	MSFC	1	1/21/2009	1/21/2010	1020	1000
CAPACITIVE ACCELEROMETER	PCB PIEZOTRONICS	3701M15	2599	MSFC	1	1/21/2009	1/21/2010	974	991
CAPACITIVE ACCELEROMETER	PCB PIEZOTRONICS	3701M15	2601	MSFC	1	1/22/2009	1/22/2010	1000	988
CAPACITIVE ACCELEROMETER	PCB PIEZOTRONICS	3701M15	2603	MSFC	1	1/21/2009	1/21/2010	1030	984
CAPACITIVE ACCELEROMETER	PCB PIEZOTRONICS	3701M15	2605	MSFC	1	1/22/2009	1/22/2010	987	984
CAPACITIVE ACCELEROMETER	PCB PIEZOTRONICS	3701M15	2606	MSFC	1	1/22/2009	1/22/2010	1020	987
CAPACITIVE ACCELEROMETER	PCB PIEZOTRONICS	3701M15	2607	MSFC	1	1/22/2009	1/22/2010	1010	983
CAPACITIVE ACCELEROMETER	PCB PIEZOTRONICS	3701M15	2608	MSFC	1	1/22/2009	1/22/2010	1010	985
CAPACITIVE ACCELEROMETER	PCB PIEZOTRONICS	3701M15	2609	MSFC	1	1/21/2009	1/21/2010	1030	981
CAPACITIVE ACCELEROMETER	PCB PIEZOTRONICS	3701M15	2610	MSFC	1	1/22/2009	1/22/2010	1000	983
CAPACITIVE ACCELEROMETER	PCB PIEZOTRONICS	3701M15	2611	MSFC	1	1/21/2009	1/21/2010	1020	994
CAPACITIVE ACCELEROMETER	PCB PIEZOTRONICS	3701M15	2612	MSFC	1	1/21/2009	1/21/2010	1040	988
CAPACITIVE ACCELEROMETER	PCB PIEZOTRONICS	3701M15	2613	MSFC	1	1/21/2009	1/21/2010	1010	995
CAPACITIVE ACCELEROMETER	PCB PIEZOTRONICS	3701M15	2614	MSFC	1	1/22/2009	1/22/2010	1040	974
CAPACITIVE ACCELEROMETER	PCB PIEZOTRONICS	3701M15	2615	MSFC	1	1/22/2009	1/22/2010	1050	992
CAPACITIVE ACCELEROMETER	PCB PIEZOTRONICS	3701M15	2670	MSFC	1	1/22/2009	1/22/2010	1050	992
CAPACITIVE ACCELEROMETER	PCB PIEZOTRONICS	3701M15	2671	MSFC	1	1/22/2009	1/22/2010	1030	984
CAPACITIVE ACCELEROMETER	PCB PIEZOTRONICS	3701M15	2672	MSFC	1	1/21/2009	1/21/2010	991	986
CAPACITIVE ACCELEROMETER	PCB PIEZOTRONICS	3701M15	2673	MSFC	1	1/22/2009	1/22/2010	1030	985
CAPACITIVE ACCELEROMETER	PCB PIEZOTRONICS	3701M15	2675	MSFC	1	1/22/2009	1/22/2010	1030	988
CAPACITIVE ACCELEROMETER	PCB PIEZOTRONICS	3701M15	2676	MSFC	1	1/21/2009	1/21/2010	943	991
CAPACITIVE ACCELEROMETER	PCB PIEZOTRONICS	3701M15	2679	MSFC	1	1/22/2009	1/22/2010	1030	981
CAPACITIVE ACCELEROMETER	PCB PIEZOTRONICS	3701M15	8138	MSFC	1	1/21/2009	1/21/2010	1010	976
CAPACITIVE ACCELEROMETER	PCB PIEZOTRONICS	3701M15	8139	MSFC	1	1/21/2009	1/21/2010	985	977
CAPACITIVE ACCELEROMETER	PCB PIEZOTRONICS	3701M15	8140	MSFC	1	1/21/2009	1/21/2010	1060	1020
CAPACITIVE ACCELEROMETER	PCB PIEZOTRONICS	3701M15	8141	MSFC	1	1/21/2009	1/21/2010	1010	977
CAPACITIVE ACCELEROMETER	PCB PIEZOTRONICS	3701M15	8142	MSFC	1	1/21/2009	1/21/2010	1020	999
CAPACITIVE ACCELEROMETER	PCB PIEZOTRONICS	3701M15	8156	MSFC	1	1/21/2009	1/21/2010	941	990
CAPACITIVE ACCELEROMETER	PCB PIEZOTRONICS	3701M15	8157	MSFC	1	1/21/2009	1/21/2010	977	999

Table B.1. FTV Equipment List (3 of 3)

	MSFC ACCELEROMETERS								
NAME	**MANUFACTURER**	**MODEL**	**SERIAL**	**OWNER**	**QTY**	**CAL DATE**	**CAL DUE**	**159.2Hz SENS (mV/g)**	**DC SENS (mV/g)**
CAPACITIVE ACCELEROMETER	PCB PIEZOTRONICS	3701M15	8158	MSFC	1	1/21/2009	1/21/2010	1010	987
CAPACITIVE ACCELEROMETER	PCB PIEZOTRONICS	3701M15	8159	MSFC	1	1/21/2009	1/21/2010	1010	997
CAPACITIVE ACCELEROMETER	PCB PIEZOTRONICS	3701M15	8160	MSFC	1	1/21/2009	1/21/2010	994	983
CAPACITIVE ACCELEROMETER	PCB PIEZOTRONICS	3701M15	8161	MSFC	1	1/21/2009	1/21/2010	932	980
CAPACITIVE ACCELEROMETER	PCB PIEZOTRONICS	3701M15	8162	MSFC	1	1/21/2009	1/21/2010	941	965
CAPACITIVE ACCELEROMETER	PCB PIEZOTRONICS	3701M15	8163	MSFC	1	1/21/2009	1/21/2010	1030	981
CAPACITIVE ACCELEROMETER	PCB PIEZOTRONICS	3701M15	8164	MSFC	1	1/21/2009	1/21/2010	972	1000
CAPACITIVE ACCELEROMETER	PCB PIEZOTRONICS	3701M15	8165	MSFC	1	1/21/2009	1/21/2010	986	980
CAPACITIVE ACCELEROMETER	PCB PIEZOTRONICS	3701M15	8166	MSFC	1	1/21/2009	1/21/2010	979	992
CAPACITIVE ACCELEROMETER	PCB PIEZOTRONICS	3701M15	8167	MSFC	1	1/21/2009	1/21/2010	1040	989
CAPACITIVE ACCELEROMETER	PCB PIEZOTRONICS	3701M15	8168	MSFC	1	1/21/2009	1/21/2010	998	984
CAPACITIVE ACCELEROMETER	PCB PIEZOTRONICS	3701M15	8169	MSFC	1	1/21/2009	1/21/2010	1040	990
CAPACITIVE ACCELEROMETER	PCB PIEZOTRONICS	3701M15	8170	MSFC	1	1/21/2009	1/21/2010	1010	981
CAPACITIVE ACCELEROMETER	PCB PIEZOTRONICS	3701M15	8171	MSFC	1	1/21/2009	1/21/2010	975	985
CAPACITIVE ACCELEROMETER	PCB PIEZOTRONICS	3701M15	8172	MSFC	1	1/22/2009	1/22/2010	981	984
CAPACITIVE ACCELEROMETER	PCB PIEZOTRONICS	3701M15	8173	MSFC	1	1/21/2009	1/21/2010	961	979
CAPACITIVE ACCELEROMETER	PCB PIEZOTRONICS	3701M15	8174	MSFC	1	1/21/2009	1/21/2010	951	972
CAPACITIVE ACCELEROMETER	PCB PIEZOTRONICS	3701M15	8175	MSFC	1	1/21/2009	1/21/2010	962	999
CAPACITIVE ACCELEROMETER	PCB PIEZOTRONICS	3701M15	8176	MSFC	1	1/21/2009	1/21/2010	929	984
CAPACITIVE ACCELEROMETER	PCB PIEZOTRONICS	3701M15	8177	MSFC	1	1/21/2009	1/21/2010	961	983
CAPACITIVE ACCELEROMETER	PCB PIEZOTRONICS	3701M15	8178	MSFC	1	1/21/2009	1/21/2010	1090	981
CAPACITIVE ACCELEROMETER	PCB PIEZOTRONICS	3701M15	8179	MSFC	1	1/21/2009	1/21/2010	978	980
CAPACITIVE ACCELEROMETER	PCB PIEZOTRONICS	3701M15	8180	MSFC	1	1/21/2009	1/21/2010	992	994
CAPACITIVE ACCELEROMETER	PCB PIEZOTRONICS	3701M15	8181	MSFC	1	1/21/2009	1/21/2010	1040	988
CAPACITIVE ACCELEROMETER	PCB PIEZOTRONICS	3701M15	8182	MSFC	1	1/21/2009	1/21/2010	1000	996
CAPACITIVE ACCELEROMETER	PCB PIEZOTRONICS	3711D1FA3G	517	MSFC	1	1/22/2009	1/22/2010	658	702
CAPACITIVE ACCELEROMETER	PCB PIEZOTRONICS	3711D1FA3G	518	MSFC	1	1/22/2009	1/22/2010	661	694
CAPACITIVE ACCELEROMETER	PCB PIEZOTRONICS	3711D1FA3G	519	MSFC	1	1/22/2009	1/22/2010	659	696
	LaRC ACCELEROMETERS								
NAME	**MANUFACTURER**	**MODEL**	**SERIAL**	**OWNER**	**QTY**	**CAL DATE**	**CAL DUE**	**30Hz SENS (mV/g)**	**DC SENS (mV/g)**
CAPACITIVE ACCELEROMETER	PCB PIEZOTRONICS	3701G3FA3G	2020	LaRC	1	10/1/2008	10/1/2009	991.25	996.6
CAPACITIVE ACCELEROMETER	PCB PIEZOTRONICS	3701G3FA3G	2021	LaRC	1	9/29/2008	9/29/2009	998.74	1009.3
CAPACITIVE ACCELEROMETER	PCB PIEZOTRONICS	3701G3FA3G	2022	LaRC	1	10/1/2008	10/1/2009	998.93	995.9
CAPACITIVE ACCELEROMETER	PCB PIEZOTRONICS	3701G3FA3G	2023	LaRC	1	10/1/2008	10/1/2009	996.69	991.0
CAPACITIVE ACCELEROMETER	PCB PIEZOTRONICS	3701G3FA3G	2026	LaRC	1	9/29/2008	9/29/2009	993.12	991.0
CAPACITIVE ACCELEROMETER	PCB PIEZOTRONICS	3701G3FA3G	2027	LaRC	1	9/29/2008	9/29/2009	997.99	1003.9
CAPACITIVE ACCELEROMETER	PCB PIEZOTRONICS	3701G3FA3G	2028	LaRC	1	9/24/2008	9/24/2009	992.45	989.8
CAPACITIVE ACCELEROMETER	PCB PIEZOTRONICS	3701G3FA3G	2029	LaRC	1	10/1/2008	10/1/2009	998.67	998.2
CAPACITIVE ACCELEROMETER	PCB PIEZOTRONICS	3701G3FA3G	2095	LaRC	1	9/24/2008	9/24/2009	995.46	982.0
CAPACITIVE ACCELEROMETER	PCB PIEZOTRONICS	3701G3FA3G	2096	LaRC	1	9/24/2008	9/24/2009	986.96	977.7
CAPACITIVE ACCELEROMETER	PCB PIEZOTRONICS	3701G3FA3G	3021	LaRC	1	9/24/2008	9/24/2009	1004.83	996.0
CAPACITIVE ACCELEROMETER	PCB PIEZOTRONICS	3701G3FA3G	3022	LaRC	1	10/1/2008	10/1/2009	1002.03	999.7
CAPACITIVE ACCELEROMETER	PCB PIEZOTRONICS	3701G3FA3G	3025	LaRC	1	9/16/2008	9/16/2009	1000.99	997.8
CAPACITIVE ACCELEROMETER	PCB PIEZOTRONICS	3701G3FA3G	3051	LaRC	1	9/22/2008	9/22/2009	992.82	n/a

Table B.2. Tap Test Equipment List

		DATA ACQUISITION SYSTEM EQUIPMENT						
NAME	**MANUFACTURER**	**MODEL**	**SERIAL**	**OWNER**	**QTY**	**CAL DATE**	**CAL DUE**	
DATA ACQUISITION ANALYZER	M+P INTERNATIONAL	VIBPILOT-8	B080063	LaRC	1	6/29/2009	6/29/2010	
LAPTOP	ACER	TRAVELMATE 8204WLMI	LXTAX0603460909FCCEM15	LaRC	1	n/a	n/a	
		ICP INSTRUMENTATION						
NAME	**MANUFACTURER**	**MODEL**	**SERIAL**	**OWNER**	**QTY**	**CAL DATE**	**CAL DUE**	**SENS**
IMPACT HAMMER	PCB PIEZOTRONICS	086B20	4095	LaRC	1	4/9/2009	4/9/2010	1.08 mV/lbf
ICP ACCELEROMETER	PCB PIEZOTRONICS	T333B42	14739	LaRC	1	3/25/2009	3/25/2010	519.44 mV/g
ICP ACCELEROMETER	PCB PIEZOTRONICS	T333B42	14748	LaRC	1	3/25/2009	3/25/2010	519.25 mV/g
ICP ACCELEROMETER	PCB PIEZOTRONICS	333B42	38872	LaRC	1	4/9/2009	4/9/2010	499.86 mV/g

Appendix C: Instrumentation Setup and Channel Mapping

Table C.1. Instrumentation Locations

	FTV Coordinates		MLP Coordinates			
Location Number	X-station	Angle	X-station	Y-station	Z-station	Description
1	199.4	180				LAS (Pre-Installed)
2	402.5	180				LAS (Pre-Installed)
3	568.3	180				LAS (Pre-Installed)
4	812.5	0				Service Module (Internal)
5	1063.5	0				US-7 (Internal)
6	1260.5	0				US-5 (Internal)
7	1494	0				US-3 (Internal)
8	1757.25	0				US-1 (Internal)
9	1985.5	0				IS-1 (Internal)
10	2240.4	0				Forward Skirt (External)
11	2232.9	0				5^{th} Segment (External)
12	2557.14	0				5^{th} Segment (External)
13	2557.14	45				5^{th} Segment - E-main shaker 1
14	2557.14	135				5^{th} Segment - E-main shaker 2
15	2858.9	0				Fwd Segment (External)
16	2858.9	45				Fwd Segment - B-deck shaker 1
17	2858.9	135				Fwd Segment - B-deck shaker 2
18	3202.5	0				Fwd Center Segment (External)
19	3524.0	0				Aft Center Segment (External)
20	3756.1	0				Aft Booster (External)
21	3903.9	0				Aft Booster (External)
22	4009.7	30				Holddown Post #6
23	4003.7	270				Aft Skirt
24	1023.8	20				US-7 FWD RRGU (Internal)
25	1761.5	2				US-1 FTINU (Internal)
26	3963.7	240				AFT RRGU (Internal)
27			0	0	0	MLP Corner 3-4
28			958	0	0	MLP Side 4
29			1895.9	0	0	MLP Corner 1-4
30			1895.9	-798	0	MLP Side 1
31			1895.9	-1596	0	MLP Corner 1-2
32			958	-1596	0	MLP Side 2
33			0	-1596	0	MLP Corner 2-3
34			0	-798	0	MLP Side 3
35						Holddown Post #5 Strain (160 με/V)
36						Holddown Post #6 Strain (160 με/V)
37						Holddown Post #7 Strain (160 με/V)
38						Holddown Post #8 Strain (160 με/V)
39	813.5	180				Service Module (Internal)
40	2557.14	180				5^{th} Segment (External)
41	3899.85	180				Aft Booster (External)
42	4009.7	210				Holddown Post #7
43	4009.7	150				Holddown Post #8
44	4009.7	330				Holddown Post #5
113	2557.14	45				5^{th} Segment - E-main shaker 1 (Raw ICP output)
114	2557.14	135				5^{th} Segment - E-main shaker 2 (Raw ICP output)
116	2858.9	45				Fwd Segment - B-deck shaker 1 (Raw ICP output)
117	2858.9	135				Fwd Segment - B-deck shaker 2 (Raw ICP output)
(110)	4003.7	330				(Tap test only) Aft Skirt Tap Location
(111)	4003.7	300				(Tap test only) Aft Skirt Tap Location
(112)	4003.7	270				(Tap test only) Aft Skirt Tap Location
(113)	4003.7	240				(Tap test only) Aft Skirt Tap Location
(114)	4003.7	210				(Tap test only) Aft Skirt Tap Location

Table C.2. Instrumentation Orientations

Location Number	Transformation from FTV-axes to Measurement-axes	X-Axis Accel Orientation	Y-Axis Accel Orientation	Z-Axis Accel Orientation	Load Cell Orientation
1			-Y	Z	
2			-Y	Z	
3			-Y	Z	
4		-X	Y	-Z	
5			Y	-Z	
6			Y	-Z	
7		-X	Y	-Z	
8			Y	-Z	
9		-X	Y	-Z	
10			Y	Z	
11			Y	Z	
12		-X	Y	Z	
13	45° about X-axis			Z	-Z
14	135° about X-axis			Z	-Z
15			Y	Z	
16	45° about X-axis			Z	-Z
17	135° about X-axis			Z	-Z
18		-X	Y	Z	
19			Y	Z	
20			Y	Z	
21			Y	Z	
22		-X	Y	Z	
23		-X	Y	Z	
24	20° about X-axis	-X	-Y	Z	
25	2° about X-axis	X	Y	Z	
26	330° about X-axis	X	-Y	Z	
27		-X	Y	Z	
28		-X	Y	Z	
29		-X	Y	Z	
30		-X	Y	Z	
31		-X	Y	Z	
32		-X	Y	Z	
33		-X	Y	Z	
34		-X	Y	Z	
35		X			
36		X			
37		X			
38		X			
39			Y		
40			Y		
41			Y		
42		-X	Y	Z	
43		-X			
44		-X			
113	45° about X-axis				-Z
114	135° about X-axis				-Z
116	45° about X-axis				-Z
117	135° about X-axis				-Z
(110)	330° about X-axis				-Z
(111)	300° about X-axis				-Z
(112)	270° about X-axis				-Z
(113)	240° about X-axis				-Z
(114)	210° about X-axis				-Z

Table C.3. Instrumentation Notes

Location Number	Notes
1	
2	
3	
4	
5	
6	
7	
8	
9	
10	
11	
12	
13	Z-axis is in radial direction for this location
14	Z-axis is in radial direction for this location
15	
16	Z-axis is in radial direction for this location
17	Z-axis is in radial direction for this location
18	
19	
20	
21	
22	
23	
24	Z-axis is in radial direction for this location
25	
26	Not connected until FTV-P10 test. Z accelerometer was switched from 2586 to 2583 before FTV-4 test. Y-axis is in radial direction for this location
27	
28	
29	
30	
31	
32	
33	
34	
35	
36	
37	
38	
39	
40	Not connected until FTV-P10 test
41	Not connected until FTV-P10 test
42	Not connected until FTV-P10 test
43	Not connected until FTV-P10 test
44	Not connected until FTV-P10 test
113	Not connected until FTV-11 test
114	Not connected until FTV-11 test
116	Not connected until FTV-11 test
117	Not connected until FTV-11 test
(110)	
(111)	
(112)	
(113)	
(114)	

Table C.4. Transducer Channel Setup (1 of 2)

TRANSDUCER CHANNELS								
Channel	**Usage**	**Name**	**EU**	**Sensitivity**	**Cal Type**	**Input Mode**	**Model**	**Serial**
1	Excitation	FTV.13.Z-	lbf	5.549	mV/EU	Voltage	223M13	1616
2	Excitation	FTV.14.Z-	lbf	5.528	mV/EU	Voltage	223M13	1618
3	Excitation	FTV.16.Z-	lbf	5.410	mV/EU	Voltage	223M13	1614
4	Excitation	FTV.17.Z-	lbf	5.148	mV/EU	Voltage	223M13	1615
5	Response	FTV.13.Z	g	988	mV/EU	Voltage	3701M15	2612
6	Response	FTV.14.Z	g	997	mV/EU	Voltage	3701M15	2582
7	Response	FTV.16.Z	g	984	mV/EU	Voltage	3701M15	2671
8	Response	FTV.17.Z	g	981	mV/EU	Voltage	3701M15	2609
9	Response	FTV.10.Y	g	1000	mV/EU	Voltage	3701M15	8164
10	Response	FTV.10.Z	g	1020	mV/EU	Voltage	3701M15	8140
11	Response	FTV.11.Y	g	985	mV/EU	Voltage	3701M15	2608
12	Response	FTV.11.Z	g	983	mV/EU	Voltage	3701M15	2610
13	Response	FTV.12.X-	g	999	mV/EU	Voltage	3701M15	8142
14	Response	FTV.12.Y	g	983	mV/EU	Voltage	3701M15	8160
15	Response	FTV.12.Z	g	975	mV/EU	Voltage	3701M15	2562
16	Response	FTV.15.Y	g	980	mV/EU	Voltage	3701M15	8165
17	Response	FTV.15.Z	g	991	mV/EU	Voltage	3701M15	2587
18	Response	FTV.18.X-	g	980	mV/EU	Voltage	3701M15	2570
19	Response	FTV.18.Y	g	975	mV/EU	Voltage	3701M15	2576
20	Response	FTV.18.Z	g	981	mV/EU	Voltage	3701M15	8163
21	Response	FTV.1.Y-	g	997	mV/EU	Voltage	3701G3FA3G	2020
22	Response	FTV.1.Z	g	1009	mV/EU	Voltage	3701G3FA3G	2021
23	Response	FTV.2.Y-	g	996	mV/EU	Voltage	3701G3FA3G	2022
24	Response	FTV.2.Z	g	991	mV/EU	Voltage	3701G3FA3G	2023
25	Response	FTV.3.Y-	g	991	mV/EU	Voltage	3701G3FA3G	2026
26	Response	FTV.3.Z	g	1004	mV/EU	Voltage	3701G3FA3G	2027
27	Response	FTV.4.X-	g	993	mV/EU	Voltage	3701G3FA3G	3051
28	Response	FTV.4.Y	g	1000	mV/EU	Voltage	3701G3FA3G	3022
29	Response	FTV.4.Z-	g	998	mV/EU	Voltage	3701G3FA3G	3025
30	Response	FTV.24.X-	g	994	mV/EU	Voltage	3701M15	2611
31	Response	FTV.24.Y-	g	982	mV/EU	Voltage	3701M15	2571
32	Response	FTV.24.Z	g	965	mV/EU	Voltage	3701M15	8162
33	Response	FTV.5.Y	g	980	mV/EU	Voltage	3701M15	8179
34	Response	FTV.5.Z-	g	990	mV/EU	Voltage	3701M15	8169
35	Response	FTV.6.Y	g	985	mV/EU	Voltage	3701M15	8171
36	Response	FTV.6.Z-	g	990	mV/EU	Voltage	3701M15	8156
37	Response	FTV.7.X-	g	989	mV/EU	Voltage	3701M15	8167
38	Response	FTV.7.Y	g	976	mV/EU	Voltage	3701M15	8138
39	Response	FTV.7.Z-	g	984	mV/EU	Voltage	3701M15	2579
40	Response	FTV.8.Y	g	984	mV/EU	Voltage	3701M15	8176
41	Response	FTV.8.Z-	g	980	mV/EU	Voltage	3701M15	8161
42	Response	FTV.25.X	g	988	mV/EU	Voltage	3701M15	2601
43	Response	FTV.25.Y	g	983	mV/EU	Voltage	3701M15	2584
44	Response	FTV.25.Z	g	991	mV/EU	Voltage	3701M15	2599
45	Response	FTV.9.X-	g	986	mV/EU	Voltage	3701M15	2672
46	Response	FTV.9.Y	g	995	mV/EU	Voltage	3701M15	2613
47	Response	FTV.9.Z-	g	992	mV/EU	Voltage	3701M15	2670
48	Response	FTV.19.Y	g	988	mV/EU	Voltage	3701M15	2596
49	Response	FTV.19.Z	g	988	mV/EU	Voltage	3701M15	2675
50	Response	FTV.20.Y	g	985	mV/EU	Voltage	3701M15	2673
51	Response	FTV.20.Z	g	974	mV/EU	Voltage	3701M15	2614
52	Response	FTV.21.Y	g	978	mV/EU	Voltage	3701G3FA3G	2096

Table C.4. Transducer Channel Setup (2 of 2)

TRANSDUCER CHANNELS								
Channel	Usage	Name	EU	Sensitivity	Cal Type	Input Mode	Model	Serial
53	Response	FTV.21.Z	g	982	mV/EU	Voltage	3701G3FA3G	2095
54	Response	FTV.22.X-	g	996	mV/EU	Voltage	3701G3FA3G	3021
55	Response	FTV.22.Y	g	990	mV/EU	Voltage	3701G3FA3G	2028
56	Response	FTV.22.Z	g	998	mV/EU	Voltage	3701G3FA3G	2029
57	Response	FTV.23.X-	g	992	mV/EU	Voltage	3701M15	2615
58	Response	FTV.23.Y	g	988	mV/EU	Voltage	3701M15	2563
59	Response	FTV.23.Z	g	977	mV/EU	Voltage	3701M15	8141
60	Response	FTV.26.X	g	987	mV/EU	Voltage	3701M15	8158
61	Response	FTV.26.Y-	g	984	mV/EU	Voltage	3701M15	2578
62	Response	FTV.26.Z	g	986	mV/EU	Voltage	3701M15	2583
63	Response	FTV.28.X-	g	991	mV/EU	Voltage	3701M15	2569
64	Response	FTV.28.Y	g	984	mV/EU	Voltage	3701M15	2603
65	Response	FTV.28.Z	g	983	mV/EU	Voltage	3701M15	8177
66	Response	FTV.29.X-	g	987	mV/EU	Voltage	3701M15	2606
67	Response	FTV.29.Y	g	984	mV/EU	Voltage	3701M15	2605
68	Response	FTV.29.Z	g	1000	mV/EU	Voltage	3701M15	2598
69	Response	FTV.30.X-	g	989	mV/EU	Voltage	3701M15	2577
70	Response	FTV.30.Y	g	984	mV/EU	Voltage	3701M15	8168
71	Response	FTV.30.Z	g	997	mV/EU	Voltage	3701M15	8159
72	Response	FTV.31.X-	g	981	mV/EU	Voltage	3701M15	8178
73	Response	FTV.31.Y	g	988	mV/EU	Voltage	3701M15	8181
74	Response	FTV.31.Z	g	977	mV/EU	Voltage	3701M15	8139
75	Response	FTV.32.X-	g	986	mV/EU	Voltage	3701M15	2592
76	Response	FTV.32.Y	g	997	mV/EU	Voltage	3701M15	2597
77	Response	FTV.32.Z	g	994	mV/EU	Voltage	3701M15	8180
78	Response	FTV.33.X-	g	992	mV/EU	Voltage	3701M15	8166
79	Response	FTV.33.Y	g	992	mV/EU	Voltage	3701M15	2585
80	Response	FTV.33.Z	g	983	mV/EU	Voltage	3701M15	2607
81	Response	FTV.34.X-	g	981	mV/EU	Voltage	3701M15	2679
82	Response	FTV.34.Y	g	990	mV/EU	Voltage	3701M15	2591
83	Response	FTV.34.Z	g	983	mV/EU	Voltage	3701M15	2589
84	Response	FTV.27.X-	g	995	mV/EU	Voltage	3701M15	2595
85	Response	FTV.27.Y	g	978	mV/EU	Voltage	3701M15	2588
86	Response	FTV.27.Z	g	981	mV/EU	Voltage	3701M15	8170
87	Response	FTV.35.X	V	1000	mV/EU	Voltage	n/a	KMSGF509A
88	Response	FTV.36.X	V	1000	mV/EU	Voltage	n/a	KMSGF609A
89	Response	FTV.37.X	V	1000	mV/EU	Voltage	n/a	KMSGF709A
90	Response	FTV.38.X	V	1000	mV/EU	Voltage	n/a	KMSGF809A
91	Response	FTV.39.Y	g	990	mV/EU	Voltage	3701M15	2580
92	Response	FTV.40.Y	g	991	mV/EU	Voltage	3701M15	2676
93	Response	FTV.41.Y	g	999	mV/EU	Voltage	3701M15	8175
94	Response	FTV.42.X-	g	972	mV/EU	Voltage	3701M15	8174
95	Response	FTV.42.Y	g	996	mV/EU	Voltage	3701M15	8182
96	Response	FTV.42.Z	g	988	mV/EU	Voltage	3701M15	2581
97	Response	FTV.43.X-	g	984	mV/EU	Voltage	3701M15	8172
98	Response	FTV.44.X-	g	979	mV/EU	Voltage	3701M15	8173
99	Response	Source1	V	1000	mV/EU	Voltage		
100	Response	Source2	V	1000	mV/EU	Voltage		
101	Response	FTV.113.Z-	V	1000	mV/EU	Voltage	223M13	1616
102	Response	FTV.114.Z-	V	1000	mV/EU	Voltage	223M13	1618
103	Response	FTV.116.Z-	V	1000	mV/EU	Voltage	223M13	1614
104	Response	FTV.117.Z-	V	1000	mV/EU	Voltage	223M13	1615

Table C.5. Acquisition Channel Setup (1 of 2)

DAS	INPUT CHANNELS				
Channel	Coupling	Range	Offset	Pre-gain	Weighting
1	DC Gnd	5 V	0	1	Off
2	DC Gnd	5 V	0	1	Off
3	DC Gnd	5 V	0	1	Off
4	DC Gnd	5 V	0	1	Off
5	DC Gnd	1 V	0	1	Off
6	DC Gnd	1 V	0	1	Off
7	DC Gnd	1 V	0	1	Off
8	DC Gnd	1 V	0	1	Off
9	DC Gnd	1 V	0	1	Off
10	DC Gnd	1 V	0	1	Off
11	DC Gnd	1 V	0	1	Off
12	DC Gnd	1 V	0	1	Off
13	DC Gnd	1 V	0	1	Off
14	DC Gnd	1 V	0	1	Off
15	DC Gnd	1 V	0	1	Off
16	DC Gnd	1 V	0	1	Off
17	DC Gnd	1 V	0	1	Off
18	DC Gnd	1 V	0	1	Off
19	DC Gnd	1 V	0	1	Off
20	DC Gnd	1 V	0	1	Off
21	DC Gnd	1 V	0	1	Off
22	DC Gnd	1 V	0	1	Off
23	DC Gnd	1 V	0	1	Off
24	DC Gnd	1 V	0	1	Off
25	DC Gnd	1 V	0	1	Off
26	DC Gnd	1 V	0	1	Off
27	DC Gnd	1 V	0	1	Off
28	DC Gnd	1 V	0	1	Off
29	DC Gnd	1 V	0	1	Off
30	DC Gnd	1 V	0	1	Off
31	DC Gnd	1 V	0	1	Off
32	DC Gnd	1 V	0	1	Off
33	DC Gnd	1 V	0	1	Off
34	DC Gnd	1 V	0	1	Off
35	DC Gnd	1 V	0	1	Off
36	DC Gnd	1 V	0	1	Off
37	DC Gnd	1 V	0	1	Off
38	DC Gnd	1 V	0	1	Off
39	DC Gnd	1 V	0	1	Off
40	DC Gnd	1 V	0	1	Off
41	DC Gnd	1 V	0	1	Off
42	DC Gnd	1 V	0	1	Off
43	DC Gnd	1 V	0	1	Off
44	DC Gnd	1 V	0	1	Off
45	DC Gnd	1 V	0	1	Off
46	DC Gnd	1 V	0	1	Off
47	DC Gnd	1 V	0	1	Off
48	DC Gnd	1 V	0	1	Off
49	DC Gnd	1 V	0	1	Off
50	DC Gnd	1 V	0	1	Off
51	DC Gnd	1 V	0	1	Off
52	DC Gnd	1 V	0	1	Off

Table C.5. Acquisition Channel Setup (2 of 2)

DAS	INPUT CHANNELS				
Channel	Coupling	Range	Offset	Pre-gain	Weighting
53	DC Gnd	1 V	0	1	Off
54	DC Gnd	1 V	0	1	Off
55	DC Gnd	1 V	0	1	Off
56	DC Gnd	1 V	0	1	Off
57	DC Gnd	1 V	0	1	Off
58	DC Gnd	1 V	0	1	Off
59	DC Gnd	1 V	0	1	Off
60	DC Gnd	1 V	0	1	Off
61	DC Gnd	1 V	0	1	Off
62	DC Gnd	1 V	0	1	Off
63	DC Gnd	1 V	0	1	Off
64	DC Gnd	1 V	0	1	Off
65	DC Gnd	1 V	0	1	Off
66	DC Gnd	1 V	0	1	Off
67	DC Gnd	1 V	0	1	Off
68	DC Gnd	1 V	0	1	Off
69	DC Gnd	1 V	0	1	Off
70	DC Gnd	1 V	0	1	Off
71	DC Gnd	1 V	0	1	Off
72	DC Gnd	1 V	0	1	Off
73	DC Gnd	1 V	0	1	Off
74	DC Gnd	1 V	0	1	Off
75	DC Gnd	1 V	0	1	Off
76	DC Gnd	1 V	0	1	Off
77	DC Gnd	1 V	0	1	Off
78	DC Gnd	1 V	0	1	Off
79	DC Gnd	1 V	0	1	Off
80	DC Gnd	1 V	0	1	Off
81	DC Gnd	1 V	0	1	Off
82	DC Gnd	1 V	0	1	Off
83	DC Gnd	1 V	0	1	Off
84	DC Gnd	1 V	0	1	Off
85	DC Gnd	1 V	0	1	Off
86	DC Gnd	1 V	0	1	Off
87	DC Gnd	10 V	0	1	Off
88	DC Gnd	10 V	0	1	Off
89	DC Gnd	10 V	0	1	Off
90	DC Gnd	10 V	0	1	Off
91	DC Gnd	1 V	0	1	Off
92	DC Gnd	1 V	0	1	Off
93	DC Gnd	1 V	0	1	Off
94	DC Gnd	1 V	0	1	Off
95	DC Gnd	1 V	0	1	Off
96	DC Gnd	1 V	0	1	Off
97	DC Gnd	1 V	0	1	Off
98	DC Gnd	1 V	0	1	Off
99	DC Gnd	5 V	0	1	Off
100	DC Gnd	5 V	0	1	Off
101	DC Gnd	20 V	0	1	Off
102	DC Gnd	20 V	0	1	Off
103	DC Gnd	20 V	0	1	Off
104	DC Gnd	20 V	0	1	Off

Table C.6. Channel Connectivity (1 of 2)

DAS	SIGNAL CONDITIONER CHANNELS				PATCH PANEL		VXI CHANNELS	
Channel	Box	Channel	Type	Cable	Box	Channel	Card	Group
1	7	1	ICP	BNC	10	1	1	1
2	7	2	ICP	BNC	10	2	1	1
3	7	3	ICP	BNC	10	3	1	1
4	7	4	ICP	BNC	10	4	1	1
5	3	1	Capacitive	BNC	10	5	1	2
6	3	2	Capacitive	BNC	10	6	1	2
7	3	3	Capacitive	BNC	10	7	1	2
8	3	4	Capacitive	BNC	10	8	1	2
9	3	5	Capacitive	BNC	11	1	1	3
10	3	6	Capacitive	BNC	11	2	1	3
11	3	7	Capacitive	BNC	11	3	1	3
12	3	8	Capacitive	BNC	11	4	1	3
13	3	9	Capacitive	BNC	11	5	1	4
14	3	10	Capacitive	BNC	11	6	1	4
15	3	11	Capacitive	BNC	11	7	1	4
16	3	12	Capacitive	BNC	11	8	1	4
17	3	13	Capacitive	BNC	12	1	2	1
18	3	14	Capacitive	BNC	12	2	2	1
19	3	15	Capacitive	BNC	12	3	2	1
20	3	16	Capacitive	BNC	12	4	2	1
21	1	1	Capacitive	BNC	1	1	2	2
22	1	2	Capacitive	BNC	1	2	2	2
23	1	3	Capacitive	BNC	1	3	2	2
24	1	4	Capacitive	BNC	1	4	2	2
25	1	5	Capacitive	BNC	1	5	2	3
26	1	6	Capacitive	BNC	1	6	2	3
27	1	7	Capacitive	BNC	1	7	2	3
28	1	8	Capacitive	BNC	1	8	2	3
29	1	9	Capacitive	BNC	2	1	2	4
30	1	10	Capacitive	BNC	2	2	2	4
31	1	11	Capacitive	BNC	2	3	2	4
32	1	12	Capacitive	BNC	2	4	2	4
33	2	1	Capacitive	BNC	2	5	3	1
34	2	2	Capacitive	BNC	2	6	3	1
35	2	3	Capacitive	BNC	2	7	3	1
36	2	4	Capacitive	BNC	2	8	3	1
37	2	5	Capacitive	BNC	3	1	3	2
38	2	6	Capacitive	BNC	3	2	3	2
39	2	7	Capacitive	BNC	3	3	3	2
40	2	8	Capacitive	BNC	3	4	3	2
41	2	9	Capacitive	BNC	3	5	3	3
42	2	10	Capacitive	BNC	3	6	3	3
43	2	11	Capacitive	BNC	3	7	3	3
44	2	12	Capacitive	BNC	3	8	3	3
45	2	13	Capacitive	BNC	4	1	3	4
46	2	14	Capacitive	BNC	4	2	3	4
47	2	15	Capacitive	BNC	4	3	3	4
48	4	1	Capacitive	BNC	4	4	3	4
49	4	2	Capacitive	BNC	4	5	4	1
50	4	3	Capacitive	BNC	4	6	4	1
51	4	4	Capacitive	BNC	4	7	4	1
52	4	5	Capacitive	BNC	4	8	4	1

Table C.6. Channel Connectivity (2 of 2)

DAS	SIGNAL CONDITIONER CHANNELS				PATCH PANEL		VXI CHANNELS	
Channel	Box	Channel	Type	Cable	Box	Channel	Card	Group
53	4	6	Capacitive	BNC	5	1	4	2
54	4	7	Capacitive	BNC	5	2	4	2
55	4	8	Capacitive	BNC	5	3	4	2
56	4	9	Capacitive	BNC	5	4	4	2
57	4	10	Capacitive	BNC	5	5	4	3
58	4	11	Capacitive	BNC	5	6	4	3
59	4	12	Capacitive	BNC	5	7	4	3
60	4	13	Capacitive	BNC	5	8	4	3
61	4	14	Capacitive	BNC	6	1	4	4
62	4	15	Capacitive	BNC	6	2	4	4
63	5	1	Capacitive	BNC	6	3	4	4
64	5	2	Capacitive	BNC	6	4	4	4
65	5	3	Capacitive	BNC	6	5	5	1
66	5	4	Capacitive	BNC	6	6	5	1
67	5	5	Capacitive	BNC	6	7	5	1
68	5	6	Capacitive	BNC	6	8	5	1
69	5	7	Capacitive	BNC	7	1	5	2
70	5	8	Capacitive	BNC	7	2	5	2
71	5	9	Capacitive	BNC	7	3	5	2
72	5	10	Capacitive	BNC	7	4	5	2
73	5	11	Capacitive	BNC	7	5	5	3
74	5	12	Capacitive	BNC	7	6	5	3
75	6	1	Capacitive	BNC	7	7	5	3
76	6	2	Capacitive	BNC	7	8	5	3
77	6	3	Capacitive	BNC	8	1	5	4
78	6	4	Capacitive	BNC	8	2	5	4
79	6	5	Capacitive	BNC	8	3	5	4
80	6	6	Capacitive	BNC	8	4	5	4
81	6	7	Capacitive	BNC	8	5	6	1
82	6	8	Capacitive	BNC	8	6	6	1
83	6	9	Capacitive	BNC	8	7	6	1
84	6	10	Capacitive	BNC	8	8	6	1
85	6	11	Capacitive	BNC	9	1	6	2
86	6	12	Capacitive	BNC	9	2	6	2
87			n/a	BNC	9	3	6	2
88			n/a	BNC	9	4	6	2
89			n/a	BNC	9	5	6	3
90			n/a	BNC	9	6	6	3
91	1	13	Capacitive	BNC	9	7	6	3
92	8	1	Capacitive	BNC	9	8	6	3
93	8	2	Capacitive	BNC	13	1	6	4
94	5	13	Capacitive	BNC	13	2	6	4
95	5	14	Capacitive	BNC	13	3	6	4
96	5	15	Capacitive	BNC	13	4	6	4
97	5	16	Capacitive	BNC	13	5	8	1
98	4	16	Capacitive	BNC	13	6	8	1
99					13	7	8	1
100					13	8	8	1
101	7	1	ICP	BNC	14	1	8	2
102	7	2	ICP	BNC	14	2	8	2
103	7	3	ICP	BNC	14	3	8	2
104	7	4	ICP	BNC	14	4	8	2

Appendix D: Data Acquisition Log

PRE-TEST DATA

FTV-P1: August 19, 2009; Ambient noise data for connected MLP and 1st stage sensors, 1000 mV/g sensitivity for all channels, 32Hz sample rate, 0.016Hz resolution, 5 blocks, 9 avgs (50% overlap); Frequencies appear consistent with pre-test predictions

Static load test for shaker adapter plate attachment to vehicle: August 20, 2009; B45 925 lb with peaks to 966 lbs; B135 965 lbs with peaks to 980 lbs; E135 950 lb with peaks to 975 lbs; E45 came off at low load—reattached and tested to 948 lb at 1:30 am August 21, 2009

FTV-P2: August 21, 2009; Shaker B135 Checkout, Random, 12.5Hz Bandwidth, solenoid and valve open, ~100 lb rms, need to add weight to aft end of fixture

FTV-P3: August 21, 2009; Shaker B135 Checkout, Sine Dwell, 0.17Hz, ~50 lb peak, need to restrict personnel movement on platforms where shakers are mounted

FTV-P4: August 21, 2009; Shaker B135 Checkout, Sine Dwell, 1.0625Hz

FTV-P5: August 21, 2009; Shaker B135 Checkout, Sine Dwell, 1.2031Hz

FTV-P6: August 21, 2009 (4:13-5:20am); 4 Shaker Random, 12.5Hz Bandwidth, 8 blocks, 15 avgs (50% overlap), 0.0019 Hz resolution, 8 second ramp, 35 lb-rms E45, 40 lb-rms E135, 90 lb-rms B45, 75 lb-rms B135

FTV-P7: August 24, 2009 (Start ~11:45am); Ambient noise data for all original sensor locations except for 26, 32 Hz sample rate, 0.0019 Hz resolution, 12 blocks, 23 avgs (50% overlap), location 39 is across from location 4; no restrictions on vehicle access

FTV-P8: August 24, 2009; Tap tests at Forward RRGU (24Z, 24X) and FTINU (25Z-, 25X-). 256 Hz sample rate, 0.125 Hz resolution, 8 blocks per location, 10% force window, uniform response window, first impact of 24Z was overload; FTINU not installed

FTV-P9: August 26, 2009 (~3:12am-4:20am); 4 Shaker Random, 12.5Hz Bandwidth, 7 blocks, 13 avgs (50% overlap), 0.0019 Hz resolution, 8 second ramp, 54 lb-rms E45, 56 lb-rms E135, 52 lb-rms B45, 45 lb-rms B135; ballast mass of 600 lbs added to aft end of shaker fixtures; personnel movement on E-level caused inputs to shakers on that level

FTV-P10: August 26, 2009 (~2pm); Ambient noise data beginning while High Bay 3 and 4 doors were open at top, with wind exciting the first bending modes of the vehicle. High bay 3 door was shut soon after acquisition began. 32 Hz sample rate, 0.0019 Hz resolution, 12 blocks, 23 avgs (50% overlap); bay cleared after acquisition start so no personnel effects

TEST DATA

FTV-1: August 27, 2009 (~5:19-7:02pm); 4 Shaker Random, 12.5Hz Bandwidth, 12 blocks, 23 avgs (50% overlap), 0.0019 Hz resolution, 8 second ramp, 49 lb-rms E45, 50 lb-rms E135, 54 lb-rms B45, 53 lb-rms B135; changed to battery boxes for force cells to improve low frequency

FTV-2: August 27, 2009 (~7:41-9:23pm); 4 Shaker Random, 12.5Hz Bandwidth, 12 blocks, 23 avgs (50% overlap), 0.0019 Hz resolution, 8 second ramp, 130 lb-rms E45, 129 lb-rms E135, 140 lb-rms B45, 135 lb-rms B135

FTV-3: August 27, 2009 (~10:07-11:50pm); (50lb-pk): B135 Shaker, 50 lb-pk force controlled sine sweep, 1.01 to 1.26 Hz, 0.01 Oct/min, force fluctuations as high as 100 lbs for 8 second block; changed to 2 second block and (100lb-pk): B135 Shaker, 100 lb-pk force controlled sine sweep, 1.01 to 1.26 Hz, 0.01 Oct/min, force control issues persist; try constant voltage (100lb-pk,OpenLoop): B135 Shaker, 100 lb-pk open loop sine sweep, 1.01 to 1.26 Hz, 0.01 Oct/min, input unstable; need to evaluate sine sweep options

Data review; August 28, 2009; good mode estimates from random data for 2nd -4th bending modes; 1st bending difficult –poor coherence and split peak; in general test mode frequencies/shapes in good agreement with pre-test predictions; damping <1%; Bad transducer identified -replaced accelerometer and cable for 26Z location(S/N 2586 replaced with S/N 2583)

FTV-4(50lb-pk): August 29. 2009 (~6:39-5:54am); B135 Shaker, 50 lb-pk force controlled sine sweep, 1.01 to 1.26 Hz, 0.01 Oct/min; instability-need to sweep each mode separately

FTV-5(50lb-pk): August 29, 2009 (~7:38-7:51am); B135 Shaker, 50 lb-pk force controlled sine sweep, 1.00 to 1.07 Hz, 0.01 Oct/min, stop when goes unstable

FTV-5(100lb-pk): August 29, 2009 (~8:05-8:15am); B135 Shaker, 100 lb-pk force controlled sine sweep, 1.00 to 1.07 Hz, 0.01 Oct/min, stop when goes unstable

FTV-5(200lb-pk): August 29, 2009 (~8:23-8:33am); B135 Shaker, 200 lb-pk force controlled sine sweep, 1.00 to 1.07 Hz, 0.01 Oct/min, stop when goes unstable

FTV-6(50lb-pk): August 29, 2009 (~9:13-9:22am); B135 Shaker, 50 lb-pk force controlled sine sweep, 1.14 to 1.26 Hz, 0.01 Oct/min, stop when goes unstable

FTV-6(100lb-pk): August 29, 2009 (~9:49-9:59am); B135 Shaker, 100 lb-pk force controlled sine sweep, 1.14 to 1.26 Hz, 0.01 Oct/min, stop when goes unstable

FTV-6(200lb-pk): August 29, 2009 (~10:05-10:15am); B135 Shaker, 200 lb-pk force controlled sine sweep, 1.14 to 1.26 Hz, 0.01 Oct/min, stop when goes unstable

FTV-7(50lb-pk): August 29, 2009 (~11:40am-noon); E45 Shaker, 50 lb-pk force controlled sine sweep, 3.29 to 3.88 Hz, 0.01 Oct/min, stopped early due to harmonic processing indication of higher frequency

FTV-7(100lb-pk): August 29, 2009 (~12:13-12:37pm); E45 Shaker, 100 lb-pk force controlled sine sweep, 3.29 to 3.88 Hz, 0.01 Oct/min

FTV-7(200lb-pk): August 29, 2009 (~12:58-1:22pm); E45 Shaker, 200 lb-pk force controlled sine sweep, 3.29 to 3.88 Hz, 0.01 Oct/min

FTV-8: August 29, 2009 (2:36pm start); Time data while exciting 1st bending modes by hand, 32 Hz sample rate, start with y direction and allow to decay ~ 310 s, then z direction and allow to decay ~ 925s. 12Z accidentally removed from patch panel during acquisition for a few seconds

FTV-9: August 29, 2009; Time data taken while attempting to excite 2nd bending modes by hand with little success, same setup parameters as FTV-8

FTV-10: August 30, 2009 (~7:30am); Tap tests at Forward RRGU (24Z, 24X), FTINU (25Z-, 25X), 1024 Hz sample rate, 0.125 Hz resolution, 8 blocks per location, 10% force window, uniform response window, first impact of 24Z was overload, strange offsets in force signal after impact for location 25

FTV-11: August 30, 2009 (8:42-10:27am); 3 Shaker Random (Filter for B45 source did not work), 6.0Hz Bandwidth, 20 blocks, 39 avgs (50% overlap), 0.0019 Hz resolution, 8 second ramp, 190 lb-rms E45, 240 lb-rms E135, 228 lb-rms B135, stopped sources for E45 & E135 early after 12 blocks (23 avgs) and B135 about 1 minute later, then stopped acquisition after response died down

FTV-12: August 30, 2009; Time data taken while exciting 1st bending modes by hand, 32 Hz sample rate, start with y direction and allow to decay twice, then z direction and allow to decay twice. end with exciting in y direction and allow to decay with shaker B135 (17Z-) attached

FTV-13: August 30, 2009; Time data during 1.06 Hz sine dwell at B135 shaker (17Z-), 32 Hz sample rate, shaker/vehicle interactions cause difficulties controlling force -unable to get clean free-decay after signal shutdown

FTV-14: August 30, 2009 (3:30pm); Tap tests at Aft RRGU (26X-, 26Y) and Aft Skirt (110Z- [330 deg], 111Z- [300 deg], 112Z- [270 deg], 113Z- [240 deg], 114Z- [210 deg]), 1024 Hz sample rate, 0.125 Hz resolution, 8 blocks per location, 10% force window, uniform response window; Aft skirt not in flight configuration:gimbal rods not connected; access platform hanging on aft skirt; Ground Carrier Assembly adds constraint/mass.

REPROCESSED SWEEP DATA

FTV-5(50lb-pk): Single block DFT of entire time history, Uniform window

FTV-5(100lb-pk): Single block DFT of entire time history, Uniform window

FTV-5(200lb-pk): Single block DFT of entire time history, Uniform window

FTV-6(50lb-pk): Single block DFT of entire time history, Uniform window

FTV-6(100lb-pk): Single block DFT of entire time history, Uniform window

FTV-6(200lb-pk): Single block DFT of entire time history, Uniform window

FTV-7(50lb-pk): Single block DFT of entire time history, Hanning window

FTV-7(100lb-pk): Single block DFT of entire time history, Hanning window

FTV-7(200lb-pk): Single block DFT of entire time history, Hanning window

NOTES:

1. Pre-test data up to FTV-P6 only had the following accelerometers connected to the DAS: 10, 16, 19-23, 27-34

2. The following channels have local coordinate systems that are rotated about the X-axis: 13 (45 deg), 14 (135 deg), 16 (45 deg), 17 (135 deg), 24 (20 deg), 25 (330 deg)

3. Pre-test data from FTV-P7 to FTV-P9 did not have the following accelerometers installed: 26, 40-44

4. Instabilities were observed near resonances of the FTV-3 sine sweeps.

5. Units of universal files and throughput files are in SI units (N for force, m/s^2 for acceleration)

6. Switched out accelerometers at location 26Z before FTV-4 (S/N 2586 replaced with S/N 2583)

7. Added inputs for the ICP signals from the load cells for FTV-11 and later datasets (listed as locations 113, 114, 116, 117)

Appendix E: Test Mode Shapes

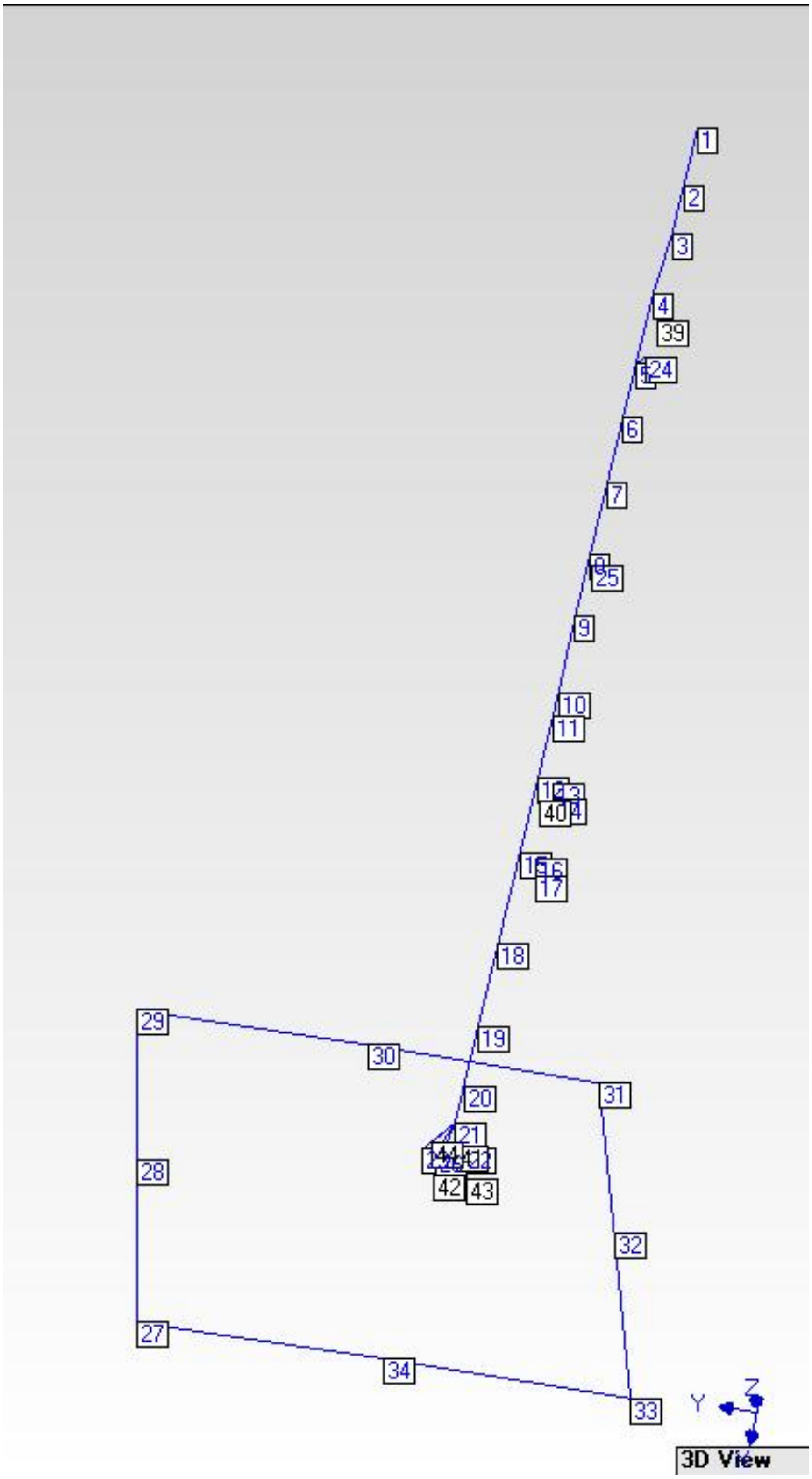

Figure E.1. Test geometry with measurement points labeled.

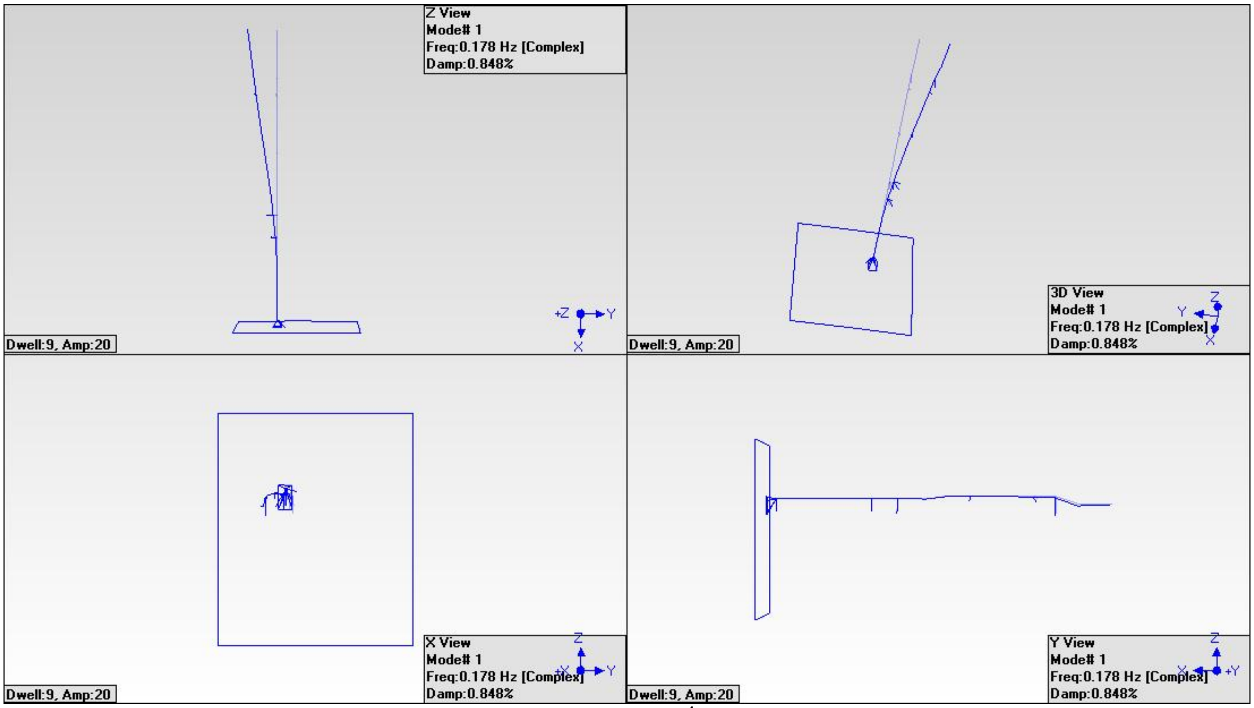

Figure E.2. Test mode 1; 1st Bending Y-Axis.

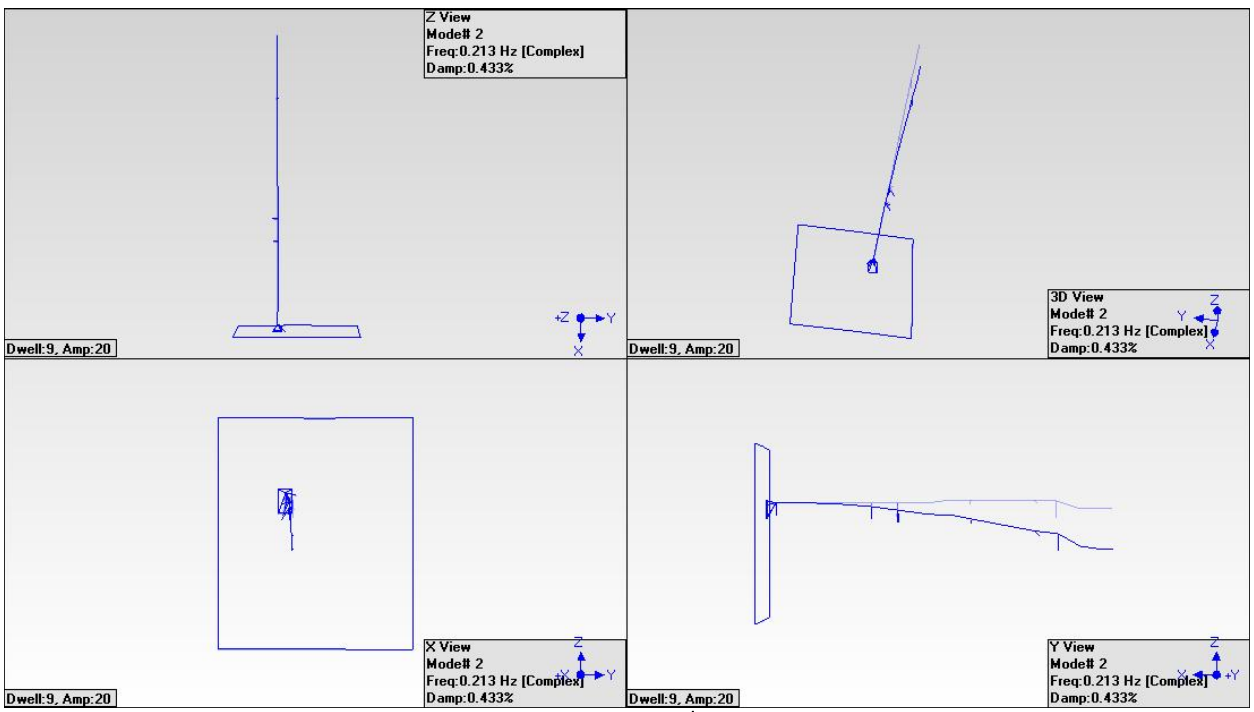

Figure E.3. Test mode 2; 1st Bending Z-Axis.

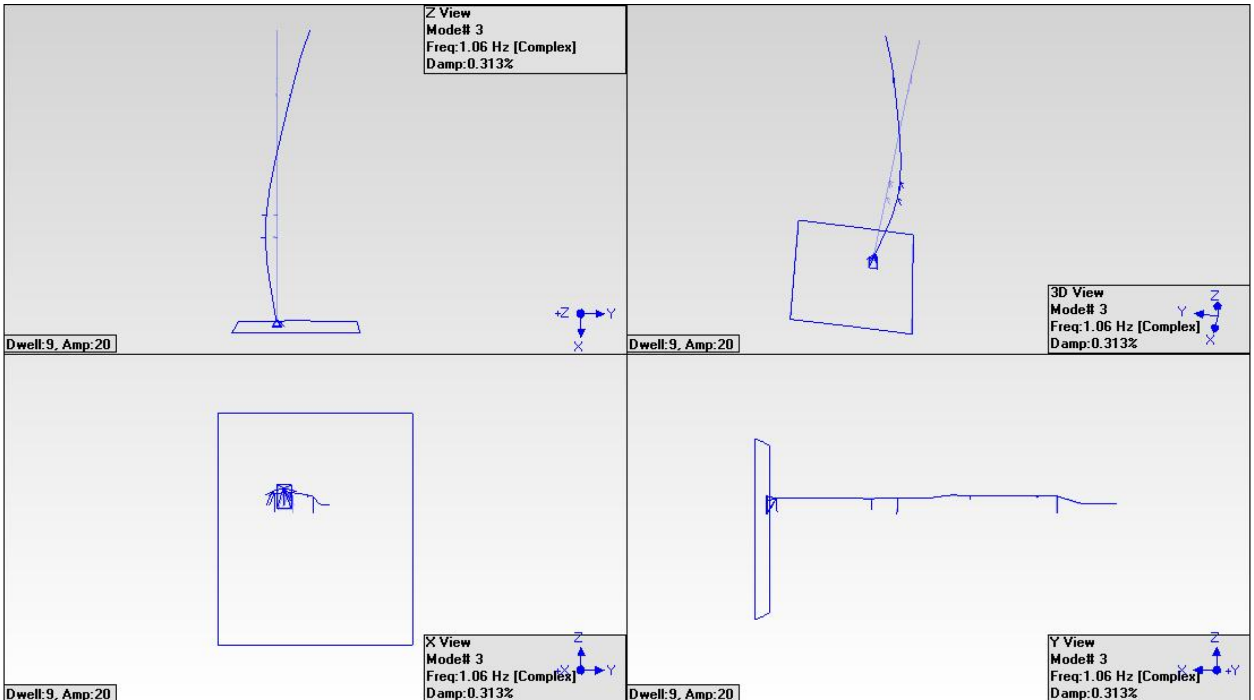

Figure E.4. Test mode 3; 2nd Bending Y-Axis.

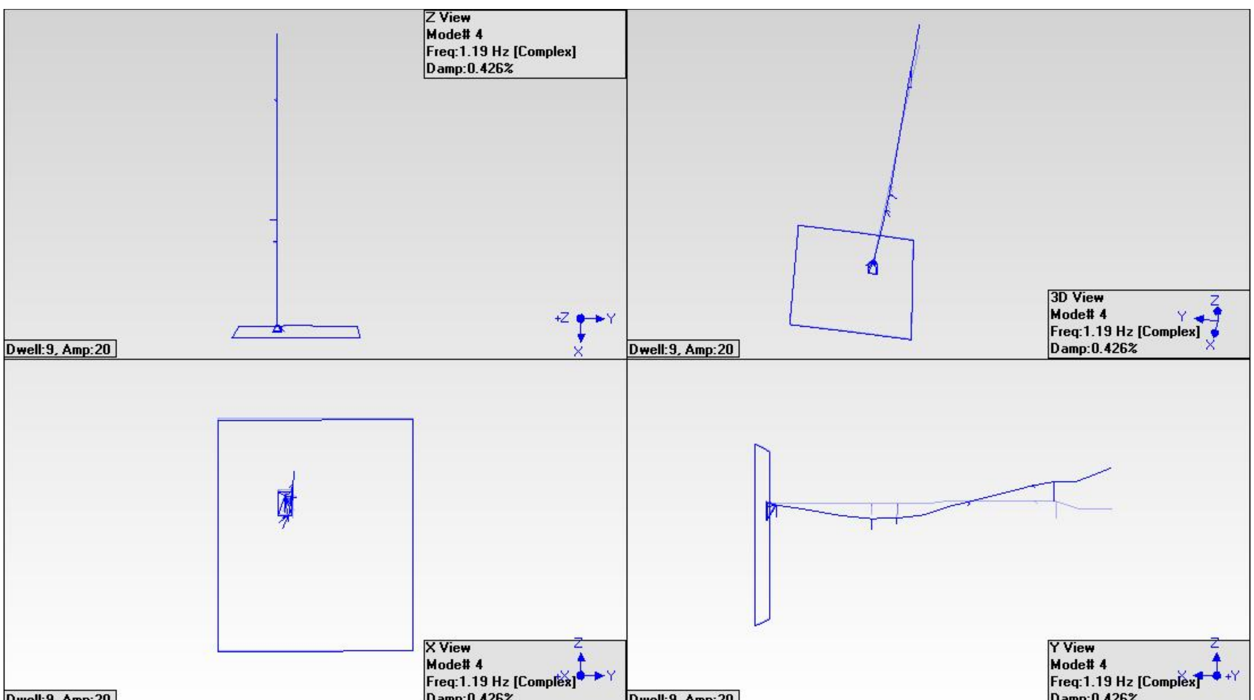

Figure E.5. Test mode 4; 2nd Bending Z-Axis.

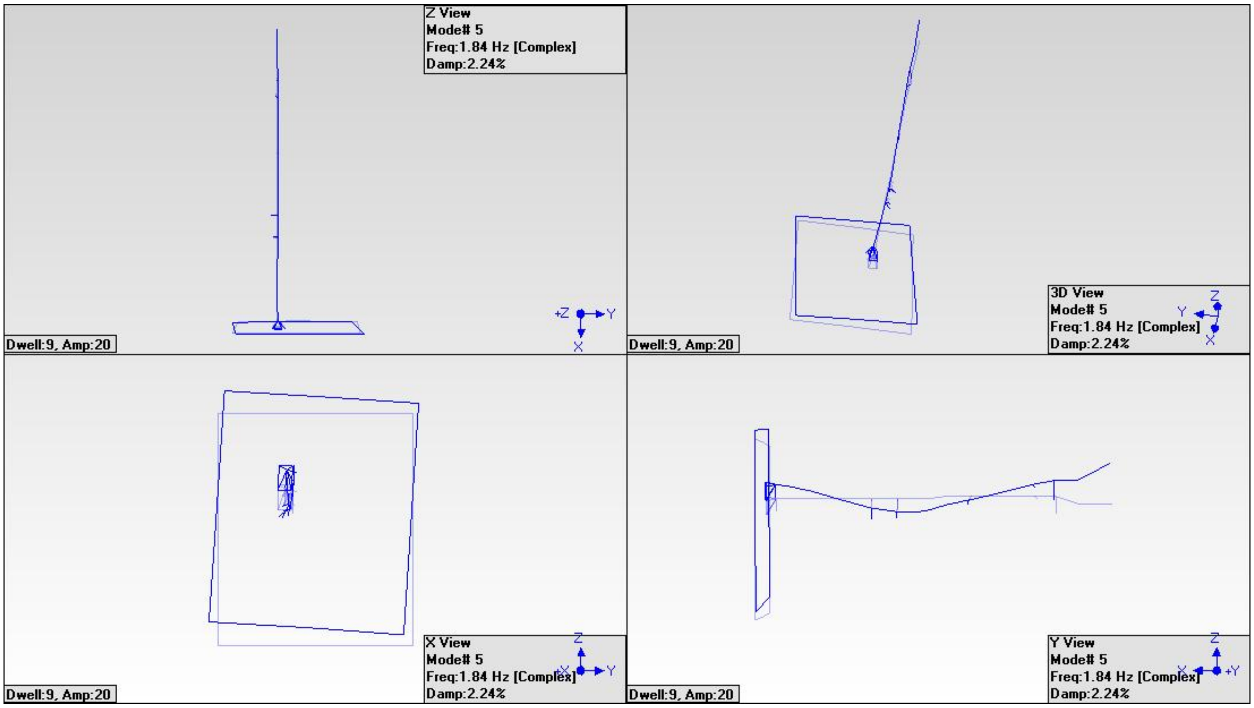

Figure E.6. Test mode 5; MLP/FTV System mode Z-Axis.

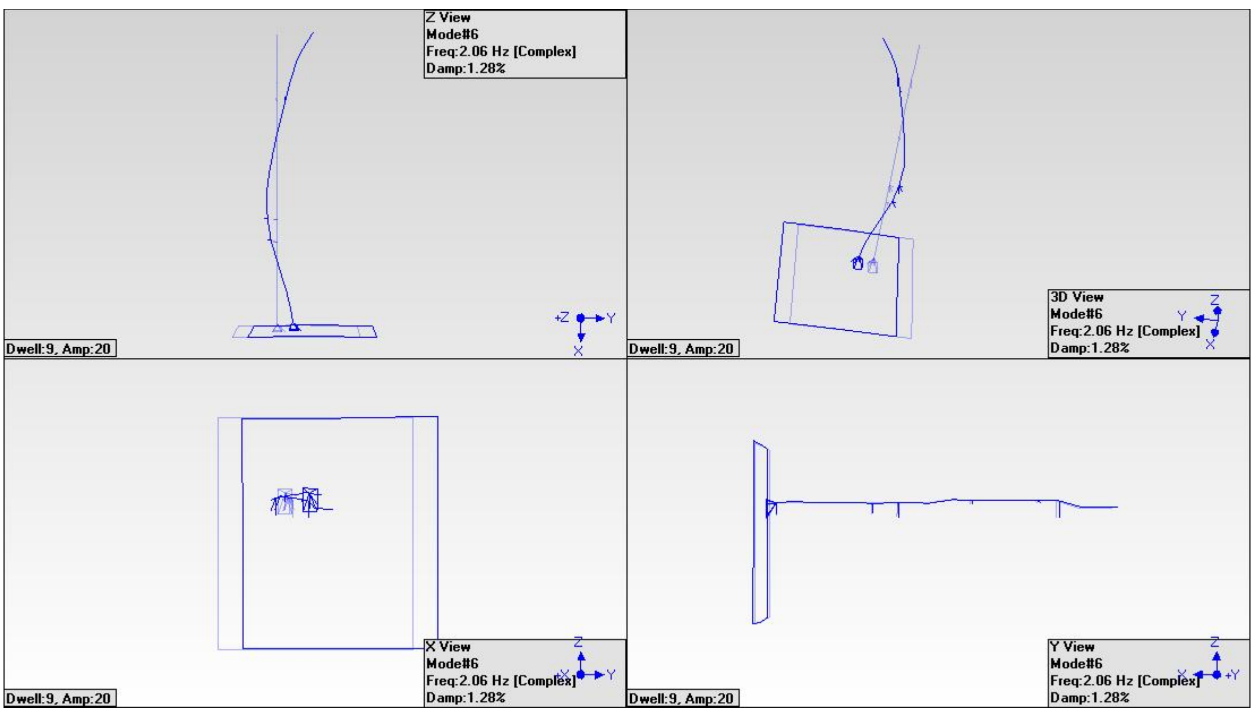

Figure E.7. Test mode 6; MLP/FTV System mode Y-Axis.

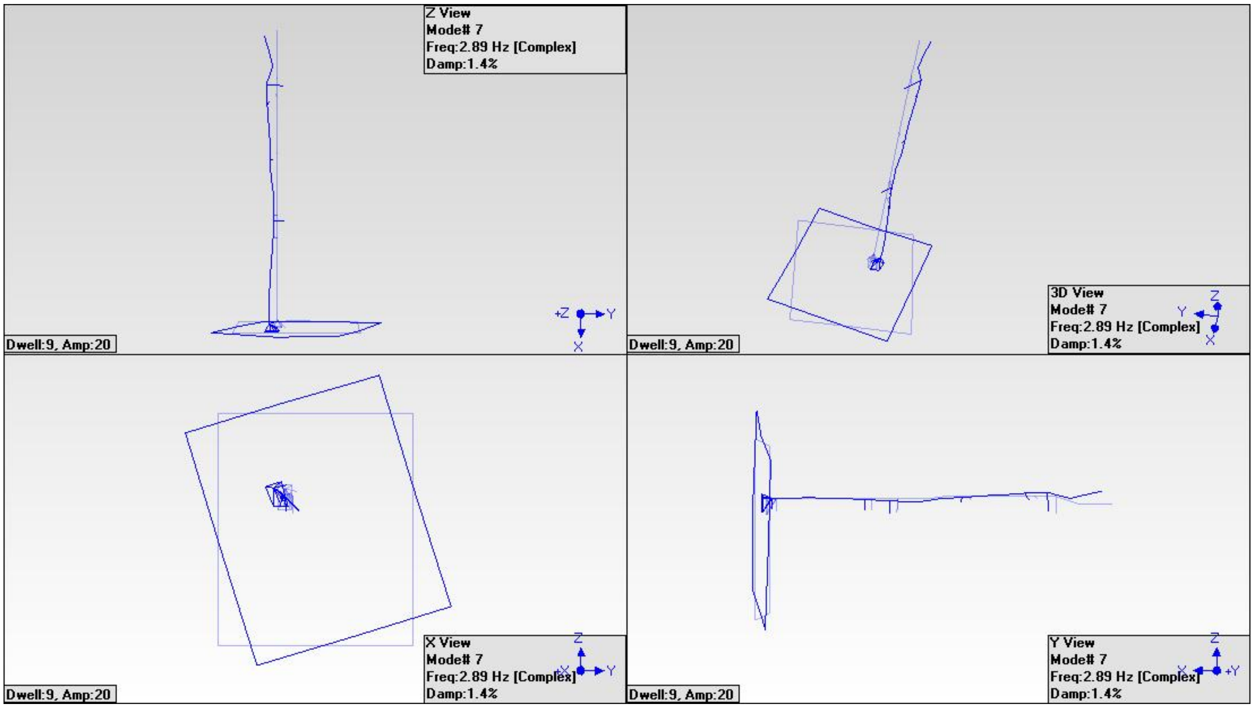

Figure E.8. Test mode 7; MLP/FTV System torsion mode.

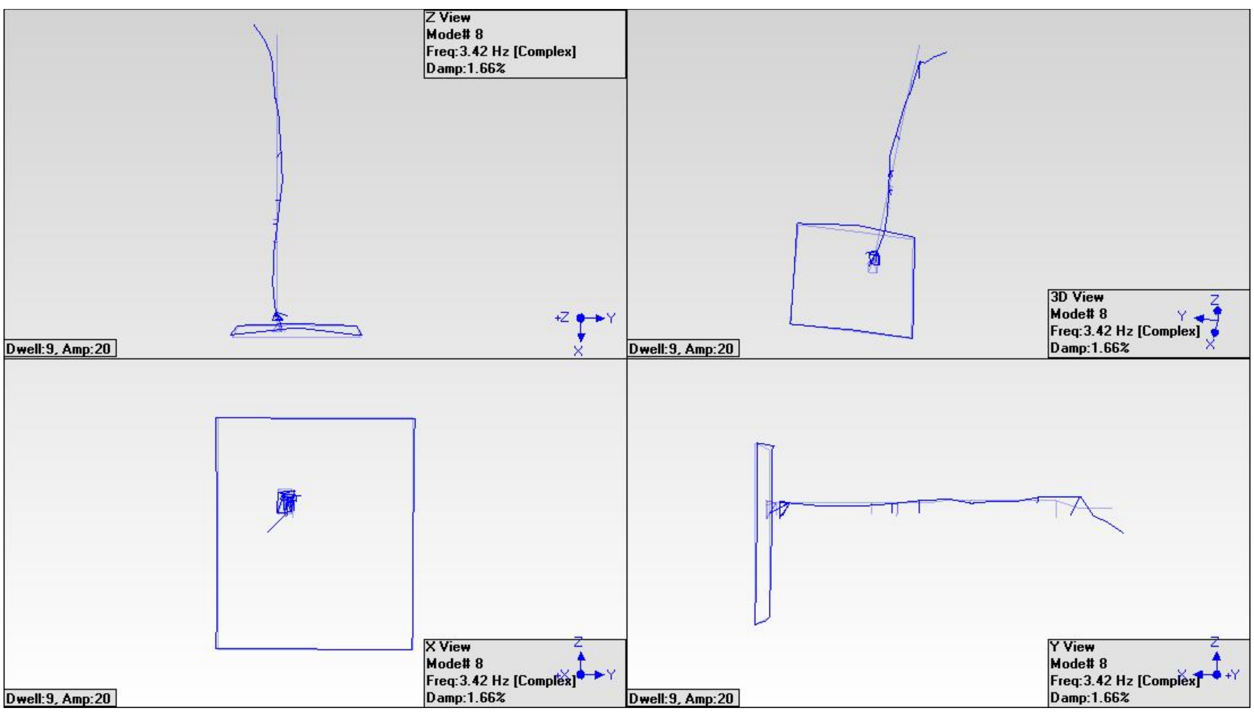

Figure E.9. Test mode 8; MLP/FTV System mode X-Axis.

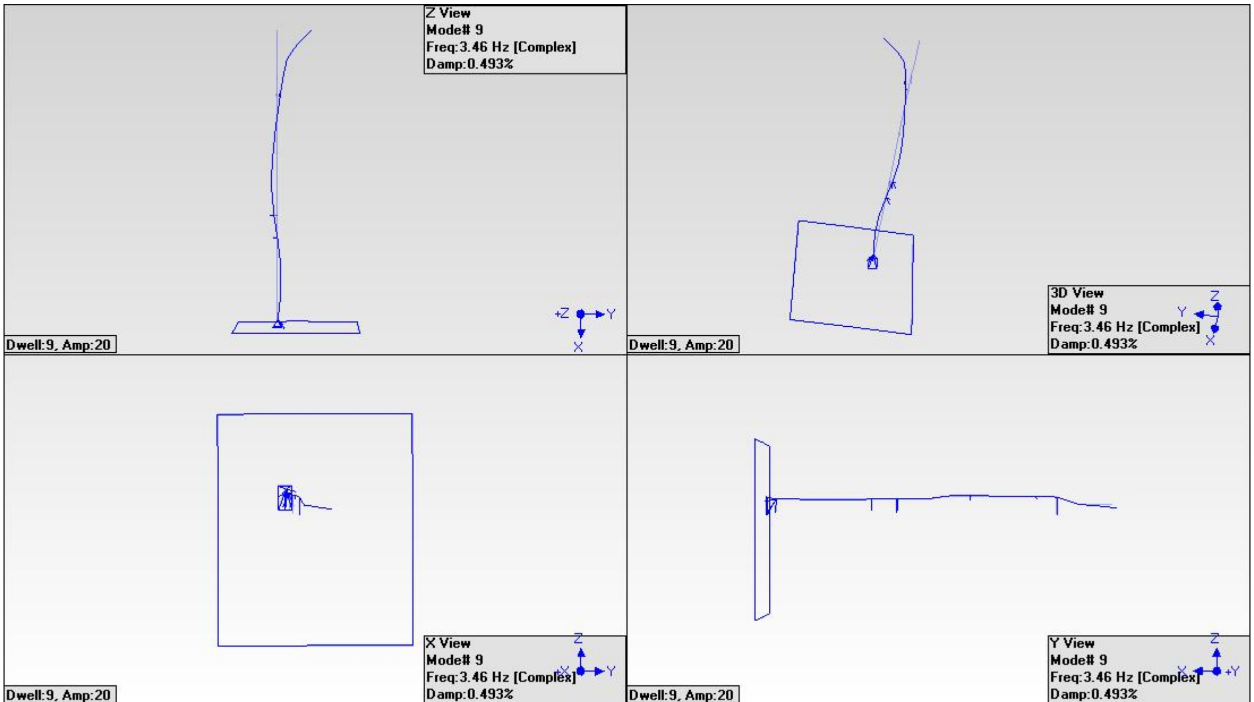

Figure E.10. Test mode 9; 3rd Bending Y-Axis.

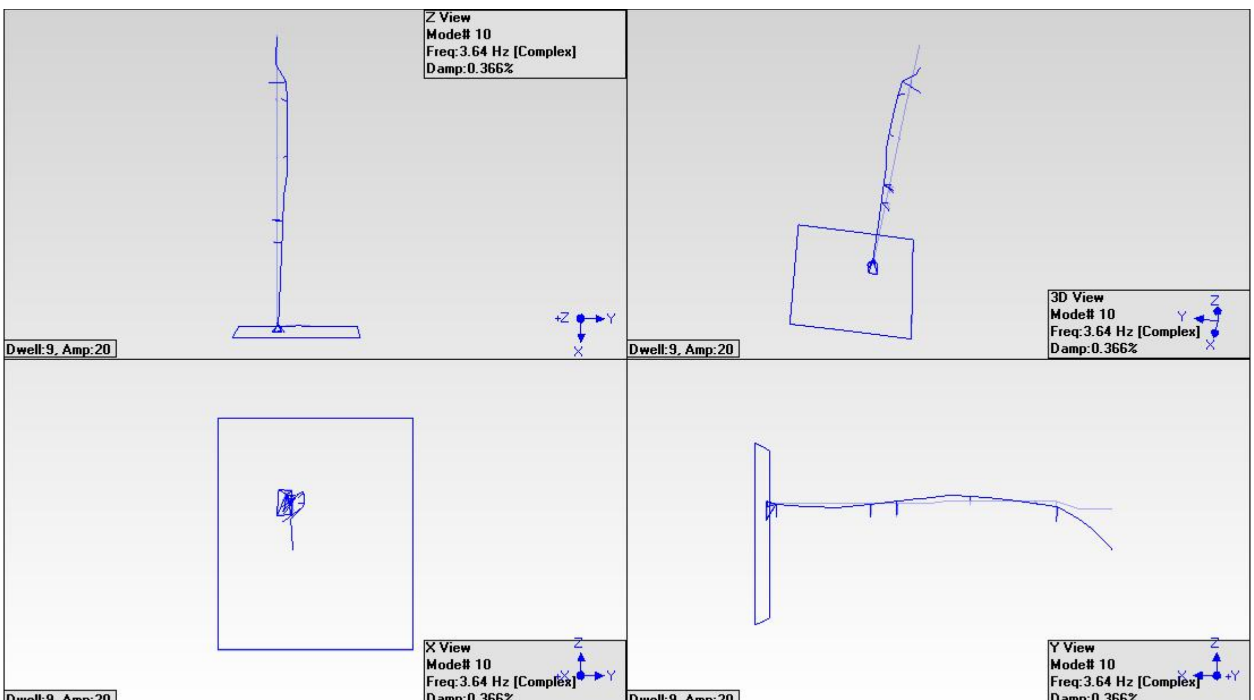

Figure E.11. Test mode 10; 3rd Bending Z-Axis and Torsion.

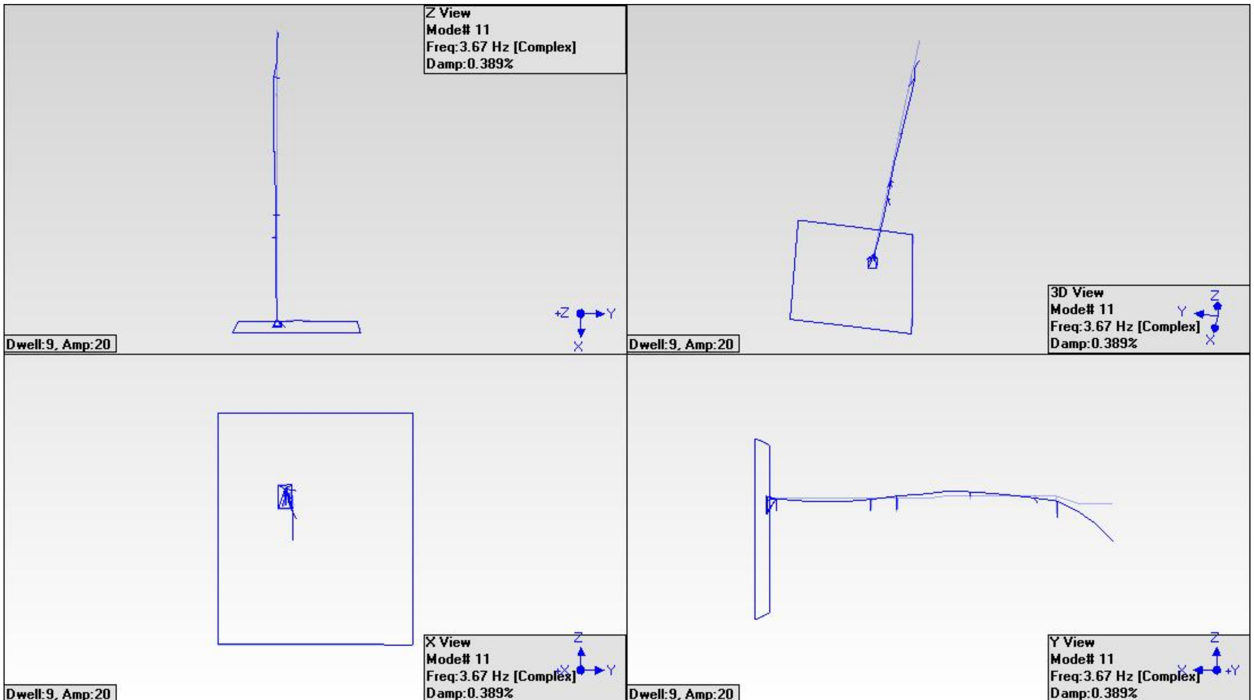

Figure E.12. Test mode 11; 3rd Bending Z-Axis.

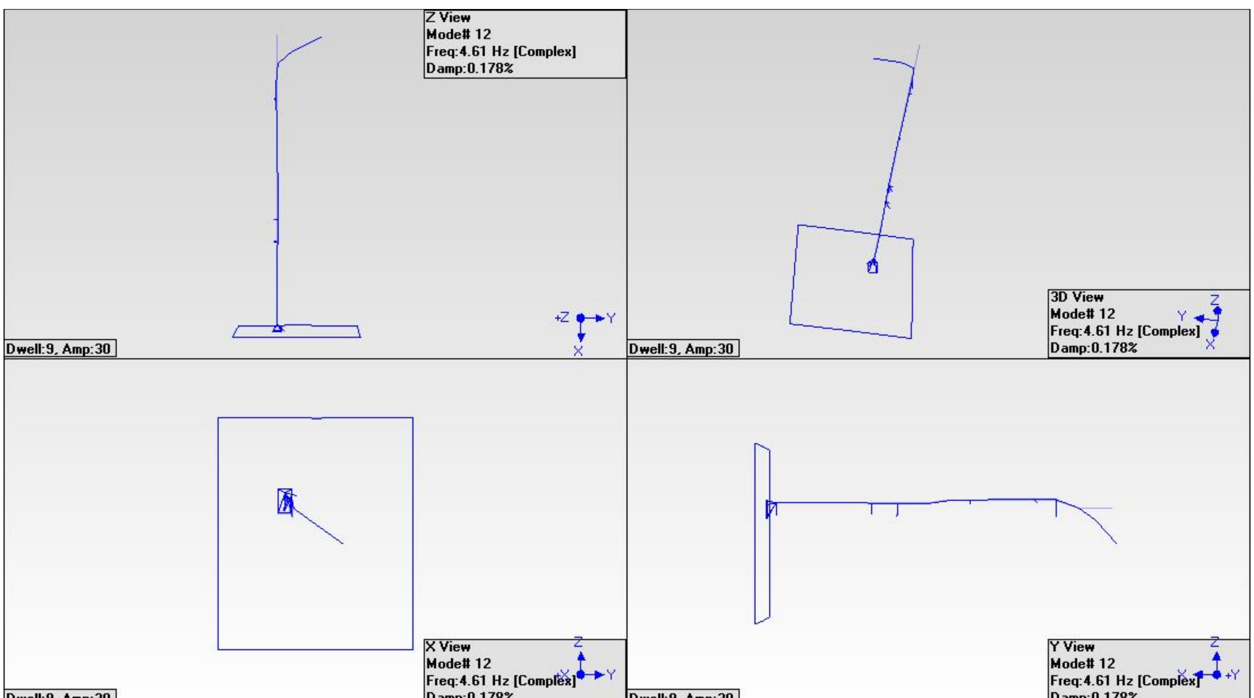

Figure E.13. Test mode 12; 4th Bending (45°).

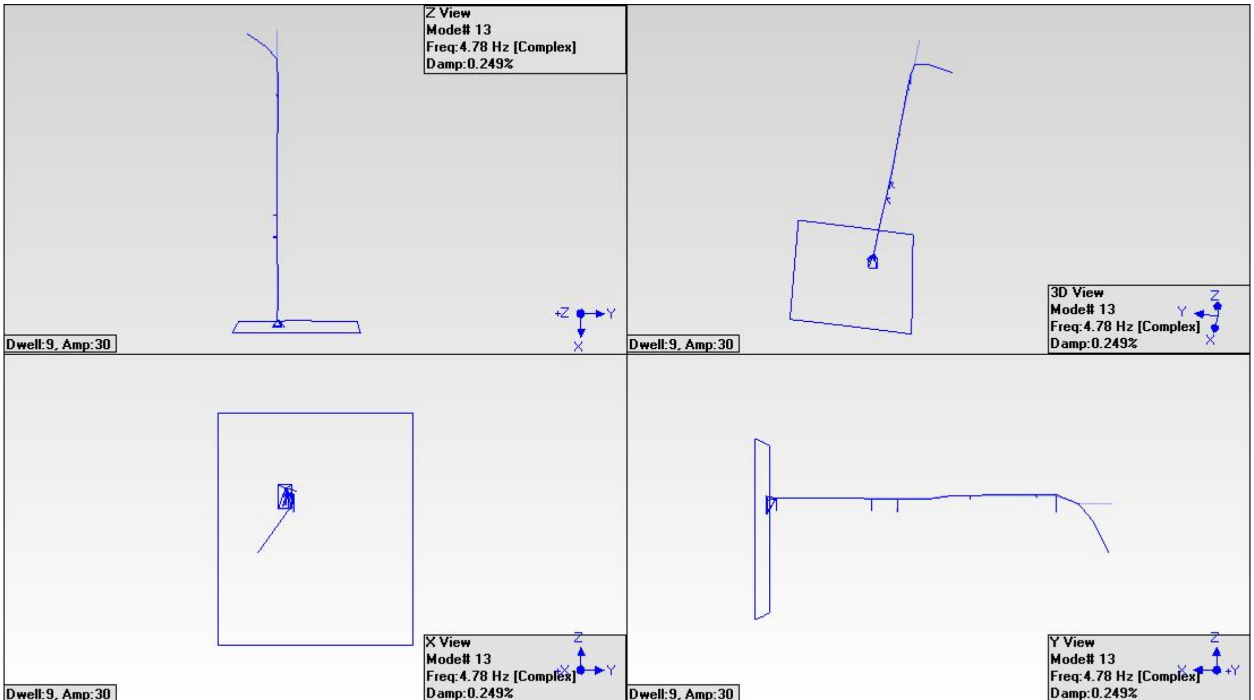

Figure E.14. Test mode 13; 4^{th} Bending (135°).

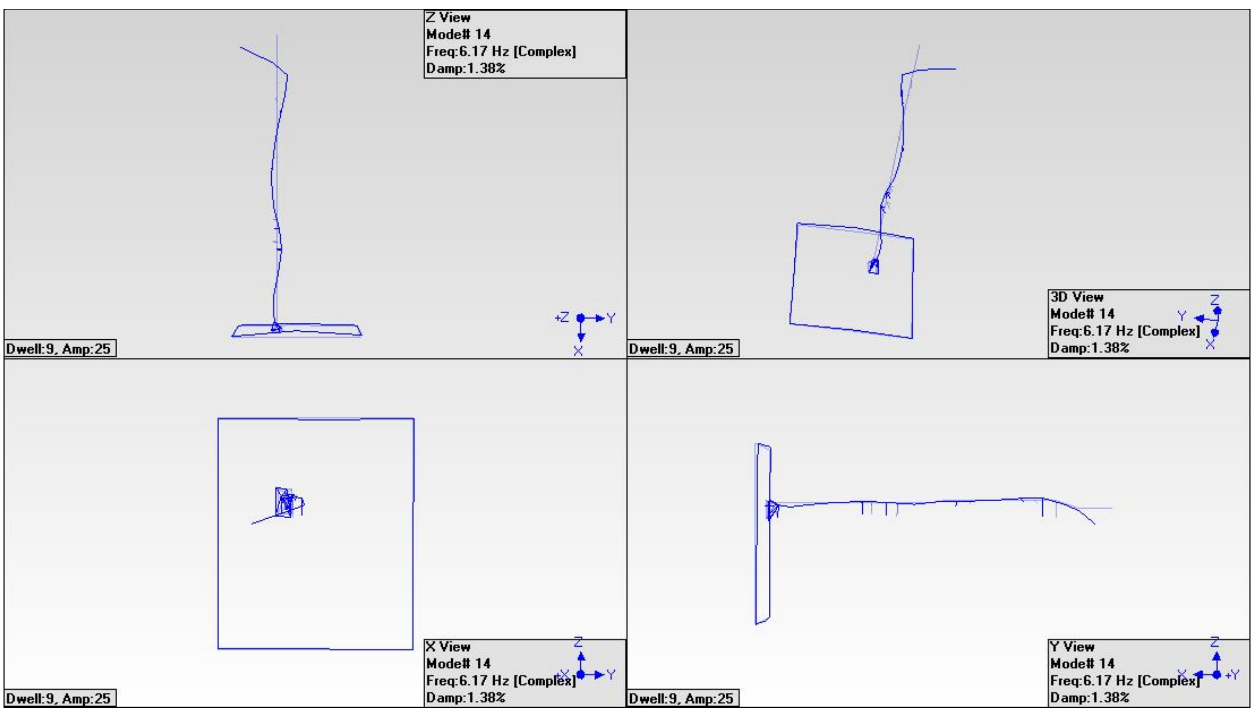

Figure E.15. Test mode 14; MLP/FTV System mode.

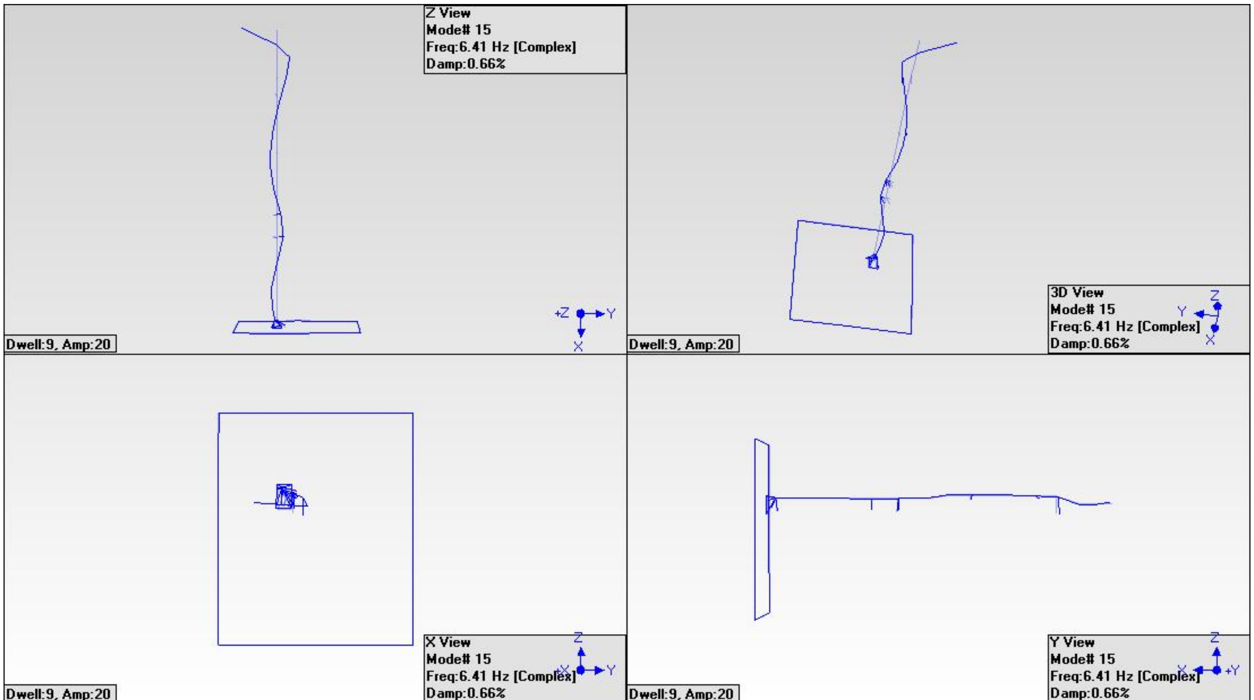

Figure E.16. Test mode 15; 5th Bending Y-Axis.

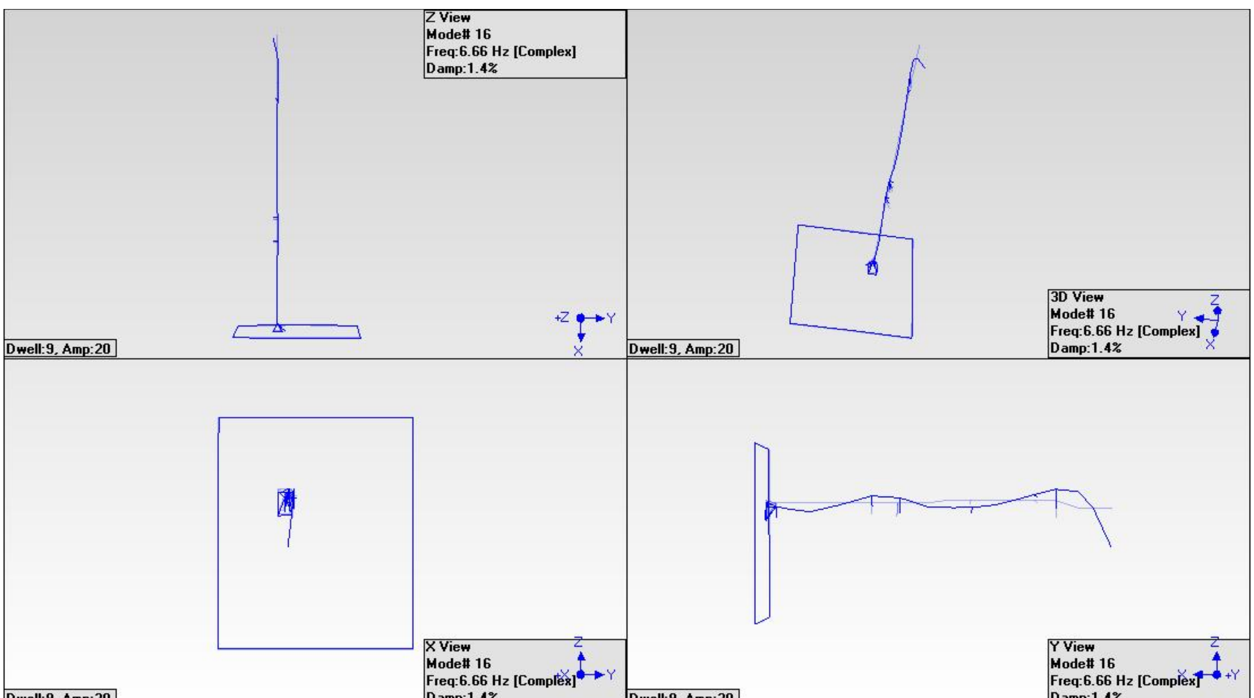

Figure E.17. Test mode 16; 5th Bending Z-Axis.

REPORT DOCUMENTATION PAGE	*Form Approved OMB No. 0704-0188*

1. REPORT DATE *(DD-MM-YYYY)*	2. REPORT TYPE	3. DATES COVERED *(From - To)*
01- 01 - 2010	Technical Memorandum	

4. TITLE AND SUBTITLE	5a. CONTRACT NUMBER
Ares I-X Flight Test Vehicle Modal Test	
	5b. GRANT NUMBER
	5c. PROGRAM ELEMENT NUMBER
6. AUTHOR(S)	**5d. PROJECT NUMBER**
Buehrle, Ralph D.; Templeton, Justin D.; Reaves, Mercedes, C.; Horta, Lucas G.; Gaspar, James L.; Bartoletta, Paul A.; Parks, Russel A.; Lazor, Daniel R.	5e. TASK NUMBER
	5f. WORK UNIT NUMBER 136905.10.10.20.20

7. PERFORMING ORGANIZATION NAME(S) AND ADDRESS(ES)	8. PERFORMING ORGANIZATION REPORT NUMBER
NASA Langley Research Center Hampton, VA 23681-2199	L-19797
9. SPONSORING/MONITORING AGENCY NAME(S) AND ADDRESS(ES)	**10. SPONSOR/MONITOR'S ACRONYM(S)**
National Aeronautics and Space Administration Washington, DC 20546-0001	NASA
	11. SPONSOR/MONITOR'S REPORT NUMBER(S) NASA/TM-2010-216182

12. DISTRIBUTION/AVAILABILITY STATEMENT
Unclassified - Unlimited
Subject Category 18
Availability: NASA CASI (443) 757-5802

13. SUPPLEMENTARY NOTES

14. ABSTRACT

The first test flight of NASA's Ares I crew launch vehicle, called Ares I-X, was launched on October 28, 2009. Ares I-X used a 4-segment reusable solid rocket booster from the Space Shuttle heritage with mass simulators for the 5th segment, upper stage, crew module and launch abort system. Flight test data will provide important information on ascent loads, vehicle control, separation, and first stage reentry dynamics. As part of hardware verification, a series of modal tests were designed to verify the dynamic finite element model (FEM) used in loads assessments and flight control evaluations. Based on flight control system studies, the critical modes were the first three free-free bending mode pairs. Since a test of the free-free vehicle was not practical within project constraints, modal tests for several configurations during vehicle stacking were defined to calibrate the FEM. Test configurations included two partial stacks and the full Ares I-X flight test vehicle on the Mobile Launcher Platform. This report describes the test requirements, constraints, pre-test analysis, test execution and results for the Ares I-X flight test vehicle modal test on the Mobile Launcher Platform. Initial comparisons between pre-test predictions and test data are also presented.

15. SUBJECT TERMS
Flight test vehicles; Modal parameters; Modal test

16. SECURITY CLASSIFICATION OF:			17. LIMITATION OF ABSTRACT	18. NUMBER OF PAGES	19a. NAME OF RESPONSIBLE PERSON
a. REPORT	b. ABSTRACT	c. THIS PAGE			STI Help Desk (email: help@sti.nasa.gov)
					19b. TELEPHONE NUMBER *(Include area code)*
U	U	U	UU	94	(443) 757-5802